HIGH PRECISION LATTICE QCD: PERTURBATIONS IN A NON-PERTURBATIVE WORLD

A Dissertation

Presented to the Faculty of the Graduate School

of Cornell University

in Partial Fulfillment of the Requirements for the Degree of

Doctor of Philosophy

by

Quentin John Mason

January 2004

AUTOMATED LATTICE PERTURBATION THEORY

Quentin John Mason, Ph.D.

Cornell University 2004

The High-Precision QCD collaboration has embarked on a ground-breaking survey of strongly interacting Standard Model phenomenology from lattice QCD using the improved staggered action for light quarks, NRQCD for the heavy quarks and one-loop Symanzik improved gluons. This program requires one- and two-loop perturbative renormalisations of action parameters, matrix elements and currents. The current techniques for lattice perturbation theory are very cumbersome and inflexible, built for individual one-loop applications. Very few two-loop results are known, even for the simplest actions. A new method for performing perturbative calculations in Lattice QCD is presented. The combination of easily determining Feynman rules for arbitrary actions and automated diagram generation has enabled the calculation of six related three-loop quantities for several different actions including the most highly improved, "Asqtad" that is being used for the most realistic lattice simulations ever. The necessity of choosing an appropriate scheme and scale for lattice expansions is demonstrated. Further improvements to the scaling in the quark sector are investigated and a new action with three times smaller errors is obtained. The connection between the lattice and continuum couplings is determined to two-loops for these actions which is a pre-requisite for any future perturbative calculations. Third-order Wilson loops up to 2×2 are calculated for the first time which can be used to determine the strong coupling

constant at energies relevant to simulations and to experimenters. The quark mass is renormalised to one-loop in order to determine the mass of the strange quark and compare to sum rules.

BIOGRAPHICAL SKETCH

Quentin John Mason was born April 28th, 1977 to Canadian parents in Newport Pagnell, England. After attending the local state school for a short time he was dispatched to cram for entrance to Bedford Modern; a private school. It was there that he discovered water-polo after being put off by rugby, and has played all 15+ seasons since; some of them at a national level included England Trials. He began to distinguish himself in Mathematics at GCSE and subsequently also Physics through S-level. Originally intending to be a mathematician it was the wise council of the school that physics would be a better choice, for which he is very grateful. It was summers canoe tripping at Camp Pathfinder, Algonquin Park, that he learned about real physical adversity and the inward insights of living on the edge; constantly being challenged. At St. John's College, Oxford he took up rowing, in his novice year with the college 1st VIII behind several multiple Blues-winners, in the second year with the Oxford Lightweights at Henley Royal and later rowing through his Finals, including several days of arriving at races with a gown and mortar-board, fresh from the exam. He coached and lead the water-polo team to avenge more than a decade of defeat at the Varsity match and to take an unprecedented second at the BUSA competition. Made a Scholar after his Prelims and receiving a gentleman's First (MPhys) after four years, he was advised to study in the USA to pursue an academic career and flew off to the wonderful natural beauty of Cornell and the surrounding area. There he discovered the joys of working until sunrise, the wonders of daily pool-time, the stopping force of rail-road ties, and that being losing everything and having to re-write the code completely from scratch is not the end of the world. He player-coached the water-polo team to Nationals for the first time and squeaked fourth place much to the chagrin of

the other teams, who could not get over the absence of a coach on deck and the presence of a petrol-can for our "gadoline". His educational parents, Prof's John and Robin Mason, instilled some small padagogy and teaching methodology in him that he tried to pass on to the various students at Cornell that he interacted with during his Teaching Assistantship. It was after discovering G. Peter Lepage and Lattice QCD in February of the first year that the unending struggle to understand and conquer lattice perturbation theory began. After three years of late nights and much angst, this thesis is the result.


o the inspiration and perspiration of those at Bedford Modern School, Camp Pathfinder, St. John's College Oxford and at Cornell who taught me; to constantly challenge and push oneself in order to better understand oneself, physics and life. To my family, for the opportunities afforded me and the support and encouragement to follow through on my dreams however far from home. Mad props to the SJC Skillz Crew.

ACKNOWLEDGEMENTS

I am very grateful for the time and interest of my supervisor, G. Peter Lepage who was never without explanations, ideas and possible checks on my calculations. I would like to acknowledge the collaboration with Howard Trottier, particularly for our friendly competition that has helped spur us both on. I certainly appreciate Martin Lüscher and Haris Panagopoulos who developed the framework of these multi-loop perturbative calculations and published diagram by diagram results for the simple unimproved action that we could exploit. I would like to thank Ron Horgan for driving our parallelisation of `VEGAS` that vastly increased my efficiency when I finally started using it, and for his encouragement and giving me a postdoc. I would like to thank Ivan and Dan for setting up the B3 computers and the rest of the physics graduates students at Cornell for letting me run parallel jobs there. So much less would have been possible without the MILC collaboration's configurations and without computer time at Fermi National Laboratory. Joachim Hein and I had some useful interactions regarding the strange quark mass calculation and the taste-changing investigation. Thanks should also go to my tutor Keith Burnett who advised me to come to the the USA, and to Sam Carr for a great atmosphere in tutorials and for suggesting the mathematics paper as a replacement to the boring option.

I would like to thank my housemates; Sami, Maurizio, Connie and Handë for putting up with me and keeping me amused with their antics. Thank you also to classmates Nick and Kerryann for general chat and light-hearted relief and to Kerryann for studying Gness with me. No thanks go to the Big Red Barn, but I would like to remember Jason and Leslie for provoking some fascinating discussions! Thanks to the Wilson computer group for finally trusting me with

administrator priviledges to fix their problems and for their funding; supporting my own computers, technical support know-how and writing this thesis. I am deeply indebted to Tim Whitwham for getting me into water-polo at school and teaching me the fundamentals so well, and to Pauly-P. for early morning lessons to the 1995 novice crew: "Our wake, your Funeral." Thank you to James Orford and Laura Mason who were inspirational people who I met through water-polo and who always knew what to say. I would like to remember the St. John's boaties for giving me the discipline/threats to get up before dawn and for keeping me cold, soaking wet and tired, just occasionally a touch dehydrated, and particularly: James, Dom, Rich, Rick, Chief, Charlotte and Nigel for many harsh insights into reality (but always fair); Susan for trying to sort me out – I never said how much it meant. I would like to thank my long gone great-grandfather who helped support me financially at university. Finally I would like to thank Dusty for always generously helping theory graduate students, particularly during the stressful job-application and thesis submission times, and for sharing her stories.

This thesis was brought to you in LaTeX with `FeynMP` diagrams, by the letter α_s and the numbers e, i, and π.

TABLE OF CONTENTS

LIST OF TABLES

LIST OF FIGURES

CHAPTER 1

INTRODUCTION

Quantum Chromo-Dynamics (QCD) is a strongly coupled field theory that describes the physics at the nuclear level on the scale of femptometers, 10^{-15}m. It is a fundamental part of the Standard Model that physicists believe explains the world that we see. Although perhaps not as successful as Quantum Electro-Dynamics which has been tested to extremely high precision with the $g-2$ experiments, QCD predicts the masses, decays and mixings of mesons and hadrons. Despite accurate measurements of these quantities at accelerators, the theoretical side is lagging — there is a lack of precision *ab-initio* calculations of many of the fundamental parameters in the theory. This has to do with "asymptotic freedom" whereby the strength of the interactions decreases at *high* energies and becomes strong at low energies where there is a non-perturbative confining phase. The basic particles – the quarks – are not experimentally observed except in composite colour singlets. The quarks strongly interact with force carrying vector bosons known as gluons and only very occasionally through electro-weak interactions.

Lattice QCD (LQCD) studies the quantum fields of quarks and gluons using a discretized version of spacetime and was first presented in 1974 by Wilson [1]. The limit of LQCD where the size of the lattice grows to infinity and the lattice spacing a decreases to zero, formally defines the continuum theory of QCD. The lattice itself provides a high-momentum cutoff to the theory of $\mathcal{O}(\pi/a)$ which is a non-perturbative regularisation. As such LQCD is a renormalisable effective field theory that has no additional free parameters over the continuum and is the only method by which a first principles determination of the physics implications of QCD may be made and tested against experiment. That is a great promise

that has by and large not been delivered upon; until recently lattice simulations have been far from realistic largely because of two factors. First, the quenched approximation where there are no fermions running in loops, is computationally far easier than dynamical simulations of quarks which require repeated inversion of enormous ill-conditioned sparse distributed matrices to update the Grassman fermion fields. Only in the last few years have simulations been performed with two light quarks (representing the u and d) and one slightly heavier dynamical s-quark. Second, the cost of simulations increases at least like $\frac{1}{a^6}$, so a small decrease in a is extremely expensive. Unfortunately it is only in the limit $a \to 0$ that the theory reproduces life. The state of the art is now 2+1 dynamical light quarks, m_s correct but with $m_u = m_d$ too heavy at between $m_s/10$ and $m_s/2$. The lattice spacings are $a^{-1} \sim 0.1$ GeV. This can only be done using a very highly improved action, "Asqtad" to reduce discretisation artifacts such as $\mathcal{O}(a, a^2)$ which would otherwise have to be fit and removed using more expensive simulations at even smaller a. These unprecedented simulations recently postdicted to less than 3% errors 9 "gold-plated" quantities that cover a range of scales from light-light to baryonic [2], finally establishing Lattice QCD as a quantitative contributor to phenomenology.

Weakly coupled perturbation theory expands the action in the bare coupling and is very important for non-perturbative simulations. Although it does not reveal the full content of the theory or provide a suitable regularisation for doing continuum perturbation theory calculations, it currently limits the accuracy of many important phenomenological quantities such as $\alpha_{\overline{\rm MS}}(m_Z)$, m_s, f_B, $B - \overline{B}$ mixing and various splittings in both the Upsilon and Psi families. Non-perturbative renormalisations and matchings could in principle be done but the improvement

required for the realistic simulations leaves many parameters, and the tuning necessary is prohibitively difficult. The High Precision Lattice QCD collaboration (HPQCD) has embarked on an ambitious program of all the one- and two-loop renormalisations necessary to make accurate *pre*dictions of forthcoming experiments at the B-factories and CLEO [3]. Lattice perturbation theory fixes the sharp cutoff and is responsible for the physics above that. It is used for improving the scaling behaviour of the gluon, light-quark and heavy-quark Lagrangians, for matching lattice operators and matrix elements to the continuum and for the renormalisation of the input parameters: quark masses and the coupling. Unfortunately lattice perturbation theory is much more difficult than in the continuum because there are no analytic integrals in any approximation and with much larger Feynman rules, more diagrams and many Lagrangians very few two-loop results are known for even the simplest actions.

In this work a new automated method and associated techniques for lattice perturbation theory are explained in §2, particularly comparing with previous approaches and continuum techniques. It shows promise with the flexibility required to do many calculations with many different actions with small enough errors for the HPQCD program.

- The most accurate light quark action is further improved to remove taste-changing effects that contribute few-percent corrections to current simulations in §3.

- The one-loop quark mass renormalisation is determined in §4 which is then used to set the strange quark mass.

- The two-loop relation between the lattice coupling and a continuum cou-

pling is calculated for four actions, and six three-loop expansions of Wilson loops are determined in §5. Combined, these results can determine the strong coupling constant $\alpha_{\overline{\rm MS}}(m_Z)$ at least as accurately as any experimental method [4]. The coupling matching is the most important lattice perturbation theory calculation because all other expansions of lattice observables must be converted to a continuum scheme for comparison to phenomenology.

CHAPTER 2

LATTICE PERTURBATION THEORY: A HOWTO

Perturbation theory on the lattice is not really any different than the continuum, it is just harder to evaluate the integrals because answers cannot be expressed in closed form. Lattice perturbation theory has historically been unconvincing with poorly convergent series which did not agree with non-perturbative simulation results. This was explained and resolved by several insights from Lepage (tadpole improvement, appropriate scale and scheme and improved staggered quarks) [5, 6, 7]. The evaluation of even one-loop quantities with unimproved actions was difficult with the computing power available at the time. Now a new method combined with these insights has enabled two and three loop calculations with improved actions, an endeavour roughly 10^8 more complex than before; resulting in convergent series which agree well with simulation.

Perturbative calculations are well known and understood in the continuum where the $\overline{\text{MS}}$ renormalisation scheme using dimensional-regularisation is dominant. This scheme is not suitable for use on the lattice for either ultra-violet (UV) or infra-red (IR) divergences. A matching calculation must therefore be performed in order to convert lattice results to the $\overline{\text{MS}}$ scheme and compare to phenomenology. This is done to two-loop (third-order) in §5.1 for the lattice coupling $\alpha_{\text{lat}} = \alpha_{\overline{\text{MS}}}\left(1 + \mathcal{O}(\alpha) + \mathcal{O}(\alpha^2) + \ldots\right)$ and for the quark mass to first order $m_{\overline{\text{MS}}}(\mu) = m\left(1 + \mathcal{O}(\alpha) + \ldots\right)$ in §4.

The lattice itself is the UV regulator — the highest momentum mode on the lattice is π/a so in a sense this is a huge simplification over the continuum, but the IR regulation can be more tricky on the lattice and is discussed in §2.4. The Feynman diagrams are constructed from propagators and vertices in the usual

way but with momentum conservation modulo $2\pi/a$ and a lot of new vertices. However the biggest difference with the continuum is that the Feynman rules are *significantly* larger — in the continuum they all fit on a single envelope for those important calculations, but on the lattice a single rule can be $5\times$ larger than Kurt Gottfried's new book [8]! There are several reasons for this explosion: the lattice pays the large cost of breaking most of the Lorentz symmetry of the continuum to retain gauge invariance, additional operators are added to improve actions to correct scaling and the vertices grow factorially in size §2.2, §2.2.5. In fact there are vertices $\mathcal{O}(\alpha^n A^m)\ \forall n, m$ just for the pure gluon action, though all but the lowest that are shared with the continuum are "irrelevant" in the renormalisation-group sense and although they cause no IR problems they must be evaluated to get gauge-invariant answers.

After introduction of some notation and the various lattice actions in §2.1, an old algorithm for making lattice Feynman rules is briefly reviewed in §2.2, and extended to vertices required for three-loop calculations, improved staggered quarks and background fields in §2.2.1, §2.2.2, and §2.2.4, which inform a discussion of the various approaches to integration in perturbative calculations on the lattice in §2.2.5. An algorithm for generating the diagrams automatically in §2.3 as part of the automated method is presented along with a review of how to handle IR divergences in §2.4. Finally the re-organisation of finite perturbative series to improve convergence is discussed in §2.5.

2.1 Lattice Actions

The naïve discretisation of the continuum action with continuum gluon fields at the lattice sites breaks both Poincaré symmetry and gauge invariance. The gauge

invariance which keeps each occurrence of the coupling g in the action the same would be very difficult to restore exactly on the lattice by the addition of (an infinite number) counter terms, or approximately to even a few orders in g. The action should reduce to the continuum as a goes to zero to restore Lorentz invariance and made only from gauge invariant operators. Therefore parallel transporters U, Wilson lines of one lattice spacing, are used to connect lattice sites. The "link" fields U carry a direction Lorentz index μ, are SU(3) matrices and possess a local gauge invariance:

$$U_\mu(x) \to \Lambda(x)\, U_\mu(x)\, \Lambda^\dagger(x + a\hat{\mu}) \quad \Lambda(x) \in \mathrm{SU}(N), \tag{2.1}$$

under local gauge transformations $\Lambda(x)$. The Wilson gluon action is then made from the minimal closed loop of links, the plaquette $P_{\mu\nu}$, Symanzik improved with a rectangle $R_{\mu\nu}$ to eliminate $\mathcal{O}(a^2)$ corrections and to one-loop order with a further non-planar "corner-cube" $C_{\mu\nu\sigma}$ to eliminate $\mathcal{O}(\alpha_s a^2)$ errors by careful choice of the parameters involving a one-loop renormalisation calculation [9, 10]. Almost all perturbative results in the literature are for the unimproved Wilson gluon action, especially the very few higher loop results [11]. The most highly-improved action available and the one of most interest is that used by the MILC collaboration in their simulations and analysed by many groups including HPQCD [7, 9, 10, 12]. It is one-loop improved Symanzik glue including plaquette tadpole improvement factors of u_0:

$$S_G = \beta_{pl} \sum_{x;\mu<\nu} (1 - P_{\mu\nu}) + \beta_{rt} \sum_{x;\mu\neq\nu} (1 - R_{\mu\nu}) + \beta_{pg} \sum_{x;\mu<\nu<\sigma} (1 - C_{\mu\nu\sigma}), \tag{2.2a}$$

where the choice of parameters for SU(3) is

$$\begin{aligned}\beta_{pl} =& \frac{10}{g^2},\\ \beta_{rt} =& -\frac{\beta_{pl}}{20u_0^2}(1+0.4805\alpha_s),\\ \beta_{pg} =& -\frac{\beta_{pl}}{u_0^2}0.03325\alpha_s,\end{aligned} \tag{2.2b}$$

and the loops are:

$$P_{\mu\nu} = \frac{1}{3}\,\mathrm{Re}\,\mathrm{Tr}$$

$$R_{\mu\nu} = \frac{1}{3}\,\mathrm{Re}\,\mathrm{Tr}$$

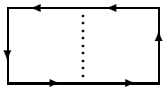

$$C_{\mu\nu\sigma} = \frac{1}{3}\,\mathrm{Re}\,\mathrm{Tr}$$

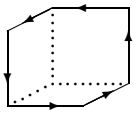

. (2.2c)

Lepage and Mackenzie [5] showed that tadpole diagrams are a large contribution to lattice perturbative results, causing the series to diverge at unexpectedly low order and to disagree with non-perturbatively measured values. The matching of lattice operators with continuum operators is based on the expansion (2.10):

$$U_\mu(x) \equiv e^{igaA_\mu} \rightarrow 1 + iga\,A_\mu + \ldots, \tag{2.3}$$

when the lattice spacing a is small. However, higher order terms in the expansion of U_μ contain additional factors of $(ga\,A_\mu)^{2n}$ and are formally of that order, but the contraction of these A_μ's with each other generates ultra-violet "tadpole" diagrams that diverge $\propto \frac{1}{a^{2n}}$ which cancel those a's in the numerator. These higher order terms are then actually of order α^n and are not being suppressed by powers of a small lattice spacing a and so are very large. If the quantity being calculated is sensitive to low-energy scale physics which is the whole point of being on the lattice then $\alpha \sim \frac{1}{2}-1$ and the tadpole contribution causes a divergence in truncated

perturbation theory. Fortunately Lepage and Mackenzie also suggested a fix by noticing that the appropriate connection to the continuum gauge field should be

$$U_\mu(x) \to u_0 \left(1 + iga\, A_\mu\right), \tag{2.4}$$

where the "tadpole" factor u_0 can be chosen and should represent the mean value of the link $U_\mu(x)$. Then everywhere a link U appears in the action it should be divided by its mean tadpole value u_0. Of course some of these factors can be absorbed into redefinitions of the fields but where there are paths of differing lengths powers of $\frac{1}{u_0}$ are seen e.g. (2.2b). Two choices for u_0 are commonly used:

$$u_P \equiv \left[\langle \frac{1}{3} \operatorname{Re}\operatorname{Tr} U_\Box \rangle\right]^{\frac{1}{4}}, \tag{2.5a}$$

for the plaquette definition (gauge invariant), and

$$u_L \equiv \left\langle \operatorname{Re}\operatorname{Tr} U_\mu \right\rangle\Big|_{\text{Landau Gauge}}. \tag{2.5b}$$

for the mean-link definition. In a simulation the non-perturbative value of $u_0 = u_P$, or u_L is used, where that value is converged to for some fixed precision by iteration. The favoured mean-link definition has the disadvantage of requiring the simulation be gauge-fixed to Landau gauge in order that it be measured, and this is time-consuming. At the same time that the tadpole factor is being converged on the value of α_s to be used in (2.2b) is also self-consistently determined from the one-loop expression for a quarter of the logarithm of the plaquette (a more convergent, physical quantity than the plaquette itself)

$$u_{0,P} = 1 - 0.767098\alpha_{\text{lat}} - (1.7723 - 0.0697 n_f)\alpha_{\text{lat}} + \mathcal{O}(\alpha_{\text{lat}}^3) \tag{2.6a}$$

$$\begin{aligned} \alpha_s\Big|_{S_{glue}} &\equiv -\frac{1}{4} \ln u_P\Big|_{\mathcal{O}(\alpha_{\text{lat}})}, \\ &= \alpha_{\text{lat}} + (2.694 - 0.09087 n_f)\alpha_{\text{lat}}^2 + \mathcal{O}(\alpha_{\text{lat}}^3) \end{aligned} \tag{2.6b}$$

which after expanding the right hand sides in powers of $\alpha_{\rm lat} = g^2/(4\pi)$ gives the perturbative definition to all orders for the α_s and u_0 appearing in the action (2.2a), (2.2b). The full Feynman rules for the action up to some given order therefore require a computation of the tadpole factor u_0 at one lower order. The tree-level value is 1. Tadpole factors add one further inconvenience to perturbation theory in that the small values for the final coefficients come at the expense of large cancellations between the tadpole-like diagrams and the official tadpole counter-terms, thereby requiring somewhat superior precision per diagram in order to have an accurate answer.

The unimproved Wilson glue ($\beta_{rt} = \beta_{pg} = 0$ in (2.2a)) has a propagator that is reminiscent of the (Euclidean) continuum

$$\mathtt{GP}_{\mu\nu}(k) = \frac{1}{\hat{k}^2}\left[\delta_{\mu\nu} - (1-\xi)\frac{\hat{k}_\mu \hat{k}_\nu}{\hat{k}^2}\right], \tag{2.7}$$

where $\hat{k}_\mu = \frac{2}{a}\sin\frac{k_\mu}{2}$ is a latticised momenta. This is diagonal — proportional to $\delta_{\mu\nu}$ for Feynman gauge, $\xi = 1$, but has corrections to the continuum that start at $\mathcal{O}(a^2)$. The improved gluon propagator removes these errors but pays the significant perturbative cost of having a very complicated expression for the matrix which is off-diagonal in all covariant gauges. This is partly the reason why so few perturbative results for this action are available despite its widespread use.

Expectation values are given as usual by

$$\langle O \rangle = \frac{\int \mathcal{D}U \; O \; e^{-S[U]}}{\int \mathcal{D}U \; e^{-S[U]}} \tag{2.8}$$

where $\mathcal{D}U$ is the usual path integral but uses the de Haar measure on U. This is only a mild complication of perturbation theory as it introduces "measure" vertices of $(gA)^{2n}$ $\forall n > 0$ which essentially encodes the Jacobian of the transformation $U \to A$ via $\mathcal{D}U = e^{-S_{\rm Meas.}}\mathcal{D}A$. A derivation is given in [13, 14], explicit Feynman

rules are in §A. Feynman rules are needed for both the operator O and for terms in $S[U]$ but O is often of the form of a sum of paths and can be treated in exactly the same way as the action.

2.2 The Making of Lattice Feynman Rules

After picking an action the step of making the Feynman rules can be completely automated by computer. Several implementations exist in various languages by the HPQCD collaborators alone (`Fortran 77+95, C++, PHP, Python, Maple`), of which only `Maple` does native symbolic algebra as this capability is useful but not necessary.

Consider only perturbative expansions around the classical vacuum and situations when the functional integral can be performed by substituting the parallel transporter

$$U_\mu(x) = \exp\left(ig\int_x^{x+a\hat{\mu}} A(y)\cdot dy\right) \tag{2.9}$$

fixing the gauge, and expanding in a *weak* bare coupling g. The potential field $A_\mu(x)$ in (2.9) is an element of the Lie algebra of SU(N), and is associated with gluon particles. Making the mean-value approximation that $\int_0^a A\cdot y \to aA$, there is a free choice over where to site this average gluon field, conventionally the centre of the link reduces the size of the final vertex expressions and is more symmetrical. Explicitly then

$$U_\mu(x) = e^{igaA_\mu(x+\frac{1}{2}a\hat{\mu})}. \tag{2.10}$$

On a hypercubic lattice x denotes a lattice point and can be written $x = na$ for some $n \in \mathbb{Z}^4$. The gluon field has a Fourier decomposition appropriate to the

boundary conditions — in infinite volume this takes the form

$$A_\mu(x) = \$\!\!\!\!\!\!\int_{k,b} e^{ik\cdot(x+\frac{1}{2}a\hat{\mu})}\tilde{A}^b_\mu(k)T^b, \tag{2.11a}$$

where

$$\$\!\!\!\!\!\!\int_{k,b} = \sum_{b=1}^{N^2-1}\prod_\mu\left(\int_{-\pi/a}^{\pi/a}\frac{dk_\mu}{2\pi}\right), \tag{2.11b}$$

for T^b that are matrices in the fundamental of SU(N) which are the usual Gell-Mann matrices [4] for the case of interest, SU(3). The non-Abelian nature of this gluon "colour" quantum-number makes finding the Feynman rules more difficult because the path ordering matters. All the links in the chosen action e.g. (2.2c) are converted to exponentials by (2.10) and expanded to the requisite order in g and A. This takes only a few minutes for paths up to ~ 25 links long even for g^4A^6 but the storage required for the Fourier phase factors from (2.11) is then hundreds of megabytes. Finally vertex functions $V_r^{\mathcal{C}}$ at order $g^{r-2}A^r$ for a path $\mathcal{C}$ are then defined in the perturbative expansion by[1]

$$\begin{aligned} S(\mathcal{C}) = &\sum_{r=2}^{\infty}\frac{1}{r!}g_0^r\$\!\!\!\!\!\!\int_{k_1,a_1}\cdots\$\!\!\!\!\!\!\int_{k_r,a_r}\sum_{\mu_1}\cdots\sum_{\mu_r}(2\pi)^4\,\delta\left(\sum_{i=1}^r k_i\right)\\ &\times\tilde{A}^{a_1}_{\mu_1}(k_1)\cdots\tilde{A}^{a_r}_{\mu_r}(k_r)V_r^{\mathcal{C}}(k_1,a_1,\mu_1;\ldots;k_r,a_r,\mu_r) \end{aligned} \tag{2.12}$$

and requiring them to be totally symmetric under permutations of the momentum, colour and Lorentz index simultaneously

$$\sigma\cdot V_r^{\mathcal{C}} = V_r^{\mathcal{C}} \quad \forall\,\sigma\in\mathcal{P}_r, \tag{2.13}$$

where $\mathcal{P}_r$ is the group of permutation of r elements, and the action of $\sigma\in\mathcal{P}_r$ on a function F of r sets of arguments a_i is defined in the natural way by

$$(\sigma\cdot F)(a_1,\ldots,a_r) = F(a_{\sigma(1)},\ldots,a_{\sigma(r)}). \tag{2.14}$$

[1]The δ-function appearing is the periodic δ-function.

The vertices factorise into a colour dependent part in a Clebsch-Gordon coefficient C_r which only knows about the $\mathrm{Re}\,\mathrm{Tr}$ and r, the number of gluon fields, and a momentum-lorentz part $\tilde{Y}_r^{\mathcal{C}}$ that accumulates the phases from (2.11a) and so depends on the details of the path $\mathcal{C}$:

$$V_r^{\mathcal{C}}(k_1, a_1, \mu_1; \ldots; k_r, a_r, \mu_r) = \frac{1}{r!} \sum_{\sigma \in \mathbb{P}_r} \sigma \cdot C_r(a_1, \ldots, a_r)\ \sigma \cdot \tilde{Y}_r^{\mathcal{C}}(k_1, \mu_1; \ldots; k_r, \mu_r). \tag{2.15}$$

This symmetrisation has two very important consequences: first, it means that the vertices are symmetric under interchange of all the labels and the usual Feynman symmetry factors can be associated with a diagram, and second, that it actually reduces the algebra because of groupings and cancellations between the different $\tilde{Y}$ under permutation, particularly if momentum conservation at the vertex is invoked. The vertices can be only partially reduced in this manner however because the colour factors are not invariant under the full permutation group. The Clebsch-Gordon coefficients are defined by

$$C_r(a_1, \ldots, a_r) = \mathrm{Tr}(T^{a_1} \cdots T^{a_r}) + (-1)^r\, \mathrm{Tr}(T^{a_r} \cdots T^{a_1}), \tag{2.16}$$

where the $(-1)^r$ comes from the real projection operator in the action. (2.16) has simple properties under the subgroup $\mathcal{Z}_r$ of cyclic permutations and inversion. Reduced vertices $Y_r^{\mathcal{C}}$ are then found through

$$\widetilde{V}_r^{\mathcal{C}}(k_1, a_1, \mu_1; \ldots; k_r, a_r, \mu_r) = \frac{1}{r!} \sum_{\sigma \in \mathbb{P}_r / \mathcal{Z}_r} \sigma \cdot C_r(a_1, \ldots, a_r)\ \sigma \cdot Y_r^{\mathcal{C}}(k_1, \mu_1; \ldots; k_r, \mu_r), \tag{2.17}$$

where

$$Y_r^{\mathcal{C}} = \sum_{\sigma \in \mathbb{Z}_r} C(\sigma)\ \sigma \cdot \widetilde{Y}_r^{\mathcal{C}}, \tag{2.18}$$

and $C(\sigma)$ is the signature of the coefficients (2.16) under the permutation. At this stage the Y_r can be implemented as a subroutine taking an input of r-momenta and returning an r-tensor in the Lorentz indices with a sum over weighted complex exponentials of linear combinations of momenta. Finally because of the real-projection operator in the action the reduced vertices (2.17) have simple properties with respect to inversion of the momenta in the origin and can therefore always be reduced to a sum of sin's (odd-r vertices) or cos's (even r). This is not true for background fields in §2.2.4 which means that more expensive complex arithmetic must be used.

2.2.1 Gauge Fixing

Gauge fixing is necessary in lattice perturbation theory just as in the continuum. The method is basically the same with the only difference being that the Fadeev-Popov term is more complicated and there are vertices to all orders, $\overline{c}A^n c$ [13, 14]. These have a slightly tricky adjoint colour factor to work out, especially for twisted boundary conditions. This is old knowledge to a certain extent [13, 14, 15] but is explicitly written out for the first time for the vertices to the order necessary for three-loop computations in §A for periodic and twisted boundary conditions. Covariant gauge fixing on the lattice starts from

$$G^a = \partial^L_\mu A_\mu(x) \tag{2.19}$$

where ∂^L is a "left" lattice derivative $\partial^L_\mu f(x) = f(x) - f(x - a\hat{\mu})$. The gauge fixing condition (2.19) gets folded into the path integral in the usual fashion by inserting the identity for integrals over the gauge group manifold ${}^g\mathrm{A}$ which is the collection

of group parameters $A^a_\mu(x)$ which parameterise the link variables $U_\mu(x)$.

$$1 = \Delta_{FP}[U;G] \int \mathcal{D}g\ \delta\big(G - \partial^L_\mu\ {}^g\mathrm{A}_\mu\big)\,, \tag{2.20}$$

with Δ_{FP} being the famous Fadeev-Popov determinant. This is substituted into the path integral, but the determinant, action and operator being gauge invariant means that all the fields can be replaced by their gauge transforms ${}^g\mathrm{A}$ and a simple transformation of variables leaves:

$$\langle O[U]\rangle = \frac{1}{Z}\int \mathcal{D}U\ O[U]\ \Delta_{FP}[G,U]\ e^{-S[U]} \prod_{x,a} \delta\big(G^a - \partial^L_\mu\ \mathrm{A}^a_\mu(x)\big)\,. \tag{2.21}$$

The Fadeev-Popov determinant can be written as an integral over anti-commuting Grassman fields and the gauge condition can be averaged over with an arbitrary Gaussian weight factor ξ exactly as in the continuum. This must appear quadratically in the fields even on the lattice so the only dependence on the gauge parameter ξ is in the gluon propagator:

$$S_{GF} = \frac{\xi}{2}\sum_{x,a}\big(\partial^L_\mu A^a_\mu(x)\big)^2 = -\frac{\xi}{2}\sum_x A_\mu(x)\partial^R_\mu\partial^L_\nu A_\nu(x). \tag{2.22}$$

Feynman gauge corresponds to $\xi = 1$ and Landau gauge to $\xi = 0$. The ghost contribution to the action is then

$$S_{FP}[A,c,\overline{c}] = -\sum_x \overline{c}^A(x)\partial^L_\mu D^{AB}_\mu c^B(x). \tag{2.23}$$

D_μ is a local operator defined in (A.51) containing arbitrary powers of gA. The three-gluon – ghost vertex vanishes but all other $\overline{c}(gA)^n c$ vertices exist in lattice perturbation theory. Feynman rules are given in figure A.1.

2.2.2 Quark Rules

The continuum quark action contains only a first derivative in time — this gives the Fermi-Dirac statistics and makes the fields in the path integral's Grassman

which causes huge problems for lattice simulations. However quarks are relatively easy to handle in perturbation theory and this does not change much on the lattice. In particular the divergence from quark lines is only one power of the momenta, $1/p$ rather than two for the gluon or ghost lines and these means that the integrals are easier to handle numerically.

The simple quark formalisms can be encompassed by the Euclidean action

$$S = \sum_{\text{Flavour}} \left[\overline{\psi} \left(\gamma \cdot \Delta + m \right) \psi - \frac{r}{2} \overline{\psi} \Delta^{(2)} \psi + \frac{i}{4} c_{SW} \overline{\psi} \sigma_{\mu\nu} F_{\mu\nu} \psi \right], \tag{2.24a}$$

where

$$\Delta_\mu^{(1)} \psi(x) \equiv \frac{1}{2au_0} \Big[U_\mu(x) \psi(x + a_\mu) - U_\mu^\dagger(x - a_\mu) \psi(x - a_\mu) \Big], \tag{2.24b}$$

$$\Delta_\mu^{(2)} \psi(x) \equiv \frac{1}{au_0} \Big[U_\mu(x) \psi(x + a_\mu) + U_\mu^\dagger(x - a_\mu) \psi(x - a_\mu) \Big] - 2\psi(x), \tag{2.24c}$$

are gauge invariant first and second lattice derivatives of spinors and

$$F_{\mu\nu} \equiv \frac{1}{8} (Q_{\mu\nu} - Q_{\nu\mu}), \quad Q_{\mu\nu} = P_{\mu,\nu} + P_{\nu,-\mu} + P_{-\mu,-\nu} + P_{-\nu,\mu}, \tag{2.24d}$$

is the lattice chromo-electromagnetic field strength and the $\sigma \cdot F$ term is known as the Sheikholeslami-Wohlert Clover term [16]. The $P_{\mu,\nu} = U_\mu U_\nu U_\mu^\dagger U_\nu^\dagger$ are plaquettes. This action is widely known as the Wilson action when $c_{SW} = 0, r = 1$, which is free of doublers but has $\mathcal{O}(a)$ errors, and is known as Clover when $c_{SW} \neq 0, r = 1$, which removes $\mathcal{O}(a)$ errors for an appropriate choice of c_{SW}. The Naïve action for which $c_{SW} = r = 0$ has doublers unless it is implemented in simulation as a "staggered" action.

The unstaggered action (2.24a) poses little additional problem for perturbative calculations for any value of the parameters. It is expressed as a sum of paths connecting quark spinors which are easily added to the vertex generation program

via their Fourier decomposition:

$$\begin{aligned}\Psi_\beta(x) &= \sum_{a=1}^{N}\prod_\mu\left(\int_{-\pi/a}^{\pi/a}\frac{dp_\mu}{2\pi}\right)\; e^{ip\cdot x}\widetilde{\Psi}^a_\beta(p)\\ \overline{\Psi}_\alpha(x) &= \sum_{a=1}^{N}\prod_\mu\left(\int_{-\pi/a}^{\pi/a}\frac{dp_\mu}{2\pi}\right)\; e^{\mp ip\cdot x}\widetilde{\overline{\Psi}}^a_\alpha(p),\end{aligned} \tag{2.25}$$

appropriate for an infinite volume. This contrasts with (2.11) for the gluon fields which carry adjoint colour instead and no 4-spinor index like α or β, but must be extended to (A.38) for twisted quarks. The choice of sign is given in the anti-quark field in order to allow Feynman rules with the convention of a leaving anti-quark momentum (upper-sign), or those for which all fields are ingoing (lower-sign). Having all fields do the same thing is slightly simpler when automatically generating the diagrams á la §2.3, but is less conventional. Feynman rules for Wilson quarks are given in figure A.1.

For improved staggered the Feynman rules are hundreds of times larger because there are 4×79 separate paths which replace 4×1, all smearing the basic $\overline{\psi}U_\mu\psi$. Those paths are up to 7 links long [7]:

$$\mathcal{S} = \sum_x \overline{\psi}(x)\,\left(\gamma\cdot\Delta' - \frac{a^2}{6}\gamma\cdot\Delta^3 + m\right)\,\psi(x) \tag{2.26a}$$

where

$$\Delta_\mu\,\psi(x) \equiv \frac{1}{2au_0}\left(U_\mu(x)\,\psi(x+a\hat{\mu})\; -U^\dagger_\mu(x-a\hat{\mu})\,\psi(x-a\hat{\mu})\right).$$

and Δ'_μ is $U\to V'$ in Δ, where

$$V'_\mu(x) = \left\{\prod_{\rho\neq\mu}\left(1+\frac{a^2\,\Delta^{(2)}_\rho}{4}\right)\Bigg|_{\text{symm.}} - \sum_{\rho\neq\mu}\frac{a^2(\Delta_\rho)^2}{4}\right\}U_\mu(x). \tag{2.26b}$$

The cubed-derivative in (2.26a) is the Naik term [17] and together with the symmetrised "Fat7" smearing (see figure 3.3) and Lepage term in (2.26b) make the errors in this action as small as $\mathcal{O}(a^4, a^2\alpha_s)$ (3.11), but the Feynman rules huge!

2.2.3 Staggered Quarks

The improved action (2.26) or the naïve action (2.24a) with $R = c_{SW} = 0$ still suffer from the famous "doubling" problem. The Wilson and Clover actions have added an irrelevant operator that lifts the energies of the doublers and breaks the Chiral symmetry which is responsible for keeping the quarks massless; these actions require an additive mass renormalisation as well as the usual multiplicative one. In simulations the non-perturbative quark-mass that results in "massless" quarks must be expensively tuned. The solution for the other actions is called "staggering". The naïve quark action has an exact "doubling" symmetry under the transformation:

$$\psi(x) \to \widetilde{\psi}(x) \equiv (i\gamma_5\gamma_\rho)(-1)^{x_\rho}\psi(x), \tag{2.27}$$

which means that any small energy-momentum quark mode in the theory is equivalent to another mode with momentum $p_\rho \approx \pi/a$. This new mode is one of the doublers of the naïve quark action. The transformation can be generalised to several directions at once

$$\psi(x) \to \mathcal{B}_\zeta(x)\psi(x) \quad \overline{\psi}(x) \to \overline{\psi}(x)\mathcal{B}^\dagger_\zeta(x) \tag{2.28a}$$

where

$$\mathcal{B}_\zeta(x) \equiv \prod_\rho (i\gamma_5\gamma_\rho)^{\zeta_\rho} e^{ix\cdot\zeta\pi}, \tag{2.28b}$$

for ζ one of the 16 fourvectors with components zero or one. There is one null transformation with $\zeta = 0$ and consequently 15 doubling copies of the original quark that can be boosted across the Brillouin zone into each other by applying (2.28). These can be interpreted as sixteen equivalent flavours of quark, significantly more than desired.

Staggering actions involves a transformation step; consider the field redefinition

$$\psi(x) \to \Omega(x)\chi(x) \quad \overline{\psi}(x) \to \overline{\chi}(x)\Omega^\dagger(x) \tag{2.29}$$

into four-spinors χ, where

$$\Omega(x) \equiv \prod_\mu (\gamma_\mu)^{x_\mu}. \tag{2.30}$$

Using the fact that $\gamma^2 = 1$, it is easy to see that there are only $\{0,1\}^4 = 16$ distinct Ω's, and that they are related to the boost operator (2.28). Some algebra reveals that

$$\eta_\mu(x) \equiv \Omega^\dagger(x)\gamma_\mu\Omega(x \pm \hat{\mu}) = (-1)^{x_0+x_1+\cdots x_{\mu-1}} \tag{2.31}$$

$$1 = \Omega^\dagger(x)\Omega(x) \tag{2.32}$$

and therefore the naïve quark action becomes

$$\overline{\psi}(x)\left(\gamma\cdot\Delta + m\right)\psi(x) = \overline{\chi}(x)\left(\eta(x)\cdot\Delta(x) + m\right)\chi(x) \tag{2.33}$$

which is diagonal as it has no spinor structure! Staggered simulations throw away all but one of the four equivalent components to leave $16/4 = 4$ copies of the original quark. These copies are called "tastes" to distinguish them from the 3 different flavours of original light quarks. The tastes are done away with in simulations using the "$\sqrt{\ }$" trick. The Grassman fields cannot be represented on a computer so the quark dependence is converted into a determinant for each light quark flavour in the reverse of the Fadeev-Popov method for ghosts:

$$\det(M) = e^{-\operatorname{Tr}\ln\overline{\psi}M\psi}, \tag{2.34}$$

$$S \to S_{\text{eff}} = S_{\text{glue}} - \sum_{\text{flavour}} \ln\det M[U] \tag{2.35}$$

The trick is to quarter or halve the number of equivalent light quark tastes in M so that there are either one or two remaining real flavours of light quark by taking the fourth-root or square root of the determinant. It is clear that perturbatively this $\sqrt[4]{\ }$ step amounts to simply replacing $n_f \to \frac{1}{4}n_f$ in the action. There is still much debate as to whether there are any harmful effects in a quantum theory that does this [18], though there is no hard evidence that there any.

In terms of momentum-space perturbation theory the Fourier-transform of the staggered action (2.33) is a disaster:

$$S_{\text{stag.}} = \int_{-\pi}^{\pi} \frac{d^4p}{(2\pi)^4} \int_{-\pi}^{\pi} \frac{d^4p'}{(2\pi)^4} \widetilde{\overline{\chi}}(p') M(p',p) \chi(p), \tag{2.36}$$

$$M(p',p) = (2\pi)^4 \left\{ \sum_{\mu} \delta^{(4)}\left(p' + p + \delta^{(\mu)}\right) i \sin p_\mu + m\delta^{(4)}(p'+p) \right\}, \tag{2.37}$$

where the position dependence of the phase $\eta(x)$ has translated into an action that does not have momentum conservation! The $\delta^{(\mu)}$ come from $\eta_\mu(x) = e^{ix\cdot\delta^{(\mu)}}$, where

$$\begin{aligned} \delta^{(0)} &= (0,0,0,0) \qquad & \delta^{(1)} &= (\pi,0,0,0) \\ \delta^{(2)} &= (\pi,\pi,0,0) \qquad & \delta^{(3)} &= (\pi,\pi,\pi,0). \end{aligned} \tag{2.38}$$

The continuum trace over spinors has been replaced by a sum over these momentum fragments $\delta^{(\mu)}$ which is a much harder book-keeping exercise in anything but one-loop diagrams. Consequently perturbation theory for staggered quarks is done completely "unstaggered" and the quark loops are divided by 16 to account for the degenerate quarks running around. At one and two loops the correct n_f dependence of the universal constants of the β-function, β_0 and β_1, is only obtained after dividing by this factor. Transformations on the momentum must respect this sixteen-fold symmetry: integrands that usually have a divergence only at $p = 0$ will also exhibit problems in the other corners of the Brillouin zone. Calculations with external staggered quark-lines get messy, one example being §3.

Staggered quarks also suffer from "taste-changing" effects which are discussed in §3. These make significant contributions to perturbative series even at first order rendering them unconvergent. The basic problem is that the quark is on-shell (becoming another taste) after emitting an $\mathcal{O}(\pi/a)$ momentum gluon as shown in figure 2.1. The hard gluon makes the two quark interactions almost a four-

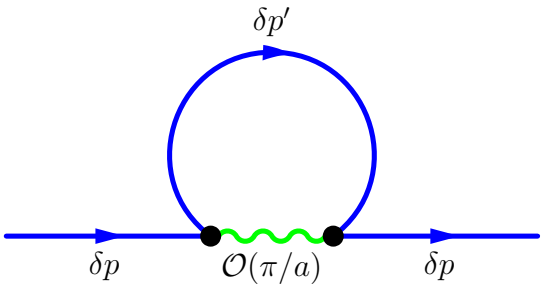

Figure 2.1: A quark tadpole that dominates quark diagrams for unimproved staggered quarks.

quark operator because of its extremely high momentum, and the soft quark loop looks like a tadpole. This type of contribution was virtually eliminated by the Fat7 smearing in improved staggered which strongly suppresses the vertices for the emission of large gluon momenta.

2.2.4 Background Field Rules

Background fields are a secondary expansion of the potential A around a fixed "classical" or external background value B: $gA \to B + gA$, where the new A is again a quantum field that can go around in internal loops, but the B is classical and therefore does not have any internal loops. The so-called "Background Field Gauge" $G^a = \partial_\mu A^a_\mu + igf^a_{bc}A^b_\mu B^c_\mu$ (cf. (2.19)) is imposed on the background fields so that explicit gauge invariance at the *quantum* level is retained. This severely

limits possible renormalisations. The gauge for the quantum fields is fixed by the $B \to 0$ limit of the background field gauge and the usual Feynman gauge can be retained even on the lattice (2.19), (2.41). When considering background n-point vertices for example the quantum fields A, ψ and c do not need wavefunction renormalisations as they only occur in loops §5.1.

On the lattice a linear substitution of background and quantum fields does not have sensible gauge transformations so an analogous expansion to (2.10) is performed:

$$U_\mu(x) \equiv U_\mu^{(Q)}(x)\, U_\mu^{(B)}(x) = e^{igaA_\mu} e^{iaB_\mu}, \tag{2.39}$$

where the exponentiated fields live at the centre of the link. The quantum and background fields then have their own separate colours which must be tracked and the number of independent colours and hence momentum-dependent contributions to each Feynman rule increases dramatically. These different contributions can not be obtained from one tensor by permutation of the arguments and must be computed separately. This is particularly true for background-gluon-quark vertices because there are no symmetrisations allowed and the largest set of vertices needed for two-loop calculations: $\overline{\psi}B^2A^2\psi$, have very different rules for $\overline{\psi}BBAA\psi$, $\overline{\psi}BABA\psi$, $\overline{\psi}BAAB\psi$, $\overline{\psi}ABBA\psi$, $\overline{\psi}ABAB\psi$ and $\overline{\psi}AABB\psi$. Once these are all tabulated along with their different colour factors they can be incorporated into the automatic diagram generation very easily. The nice properties of the pure-gluon action under inversion through the origin in momentum-space are lost and the background-gluon vertices contain expensive complex exponentials. The background gauge fixing is via

$$S_{BGF} = -\frac{1}{\xi} \operatorname{Tr} \left(D_\mu^{(-)} A_\mu \right)^2 \tag{2.40}$$

where [19]

$$D_\mu^{(-)} A_\mu(x) = A_\mu(x) - e^{-iB_\mu(x-a\hat{\mu})} A_\mu(x-a\hat{\mu}) e^{+iB_\mu(x-a\hat{\mu})}. \tag{2.41}$$

The background gauge-fixing term is invariant under background field gauge transformations

$$\begin{aligned} U_\mu^{(Q)}(x) &\to \Lambda(x)\, U_\mu^{(Q)}(x)\, \Lambda^\dagger(x) \\ U_\mu^{(B)}(x) &\to \Lambda(x)\, U_\mu^{(B)}(x)\, \Lambda^\dagger(x+a\hat{\mu}) \end{aligned} \tag{2.42}$$

which also leaves the gauge-field action invariant since it amounts to the standard transformation of the total link

$$U_\mu(x) = U_\mu^{(Q)}(x)\, U_\mu^{(B)}(x) \to \Lambda(x)\, U_\mu^{(Q)}(x)\, U_\mu^{(B)}(x)\, \Lambda^\dagger(x+a\hat{\mu}). \tag{2.43}$$

Many background-gluon vertices now depend on the gauge parameter through the exponentials in (2.41) and the gauge parameter must also be renormalised to one loop get the full background 2-point function in §5.1. Finally the ghost action in the presence of background fields is modified to

$$S_{BFP} = \overline{c} \left\{ \frac{\delta}{\delta\omega} D_\mu^{(-)} A \right\} c, \tag{2.44}$$

where $\delta\omega^a$ parameterises an infinitesimal *quantum*-field gauge transformation

$$e^{igaA_\mu(x)} \to \Lambda(x) e^{igaA_\mu(x)} e^{iaB_\mu(x)} \Lambda^\dagger(x+a\hat{\mu}) e^{-iaB_\mu(x)} \tag{2.45}$$

for infinitesimal gauge transformations $\Lambda(x) \equiv e^{\delta\omega(x)} \approx 1 + \delta\omega(x)$. The details are messy but a few of the lower order Feynman rules are given in [20] and in the continuum by [21]. Together (2.44) and (2.45) show that background-gluon-ghost vertices exist to all orders.

2.2.5 Complexity

The number of exponentials in the Feynman rule expanding to order A^r a path of l links can be strictly bounded by [13]

$$n_{r,l} \leq 2\frac{lr}{l+r}\binom{l+r}{r}, \tag{2.46}$$

which is the number of terms generated by the algorithm. However there are usually far fewer because of cancellations. The growth in terms is factorial which should be compared to the continuum where it is zero (no irrelevant operators). For example looking at the six-point vertex from the plaquette (4-links) which has no continuum analogue, (2.46) predicts $n_{6,4} \leq 1008$; it turns out that there are only 390 terms. There are 6 plaquettes in the Wilson gauge action for a total of 2340 cos's. In the improved action there are a further 12 Rectangles (of length 6) and there the total number of cos's is much higher at $31,632$. Both actions have about 40% of the total theoretical number of terms. The pure gluon action is relatively simple but it is clear that when improved a hand-calculation would be very laborious and prone to error. The number of momenta appearing in each trigonometry function in the vertex can be optimally reduced by invoking momentum conservation and translation invariance. Unfortunately for third order computations where this six-point g^4A^6 vertex is needed the quotient $\mathbb{P}_r \Big/ \mathcal{Z}_r$ from (2.14) has 60 members. This complicated momentum dependent tensor of 6 Lorentz indices has ~ 360 of the possible $4^6 = 4096$ entries non-zero, each with approximately 8 cos's for the unimproved action (2340 total) and 100 for the improved action (31,632 total). This behemoth must be evaluated 60 times with permuted arguments and different colour weights. Fortunately this vertex is a "lattice vertex" and occurs only in lattice diagrams with no IR divergences; the

integrand although complicated and expensive to evaluate is very well behaved.

The improved quark action (2.26) is significantly more complicated than the unimproved one (2.24a), and its Feynman rules are hundreds of times bigger. Unfortunately the quark and background vertices also have a reduced symmetry group under which they are invariant in (2.14) that can be summed over in (2.17), so there (2.46) is up to $(r-1)!/2$ times larger. The largest vertex by far is $\overline{\psi}B^2A^2\psi$ which includes all of $\overline{\psi}BBAA\psi, \overline{\psi}BABA\psi, \overline{\psi}BAAB\psi, \overline{\psi}ABBA\psi, \overline{\psi}ABAB\psi$ and $\overline{\psi}AABB\psi$. For quarks the invariant symmetry group in (2.14) is zero, but the permuted versions of $\overline{\psi}A^4\psi$ can be obtained by calling one vertex rule several times with permuted arguments each weighted by the different colour factor to turn the vertex into a proper Feynman rule. When background fields are also introduced vertices such as $\overline{\psi}B^2A^2\psi$, even this small simplification is broken and those six independent vertices must be determined and each called four times under $B_1 \leftrightarrow B_2$ and $A_1 \leftrightarrow A_2$. This is easily automated however. For the most expensive diagrams or the largest vertices that are only used in one or two Feynman diagrams it is possible to simplify this procedure by two methods: computing the vertex-rule with tied-momenta and pre-computing the colour weights and hence reducing the size of the tables. For example with $\overline{\psi}B^2A^2\psi$, it only occurs in one diagram with the quark and gluon fields in tadpoles so there are really only 3 independent momenta not 6 – this reduces the vertex considerably, but it is still $\sim$ 7Mb of text with 113,430 trigonometry functions (about 5$\times$ more text than Kurt Gottfried's [8] new 650 page textbook).

However it is interesting to note that most of the computer time spent on integrating Feynman diagrams is actually spent on the Lorentz sum and *not* on the evaluation of the vertices for all but the largest. The performance of the method

sketched in the following section is roughly the same for unimproved gluon actions (without assuming that the propagator is diagonal) and improved gluon actions for Lorentz dominated diagrams. Note that for analytic methods this is definitely not the case. Improved staggered quarks do add some penalty because of their huge Feynman rules, Clover fermions have a large spinor-trace penalty (4 Clover vertices connected by 4 propagators has 600,000 non-zero terms in the trace), but in general quark diagrams are less divergent than the equivalent ghost or gluon diagrams and have smaller errors.

2.3 A Guide to Automatic Diagram Generation

As a matter of convenience, but also the reduction in mistakes and human time it is desirable to automate the generation of diagrams into runnable code. In the α_s calculation presented in §5, 139 diagrams are evaluated with four different actions. The method of evaluation should be as action-agnostic as possible in order that new actions can be experimented with and expensive human time spent in optimisation and bug-fixing be reduced. Computer time is relatively cheap now, $\sim 1\$\Big/\text{MFlop}$ [18], so some leeway on simple to maintain unoptimised code that is bug-free is easily tolerated. With these goals in mind and the fact that an analytic expansion and reduction of the integrands of improved actions is prohibitively difficult §2.2.5, a naïve approach is taken. The vertices are evaluated at a given set of momenta into tensors of Lorentz indices and spinors. Diagrams are written out as sums over contracted tensors and the integrand is evaluated by adaptive Monte-Carlo with the program `VEGAS` [22,23].[2] This returns a Monte-Carlo statistical error

[2] A collaboration with Ron Horgan and Peter Lepage parallelised the `Fortran` implementation with `MPI`, the Message Passing Interface.

that decreases as the square-root of the number of integrand evaluations, hence CPU-time. The algorithm projects the integrand onto each axis and adapts by stratified importance sampling. The program works hard to minimise the cost of high-dimensional integrals and works most efficiently when the axes are suitably chosen for the shape of the integrand; pathological examples where e.g. there is a line singularity in the sum of a few variables are much harder to adapt to using this algorithm. A transformation of variables will easily rectify this situation and the accompanying Jacobian can be arranged to reduce the importance of any peaks. In particular, switching to a spherical co-ordinate system is often orders-of-magnitude more efficient than Cartesian.

To generate all the diagrams for a given expectation operator at a certain order a very simple algorithm can be used:

1. For each vertex in the expectation operator find all possible sets of vertices from the action for which the total order is correct, and compute the base weight for each set. A Feynman rule with r-identical legs appears in the action with a factor of $\frac{1}{r!}$.

   E.g. $\langle \frac{1}{3} \operatorname{Re} \operatorname{Tr} U_{\square} \rangle$, the expectation of the plaquette at $\mathcal{O}(\alpha_s^3)$ could contain a diagram made from the 2-point from the expectation, $\frac{1}{1!}$`E2` at $\mathcal{O}(g^2)$ and 2 copies of the three-point vertex from the action, $\frac{1}{3!}$`A3` at $\mathcal{O}(g)$ and two copies of the one-gluon–quark vertex, $\frac{1}{1!}$`G1Q2` at $\mathcal{O}(g)$ for a total of $\frac{1}{1!(2!3!3!)(2!1!1!)} g^6 = \frac{1}{144} g^6$.

2. For each: form the product substituting unknown momenta $\{k_i\}$, Lorentz indices $\{\mu_i\}$, colours $\{B_i; b_i\}$ and spinors $\{Z, Y, \ldots; \alpha_i\}$ where i denotes which

field the index comes from. E.g.

$$\begin{aligned}\text{Diag} = {} & \texttt{E2}(k_1, k_2; \mu_1, \mu_2)\, \texttt{A3\_1}(k_3, k_4, k_5; \mu_3, \mu_4, \mu_5)\, \texttt{A3\_2}(k_6, k_7, k_8; \mu_6, \mu_7, \mu_8) \\ & \times \texttt{G1Q2\_1}(k_9, k_{10}, k_{11}; \mu_9; \gamma^Z_{\alpha_{10},\alpha_{11}})\, \texttt{G1Q2\_2}(k_{12}, k_{13}, k_{14}; \mu_{12}; \gamma^Y_{\alpha_{13},\alpha_{14}}) \\ & \times \texttt{E2\_colour}(B_1, B_2)\, \texttt{A3\_colour}(B_3, B_4, B_5)\, \texttt{A3\_colour}(B_6, B_7, B_8) \\ & \times \texttt{G1Q2\_colour}(B_9, b_{10}, b_{11})\, \texttt{G2Q2\_colour}(B_{12}, b_{13}, b_{14}). \end{aligned} \tag{2.47}$$

3. Contract like fields together. Contracting n-fields gives $(n-1)!!$ terms. E.g. for 10 gluon fields and 4 quark fields there are 9!!×4!!=945×3 possible contractions.

4. For each possible contraction: add propagators to a local copy of (2.47) and implement the delta-functions in momentum, colour and spinors. E.g.

$$\langle \underbrace{A^B_\mu(k_1)}\, A^C_\nu(k_2)\rangle = \texttt{Gluon\_Propagator}(k_2; \mu, \nu)\ \ \delta^4_{(2\pi)}(k_1 + k_2)\delta^{BC} \tag{2.48}$$

where the overall volume factor, which depends on the boundary conditions, only needs the number of integrated momenta is best added at the end. The 4-dimensional Dirac delta-function is defined modulo 2π but as every vertex is equivalent under momentum translations of 2π this restriction is not important and one momentum can be eliminated by substituting $k_1 = -k_2$ everywhere. A second copy of the colour factor can be retained for use with twisted boundary conditions §2.4, §A, where the colour functions depend on the momentum not on separate colour indices. It is advantageous to somehow store the fact that μ and ν are connected in this gluon propagator because unimproved Wilson glue is diagonal in Feynman gauge (2.7), (like the continuum) and it is a simple but effective optimisation to choose this

gauge and exploit this feature. Using (2.48) in the example:

$$\begin{aligned}\text{Diag}_1 &= A^1_{E2}(k_1)\,\overbrace{A^2_{E2}(k_2)\quad A^3_{A3_1}(k_3)\,A^4_{A3_1}(k_4)}\,A^5_{A3_1}(k_5)\quad\ldots\\ &= \texttt{E2}(k_1,k_2;\mu_1,\mu_2)\,\texttt{A3\_1}(k_3,k_4,\texttt{-}\mathbf{k_2};\mu_3,\mu_4,\mu_5)\ \ldots\\ &\quad\times\texttt{Gluon\_Propagator}(k_2;\mu_2,\mu_5)\\ &\quad\times\texttt{E2\_colour}(B_1,B_2)\,\texttt{A3\_colour}(B_3,B_4,\mathbf{B_2})\ \ldots\end{aligned}$$

5. Compute Grassman factor for quarks and ghosts separately by either counting loops (a hard problem in mathematical graphing theory), or commute through to normal form. E.g.

$$\begin{aligned}&=\ldots\,\overbrace{\overline{\psi}^{\alpha_{10}}_{G1Q2_1}(k_{10})\,\gamma^Z_{\alpha_{10}\alpha_{11}}\,\overbrace{\psi^{\alpha_{11}}_{G1Q2_1}(k_{11})\quad\overline{\psi}^{\alpha_{11}}_{G1Q2_2}(-k_{11})}\,\gamma^Y_{\alpha_{11}\alpha_{10}}\,\psi^{\alpha_{10}}_{G1Q2_2}(-k_{10})}\ldots\\ &=\ldots\,(-1)\,\text{Tr}\left[\gamma^Y\,\overbrace{\psi_{G1Q2_2}(-k_{10})\,\overline{\psi}_{G1Q2_1}(k_{10})}\,\gamma^Z\,\overbrace{\psi_{G1Q2_1}(k_{11})\,\overline{\psi}_{G1Q2_2}(-k_{11})}\right]\end{aligned}$$

6. Implement momentum conservation at each vertex. This is easiest with a symbolic algebra system like `Maple` or `Mathematica`.

7. Reject diagram if it is:

   (a) Not 1PI (these would be removed in the path integral by the $\frac{1}{Z}$ factor as usual). Detect this because an internal propagator has a single external momentum flowing through it.

   (b) Disconnected. Detect through wrong number of independent momenta or a propagator with $p = 0$. E.g. of the other two fermion contractions one is illegal ($\overline{\psi}\overline{\psi}\psi\psi$) and the other is disconnected ($\overline{\psi}\psi\,\overline{\psi}\psi$), shown in figure 2.2. There are many more diagrams disconnected because of the gluon contractions.

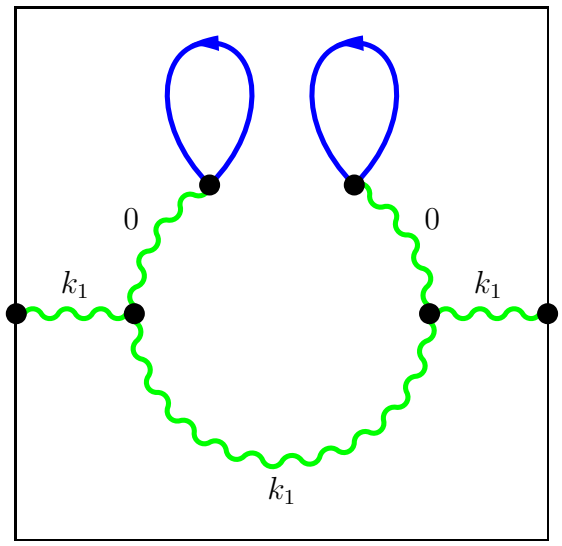

Figure 2.2: A disconnected diagram that can be very easily caught because it fails both criterion. It has four propagators with momenta of 0, one internal propagator with an "external" momenta from the expectation operator (not 1PI) and only one independent momenta, k_1, not three.

8. Add this to the final table with the base weight calculated in step (1.) multiplied by the quark and ghost Grassman factor. The quark trace and colour factor can be stored and pre-computed separately, and the newly minted diagram can be associated with a tag that lists the directions of all the propagators. This way the symmetry factors can be built up by merely adding up the factors for the unique tags. If more than one copy of a vertex is present (e.g. the example has $\texttt{A3}^2$) then check all the permutations of re-labellings to reduce the number of unique tags.

E.g. a "uniqueness" tag for the example, shown in figure 2.3, is

$$\begin{aligned}
&\texttt{GP}\Big(\{\texttt{E2},\texttt{A3_1}\}\Big)\ \texttt{GP}\Big(\{\texttt{E2},\texttt{A3_2}\}\Big)\\
&\times\texttt{GP}\Big(\{\texttt{A3_1},\texttt{A3_2}\}\Big)\ \texttt{GP}\Big(\{\texttt{A3_1},\texttt{G1Q2_1}\}\Big)\ \texttt{GP}\Big(\{\texttt{A3_2},\texttt{G1Q2_2}\}\Big)\\
&\times\texttt{QP}\Big([\texttt{G1Q2_1},\texttt{G1Q2_2}]\Big)\ \texttt{QP}\Big([\texttt{G1Q2_2},\texttt{G1Q2_1}]\Big)
\end{aligned}\tag{2.49}$$

where a set $\{\ldots\}$ is not ordered, but a list $[\ldots]$ is.

Finally for the example, this selection of vertices makes only one diagram and automatically found the continuum symmetry factor of -1, but had the quark fields also been gluons then there would also have been another diagram (often called the "eye" diagram). The non-1PI diagram made from a quark bubble followed by a gluon bubble is also discarded. The symmetry factors can also be done by hand using the usual rules from the continuum. The increase in the number of diagrams on the lattice, particularly involving more lines meeting at vertices means that there are more complicated symmetry cases that are harder to reliably compute without error.

There are only minor complications: over Feynman rules which are counter-terms (simply reduce the number of independent momenta expected), those which have many colour $\times$ vertex combinations (just be more careful) and prettying the output (substitute all the independent variables with high field-tags with the lowest ones e.g. $\{k_1, k_2, k_{10}\} \to \{k_1, k_2, k_3\}$). The very readable `C++` automatically generated for the example diagram is listed in §B, which is easily adapted to any boundary conditions or even to derivatives of the diagram with respect to coefficients in the action or to the external momenta. The code can be linked to any library that exports the necassary vertices: it is completely action agnostic.

Other programs [24, 25, 26, 27] for automating diagram generation exist but

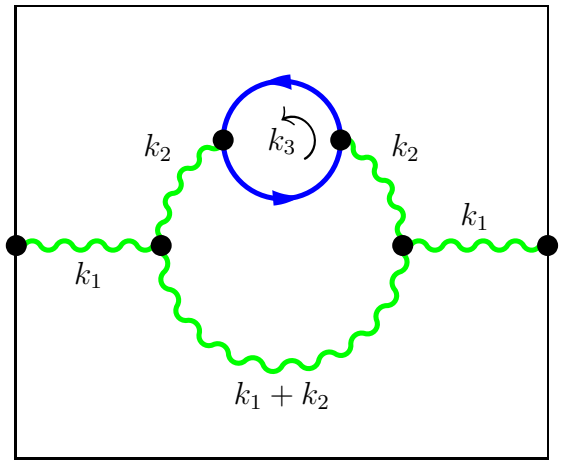

Figure 2.3: The Feynman diagram for the example being "automatically" generated. It can be tagged by (2.49), and has a final symmetry factor of -144/144=-1 just like the continuum.

currently none work well for lattice vertices; either higher order (A^5, $\overline{c}A^4c$) or those with Feynman rules made up from many colour-vertex combinations. FeynArts/FeynCalc [25] are written in `Mathematica` and QGRAF is in `Fortran+Form`, but both use a topology-based approach that does not work as easily for lattice diagrams (or vacuum loops §5.2). They do not know about lattice operators or their possible expansion in gA, but probably scale to higher loops and work for a much larger class of theories. The Euclidean metric of lattice perturbation theory combined with lack of Lorentz invariance introduces another problem: the Einstein summation convention does not apply. In the continuum indices appear only twice in every expression, whereas on the lattice several pieces may involve the same index e.g. $\hat{k}_\mu\hat{k}_\nu(1-\hat{k}_\mu^2)^2A_\mu\delta_{\mu\nu}$. On the lattice the convention is more general — *repeated* indices have an implied summation — this currently breaks all of the non-lattice specific packages, particularly those using substitution rules in `Mathematica` which rely on there being only two copies of each index in the pattern

matching. This happens a lot with Kronecker deltas which are used in computing traces, colour factors and writing out diagrams. Fixing this would require major re-writing.

2.4 Boundary Conditions, Divergences and Tricks

The lattice provides the UV cutoff so lattice integrals are UV finite, however the IR is not completely regulated by the quantised momenta. The zero-mode is numerically divergent and dropping it and taking the limit $L \to \infty$ is very difficult at more than one-loop. The numerator *and* denominator can vanish simultaneously for linear combinations of momenta and l'Hôpital's rule is very hard to implement numerically. In fact the zero-mode turns out to be of the non-Gaussian form e^{-A^4} and is important for numerical simulations in the perturbative phase (High Beta Method) [28, 29]. In the IR domain lattice integrands are identical to continuum ones and an alternative but not as yet very accurate method for lattice PT heavily exploits this fact [30, 31, 32]. For this reason the lattice shares all of the continuum IR regulators: quark masses, external momenta etc. The IR divergent diagrams are only those with a continuum analogue, which eliminates all diagrams with lattice-only "irrelevant" vertices. On the lattice with numerical evaluation of the individual diagrams internal subtractions of 1PI sub-diagrams (one-loop renormalisations of a propagator at lower order) in 2PI diagrams at *their* zero external momenta, where the sum of the divergent subtractions must vanish by gauge invariance of a massless gluon propagator is very useful. Similarly for quark propagators but here the cancellation must include an insertion of the known one-loop quark mass renormalisation. Quark actions with broken chiral symmetry, namely Wilson and Clover have an additive mass-renormalisation that must be incorporated even

for initially massless quarks. Typically these 2PI diagrams can account for $\sim \frac{1}{3}$ of the diagrams in a high-loop process, so making them IR finite with this simple technique is a big step.

The IR divergences are shared with the continuum; typically the known IR divergence at leading order in the $\frac{1}{\epsilon}$ expansion of the $\overline{\text{MS}}$ scheme agrees with the logarithmic divergence on the lattice at leading order, if done in the same gauge. The sub-leading divergences which combine one or more soft momenta with at least one hard momenta are usually not shared with the continuum because the hard-scale physics is different. Similar techniques to the continuum are in principle possible to extract the both the leading and sub-leading logarithms diagram by diagram but must instead be done numerically on the lattice point-by-point if the analytical expression is too unwieldy. This kind of ad-hoc human intervention is a large source of mistakes — so this very tricky step can be avoided by using twisted boundary conditions or evaluating at several points and fitting the logarithms.

2.4.1 Twisted Life

Twisted boundary conditions [13] add a minimal overhead to finite periodic calculations yet provide a gauge invariant gluon mass to all orders.[3] The details are relegated to appendix A, but the summary story is that by introducing a periodic SU(N) twist in $d : 2 \leq d \leq 4$ directions the effective volume is increased by a factor of N^d and so the possible number of gluon momenta are increased by N^d. The usual "colour" index of the gluons is replaced by these additional momenta that are at $\frac{2\pi}{L}\frac{1}{N}$ shifts from the original quantised momenta. Various conditions

[3]They have also been used in the continuum [9,33,34] in compact Dimensional Regularisation on a torus where they are rather more difficult than the usual methods, but are needed to match the lattice calculation for an IR divergent quantity.

reduce the plurality and allow just $N^2 - 1$ for each gluon field and in each propagator which neatly explains where the degrees of freedom went. The usual colour factors are hidden in complex momentum-dependent phases associated with the propagators and vertices but which are easier to evaluate than the usual traces of Gell-Mann matrices. The most-important feature is that the zero-mode is eliminated and the twisted-gluons receive a mass of approximately $2\pi/NL$ (it varies in direction) imposed by the minimal momenta in the twisted dimensions. The gluon mass serves as the regulator in the IR by adding a new scale which is simply fit and extrapolated away *a posteri*, however it can complicate the analysis of diagrams with multiple scales e.g. masses, and means that matching to the continuum IR can be more difficult.

2.5 Re-Organising Results to Converge

QCD is an asymptotic theory — the expectation of an operator has a formal power series that converges only asymptotically. Practically this means that the total contribution of each successive term decreases for a while and then increases without bound. Only the sum of the full infinite series gives the correct answer — the radius of convergence is zero. The problem is that in general we only know a finite but small number of terms in any perturbative series. Non-perturbative contributions to physical quantities, of which the classic example is e^{-1/g^2} are also expected, but have no Taylor expansion in the coupling. There is therefore a limit to the contribution of perturbation theory for which the signal is that the value of the last term is bigger than the previous one. At this stage the procedure is to chop the series at its smallest term, taking the next as an estimate of systematic error.

Before that point is reached however there are several important tricks that improve the convergence of perturbation theory toward the correct all-orders answer. Although any definition for the expansion parameter in an infinite series is equally valid, some choices when only a finite number of terms are known will converge faster than others. For example if an expansion parameter $\alpha_{\rm good}$ is well-behaved in a variety of cases then $\alpha_{\rm bad} \equiv \alpha_{\rm good}\,(1 - 10,000\alpha_{\rm good})$ will lead to second-order coefficients of size $\sim 10,000$ and mislead any comparison to data. Lepage [5] diagnosed the problem and showed that the bare lattice coupling was one such poor choice. To define an improved expansion parameter a new definition of the running coupling $\alpha_s(q)$ must be chosen to fix the scheme and a procedure for setting the scale q of the coupling must be established. Lepage suggested using a physical quantity to set the scheme which would provide an intuitive scale q and selected the static heavy quark potential $V(q)$. The definition of the α_V scheme is such that

$$V(q) \equiv -\frac{C_f 4\pi\,\alpha_V(q)}{q^2}, \tag{2.50}$$

to all orders and $\alpha_V(q)$ becomes the coupling strength of a gluon with momentum q. Series expressed in this scheme have smaller coefficients and converge faster than the bare coupling [5,28,29]. The scheme is now set so that $\alpha_V(q^*)$ is the appropriate expansion parameter for a process in which the typical gluon momentum is q^* and this fact can be exploited to "set the scale". Consider a gluon line in a diagram that contributes an integral I to the overall total

$$I = \alpha_V(q^*) \int d^4q\, f(q) \tag{2.51}$$

by integrating over some function of the momentum q flowing in the line. According to the renormalisation group, for large q^2 each additional vacuum loop included on

this gluon line introduces a factor $\alpha_V(q^*)\beta_0 \log(q^{*2}/q^2)$, where $\beta_0 = (11-\frac{2}{3}n_f)\Big/4\pi$. Keeping only the first order and demanding that this reproduce the full result

$$\alpha_V(q^*) \int d^4q\, f(q) \equiv \int d^4q\, \alpha_V(q) f(q) \tag{2.52}$$

as accurately as possible fixes q^*. Expanding $\alpha_V(q^*)$ and $\alpha_V(q)$ about some common scale μ:

$$\begin{aligned} \alpha_V(\mu)\left(1+\beta_0 \ln\left(\frac{q^*}{\mu}\right)^2 \alpha_V(\mu)\right) \int d^4q\, f(q) = \\ \alpha_V(\mu) \int d^4q\, f(q) + \beta_0\, \alpha_V(\mu) \int d^4q\, f(q) \ln\left(\frac{q}{\mu}\right)^2, \end{aligned} \tag{2.53}$$

and solving gives the first-order prescription for setting q^* [6]

$$\ln q^* \equiv \frac{\int d^4q\, f(q) \ln q}{\int d^4q\, f(q)}. \tag{2.54}$$

A second order prescription [35,36] is useful if the first order integral is anomalously small which can happen if the integrand $f(q)$ changes sign or has strong support at several different scales. Schemes other than the V-scheme have additive constants in the scale setting so it is best done with the formulae above and then the whole series can be converted into the final preferred scheme.

Combining the improvements of adding tadpole factors, smeared links in staggered quarks and appropriate scheme and scale setting means that lattice perturbation theory is a reliable tool for extracting continuum physics from lattice simulations, for correcting operators and the action, and for matching to phenomenological schemes such as $\overline{\rm MS}$.

CHAPTER 3

SYMANZIK IMPROVEMENT – TASTE CHANGING

Accurate simulations of the Standard Model require three light flavours of dynamical quarks. The improved staggered formalism is the only one capable of delivering large numbers of configurations with small quarks masses anytime in the near future [18]. This choice of lattice-quark discretisation has many non-degenerate pions whose masses do *not* vanish for zero quark mass. The residual masses come from mixing between the staggered copies of the quarks, and vanish like a^2. These "taste-changing" interactions are the largest remaining error in the action.

The most naïve lattice discretisation of quarks:

$$S = \overline{\psi}\,(\gamma \cdot \Delta + m)\,\psi, \tag{3.1}$$

where

$$\Delta_\mu \psi(x) = \frac{1}{2u_0}\Big[U_\mu(x)\psi(x+\hat{\mu}) - U^\dagger_\mu(x-\hat{\mu})\psi(x-\hat{\mu})\Big], \tag{3.2}$$

suffers from the infamous "doubling" problem — an additional massless mode for the quark at the opposite end of the Brillouin zone for each direction. In 4D this results in 16 extra copies of each of the n_f flavours of quark. If the vector $\zeta = (1,0,0,0), (1,1,0,0), \ldots$, in all 16 combinations, is used to describe the corners of the Brillouin zone; then naïve quarks have an exact symmetry

$$\text{quark}(p \sim 0) \quad \equiv \quad \text{quark}(p \sim \zeta\pi/a) \tag{3.3}$$

The staggered formalism uses a spinor identity to reduce this plurality to 4 copies, which are called staggered-copies or *tastes* in order to distinguish them from real

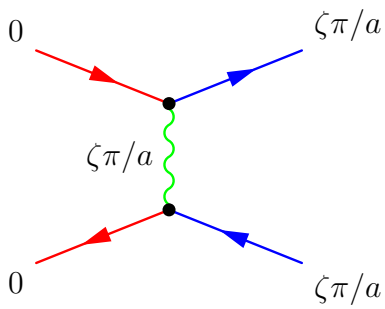

Figure 3.1: Generic tree-level taste-changing diagram for massless naïve quarks exchanging a hard gluon of momenta $\zeta\pi/a$.

flavours. These tastes then interact by hard gluon exchange as shown in figure 3.1. The gluon exchange is highly virtual with momentum $\mathcal{O}(\pi/a)$ and thus the quark-quark interaction is effectively a purely perturbative contact interaction at typical lattice spacings a, because then π/a is large.

The tree-level interaction in figure 3.1 was understood and completely removed with the introduction of the improved staggered quark action by using carefully chosen smearing to suppress high-momentum gluon emission of the form $\zeta\pi/a$ from quarks [7, 37].

Naïve staggered quarks suffer from poorly convergent perturbative expressions and large pion splittings which can also be suppressed by the use of fat links [37], §2.2.2. Staggered quarks which are improved to $\mathcal{O}(\alpha_s a^2, a^4)$ [7] significantly reduce splittings in the pion spectrum [38] and have small renormalisations [39, 40]. The goal of this chapter is to further improve staggered quarks — to effectively remove the taste-changing errors which constitute the bulk of the remaining error. This is important because these errors can amount to a few percent in quantities of interest. They are difficult to assess and remove without expensive matched simulations changing a even with "Staggered Chiral Perturbation Theory" [41, 42, 43].

If the one-loop taste-changing can be effectively eliminated then these errors would be reduced by a factor of ≈ 3 because $\alpha_s \sim 1/3$ in simulations. There are two scenarios for achieving this:

1. retain the original improved staggered action but add explicit counter-terms,
2. add further smearing to suppress these one-loop effects to comparable or below two-loop contributions.

Perturbation theory is required for the first option, and a useful investigative tool in the second. Non-perturbative simulations of new actions are expensive even in the quenched approximation. The "HYP" action [44] was originally proposed as having the desired improvement in taste-changing due to non-perturbative effects such as improved smoothness of link fields and instanton effects. This action is analysed perturbatively and the reduction in taste-changing effects is actually shown to be predicted by one-loop perturbation theory. Once perturbation theory has been confirmed as explaining the taste-changing interactions as seen in the non-perturbative simulations of e.g. bound states of pions, the relative ease of automated perturbation theory and vastly reduced CPU implementation time can be exploited for testing ideas for new actions.

3.1 Scenario 1: Add one-loop taste changing counter-terms

Taste-changing interactions involve large transfers of momenta of $\mathcal{O}(\zeta\pi/a)$ between quark lines as shown at tree level in figure 3.1. The process is easy to study in the annihilation channel and crossing can be exploited for the others. Consider

$$u\overline{u} \rightarrow \text{gluons}(\zeta\pi/a) \rightarrow d\overline{d} \tag{3.4}$$

for non-zero ζ. When ζ is zero the process occurs in real QCD dressing the π^0 and should not be removed from the lattice simulation. The unphysical process occurs when an up quark and an up anti-quark annihilate into gluons that are *off*-shell before creating a final quark-anti-quark pair that is on-shell; making a new unphysical effective contact interaction between the two quark lines: $u\overline{u}d\overline{d}$. These contact interactions can be computed order-by-order in perturbation theory. Subtracting these interactions from the lattice action is a systematic procedure for removing taste-changing effects such as the splittings between different tastes of the same meson. The tree-level interaction is eliminated completely in improved staggered quarks. The largest remaining source of error in the formalism is the one-loop effects that are calculated later on. First a general classification of 4-quark contact interactions is presented; 6-quark and higher interactions are of course present but are not relevant in todays' simulations.

Using fourvectors s, t, $\zeta = (1,0,0,0), \ldots$ to represent a spinor, taste and momentum index to the corners of the unit Brillouin zone respectively, products of gamma matrices can be written condensely:

$$\gamma_s = \prod_{\mu=0}^{3} (\gamma_\mu)^{s_\mu} . \tag{3.5}$$

An ordinary QCD local current J_s with spinor γ_s can create an on-shell meson in the staggered theory with taste t and momentum index ζ of $p_{\text{tot}} \approx \zeta\pi/a$, and is written in terms of the point split $J_s^{(\zeta,t)}$:

$$J_s^{(\zeta,t)} \equiv \overline{\psi}(x)\mathcal{B}_\zeta^\dagger \gamma_s^{(t)} \psi(x+\Delta x) \tag{3.6}$$

$$\overline{\psi}\gamma_s^{(t')}\psi \propto \overline{\chi}\gamma_{t'}\chi, \tag{3.7}$$

for staggered boost operator $\mathcal{B}$ from (2.28) ignoring the link operators U required to connect $\overline{\psi}$ and ψ, which are separated by a vector $\Delta x = s + t \pmod 2$ in lattice

units. This current is eliminated by the staggering step after (3.7) of taking only the top component of the staggered four-spinor χ unless t' is zero, and hence the gamma-matrix on the right hand side of (3.7) is the identity. This enforces $\zeta = \overline{t}$, where $\overline{t}_\mu = \sum_{\nu\neq\mu} t_\nu \pmod 2$. The currents that survive the staggering are then $J_s^{(\overline{t},t)} \equiv J_s^{(t)}$ and are equivalent to those in the standard *spinor*$\otimes$*taste* notation in the literature:

$$J_s^{(t)} \equiv \overline{\psi}(x)\gamma_s \otimes \zeta_t \psi(x) \tag{3.8}$$

$$\sim e^{i\pi\overline{t}\cdot x}\frac{1}{2}\left[\eta\overline{\psi}(x)\gamma_t^\dagger\gamma_s\psi(x+\Delta x_{st}) \pm \text{h.c.}\right]. \tag{3.9}$$

with η a phase factor of either 1 or i for Hermiticity of the spinors between the fields. The sign option is to get the correct charge eigenstate which depends on t and s. The currents and the final action that removes one-loop taste-changing are written out in detail in §C.

The form of the taste-changing contact interactions is highly constrained by the properties of the quark Lagrangian. The leading operators consist of a product of quark bilinears, one for each quark line. The gluon propagators that connect the quark lines are flavour singlets and unaffected by the quark doubling symmetry (2.27), so the unstaggered bilinears with spinor s must be flavour singlets which when staggered are diagonal in staggered spinors χ. The currents must be either singlet or octet in colour. The mass of the light quarks may be neglected because (ma) is numerically small, $\lesssim 0.05$ in current simulations, which means that the bilinears must separately be singlets under chiral transformations, and that the quark lines have an odd number of spinors. The bilinears must carry momenta of order $\zeta\pi/a$ for nonzero ζ. The only naïve-quark bilinears satisfying all of these

constraints are:

$$\begin{aligned} & e^{i\zeta\pi\cdot x}\ \overline{\psi}\gamma_\mu^{(0)}\psi && e^{i\zeta\pi\cdot x}\ \overline{\psi}\gamma_{5\mu}^{(0)}\psi \\ & e^{i\zeta\pi\cdot x}\ \overline{\psi}T^a\gamma_\mu^{(0)}\psi && e^{i\zeta\pi\cdot x}\ \overline{\psi}T^a\gamma_{5\mu}^{(0)}\psi \end{aligned} \tag{3.10}$$

where $\psi = (u, d, s)$ and T^a is a colour generator and link operators are implicit. These operators for different ζ translate one-to-one onto one-link (Vector) or three-link (Axial-vector) staggered quark operators:

$$\begin{aligned} \Delta\mathcal{L} = & \tilde{d}_V^{(1)}(1)\left(J_{5\mu\nu}^{(5\nu)}\right)^2 + d_V^{(1)}(1)\left(J_5^{(5\mu)}\right)^2 \\ & + \tilde{d}_V^{(1)}(2)\left(J_{5\nu}^{(5\mu\nu)}\right)^2 + d_V^{(1)}(2)\left(J_\nu^{(\mu\nu)}\right)^2 \\ & + \ \tilde{d}_V^{(1)}(3)\left(J_1^{(\mu)}\right)^2 + d_V^{(1)}(3)\left(J_{\mu\nu}^{(\nu)}\right)^2 \\ & \qquad\qquad + d_V^{(1)}(4)\left(J_{5\mu}^{(5)}\right)^2 \\ & + \ \tilde{d}_A^{(1)}(1)\left(J_{\mu\nu}^{(5\nu)}\right)^2 + d_A^{(1)}(1)\left(J_1^{(5\mu)}\right)^2 \\ & + \ \tilde{d}_A^{(1)}(2)\left(J_{5\nu}^{(\mu\nu)}\right)^2 + d_A^{(1)}(2)\left(J_\nu^{(5\mu\nu)}\right)^2 \\ & + \ \tilde{d}_A^{(1)}(3)\left(J_5^{(\mu)}\right)^2 + d_A^{(1)}(3)\left(J_{5\mu\nu}^{(\nu)}\right)^2 \\ & + \ \tilde{d}_A^{(1)}(4)\left(J_\mu^{(5)}\right)^2 \\ & + \left(\text{colour octet versions with } d^{(1)} \to d^{(8)}\right), \end{aligned} \tag{3.11}$$

where the sums over the repeated index ν and the direction μ are assumed. Momentum conservation in the naïve quark theory requires that the two currents in each term have the same taste (upper index), while parity and axis-interchange (the remnant of Lorentz symmetry) imply that the spinor index must match too. The terms in the Lagrangian with $\tilde{d}$, (d) coefficients are made of charge-eigenstate $C = -1$, $(C = 1)$ bilinears. The argument $d(\zeta^2)$ indicates the magnitude of the momentum transfer $\zeta\pi/a$ between the two bilinears. These contact interactions are all that can appear in dimension 6 to all orders in α_s to leading power in (am).

The chiral perturbation theory devised by Lee and Sharpe [40] which includes operators to account for staggered fermions has 8 more terms which are not doubling-eigenstates along each quark line *separately*, and 2 taste-singlets ($t = 0$) which are soft-gluon emission and important for real physics e.g. $\pi \to 2\gamma$, and should not be removed from the simulation.

The coefficients of the various operators in (3.11) are easily computed. For one-link operators each quark line should be traced over spinor labels with γ_μ, and over colour labels with either $\mathbb{I}_3$ (singlet) or T^a (octet). The result for momentum $\zeta\pi/a$ is the coefficient of the μ-th operator with currents having taste $t = \overline{\zeta}$. The axial-vector, three-link coefficients are projected out with a $\gamma_{5\mu}$.

There are five one-loop taste-changing diagrams for massless quarks. These are shown in figure 3.2 along with the effective four-quark contact term that they induce. A significant simplification for the computation with improved staggered quarks and a condition on variants is that the one-gluon emission of momentum $\zeta\pi/a$ actually vanishes. This is required for eliminating tree-level as shown in figure 3.1. For this reason the 8 diagrams that make up the one-loop renormalisation of the internal gluon all vanish, along with the 3 from one-loop wavefunction renormalisation on the external quark legs. The one-loop vertex corrections (2 continuum-like and 3 additional lattice diagrams) also vanish for the same reason leaving just five diagrams (shown in figure 3.2) of which two: 3.2(a) and 3.2(b), are familiar from continuum four-quark operators.

To actually remove all the one-loop taste-changing requires adding the terms of (3.11) to the Lagrangian. Each four-quark contact term can be individually removed in a simulation with the following trick for $d = c^2$ using anti-Hermitian

currents J:

$$\Delta\mathcal{L} = cJ\phi + \frac{1}{2}\phi^2 \qquad \equiv \qquad \Delta\mathcal{L} = -\frac{1}{2}dJ^2 \tag{3.12}$$

because the scalar field ϕ is non-propagating. The coefficients c for improved staggered quarks with improved glue are shown in table 3.1; all are around 1, decreasing with ζ^2, but the final column is always zero at this order because of symmetry.

The addition to the action requires $(8{+}1)_\mu$ ϕ's per lattice site, but for the upper half of the table the $cJ\phi$ terms are all one-link currents like the action, and can be easily accumulated in the calculation of the improved smearing with no change to the inverter. An explicit implementation is worked out in appendix C. The three-link axial-vector currents $cJ\phi$ in the lower half of the table can be made much smaller by a small change to the action [45] and are then judged to be too small so the more intricate problem of their implementation is avoided. Their small effects can be lumped in with the non-taste-changing $\mathcal{O}(\alpha_s a^2)$ errors and the two-loop taste-changing errors in the quark action.

There is a potential problem with this approach. The necessary coefficients c in the addition $cJ\phi$ quark are not guaranteed to be real which means that the total action would lose its important eigenvalue properties. Unfortunately, all the coefficients, c, turn out to be purely imaginary. The eigenvalues of the quark determinant are of the form $i\lambda{+}m$ with *real* λ for a quark action $\overline{\psi}(\text{anti-Hermitian}{+}m)\psi$. Wilson-type unstaggered quarks are a popular action for which this is not true — they suffer from so-called "exceptional" configurations when the quark matrix starts taking a long time to invert and the associated unknown systematic error involved in truncating the inversion algorithm. The closer the eigenvalues of the quark matrix are to zero the more ill-conditioned it is and harder to invert. Wilson

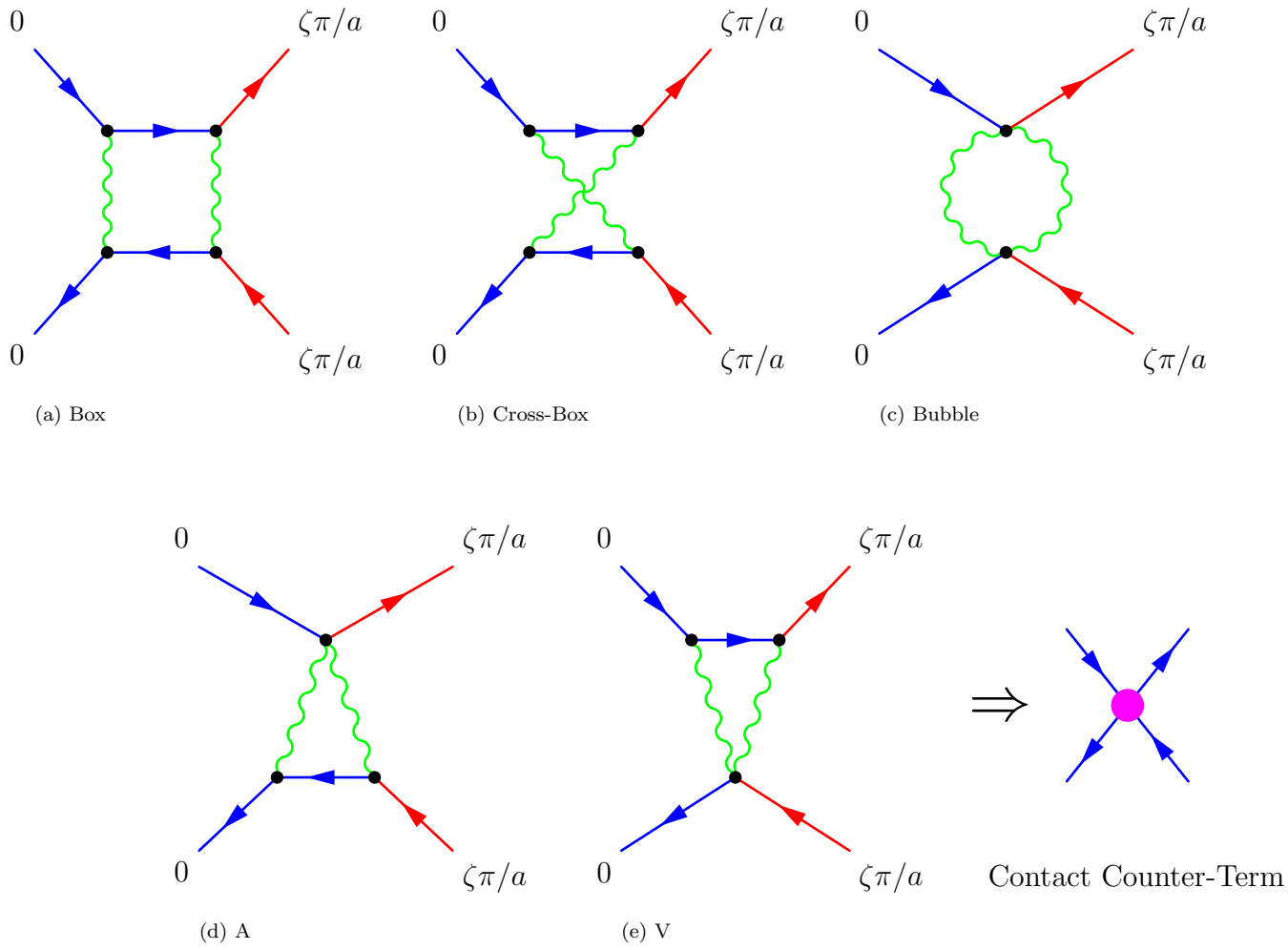

Figure 3.2: The five Feynman diagrams contributing to one-loop taste-changing for improved staggered quarks. Note that 15 other diagrams vanish due to the smearing in improved staggered.

Table 3.1: Coefficients of one-loop taste-changing counter-terms for the improved staggered action, one-loop Symanzik improved glue (Asqtad) in units of α_s.

	1-Link			
	Octet Colour		Singlet Colour	
ζ^2	$c_V^{(8)}$	$\tilde{c}_V^{(8)}$	$c_V^{(1)}$	$\tilde{c}_V^{(1)}$
1	0.880i $5\mu\otimes 5$	0.500i $5\mu\nu\otimes 5\nu$	0.643i $5\mu\otimes 5$	
2	0.435i $\nu\otimes\mu\nu$	0.438i $5\nu\otimes 5\mu\nu$	0.217i $\nu\otimes\mu\nu$	
3	0.335i $\mu\nu\otimes\nu$	0.409i $1\otimes\mu$	0.244i $\mu\nu\otimes\nu$	
4	0.300i $5\mu\otimes 5$	–	0.220i $5\mu\otimes 5$	–
	3-Link			
ζ^2	$c_A^{(8)}$	$\tilde{c}_A^{(8)}$	$c_A^{(1)}$	$\tilde{c}_A^{(1)}$
1	0.404i $1\otimes 5\mu$	0.518i $\mu\nu\otimes 5\nu$	0.295i $1\otimes 5\mu$	
2	0.228i $\nu\otimes 5\mu\nu$	0.364i $5\nu\otimes\mu\nu$	0.166i $\nu\otimes 5\mu\nu$	
3	0.198i $5\mu\nu\otimes\nu$	0.198i $5\otimes\mu$	0.145i $5\mu\nu\otimes\nu$	
4	–	0.190i $\mu\otimes 5$	–	
	$C=1$	$C=-1$	$C=1$	$C=-1$

quarks have no protection from sampling the action where the quark eigenvalues ~ 0 because $\lambda \sim im$ which is found to be increasingly likely even as m_l is around the strange quark mass, and at least a factor of 10 too large. It is not clear until simulations are done whether the very small breaking from four-quark operators with imaginary coefficients would induce this problem for staggered quarks which are already running at $m_s/10$. One possibility were exceptional configurations found would be to simulate with twice the taste-changing by adding in the currents with $c'_{\rm real} = c/i$, and then to extrapolate. Fortunately a simpler option which has results potentially almost as good has emerged which is to change the action by adding more smearing and re-unitarisation. Although removing one-loop vector-current taste-changing would be a great solution, there would still be small axial-vector interactions at one-loop, the whole gamut of two-loop taste-changing and the remaining non-taste-changing one-loop errors. Therefore settling for reducing the one-loop effects to the level of the two-loop is a reasonable approximation.

3.2 Scenario 2: further improve the staggered quark action

The size of the coefficients for a given action which are necessary to remove the one-loop taste changing can be used as a guide to the size of the mixing problem likely to be found in that quark action. There are two benchmarks in this game. The improved staggered action which has no $\mathcal{O}(a^2)$ errors, and the hypercubically blocked "HYP" action developed by Hasenfratz and Knechtli [44]. The disadvantage of the HYP action is that it is fiendishly complicated involving three different smearings, each followed by an SU(3) back-projection of the links, has an *additional* power of the volume in its unquenched algorithm which makes it prohibitively expensive and that there is no clear way to remove its $\mathcal{O}(a^2)$ discretisation errors.

Although it is difficult to extract exactly what happens with the HYP action it is clear that it involves some smearing of the side-links in combination with a lot of SU(3) back projection.

The improved staggered action involves "Fat7" smearing only the original link in the naïve action in a special way that exactly removes the tree-level taste changing, it then adds two terms (Lepage and Naik) which remove the $\mathcal{O}(a^2)$ errors. The taste-changing is about 2-3 times worse in this action than in HYP. A fairer comparison is between the Fat7-smeared action and HYP because both have similar discretisation errors. The results show that these additional $\mathcal{O}(a^2)$-improvement terms with their many side-links cost somewhat in pion splitting. Small changes to the implementation of these terms do not help very much [45]. Similarly, small changes in the basic Fat7 smearing have little effect. A defect of the Fat7 smearing is that the side-links are not smeared as can be seen in figure 3.3. Re-unitarisation of the links is a very similar operation to SU(3) projection:

$$\overline{V}_R = \mathbf{ReUnitarise}\,[V] = \frac{1}{\sqrt{V^\dagger V}} V \tag{3.13}$$

$$\overline{V}_{SU(3)} = \mathbf{Proj}_{SU(3)}\,[V] = \frac{1}{\sqrt{V^\dagger V}} V \frac{1}{(\mathrm{det} V)^3}. \tag{3.14}$$

Perturbatively at one-loop, re-unitarisation and SU(3) projection are the same. Non-perturbatively the SU(3) projection is thought to give smoother links and have better instantion behaviour. However in a simulation where the "force" term needs to be calculated for the update algorithm, the derivative of the action with respect to a particular link $U(x')$ is needed. This is relatively easy to do for re-unitarisation because the chain rule can be applied to (3.13) but not to (3.14) for HYP-smeared fermions. The latest unquenched algorithm for HYP is extremely slow and increases with volume.

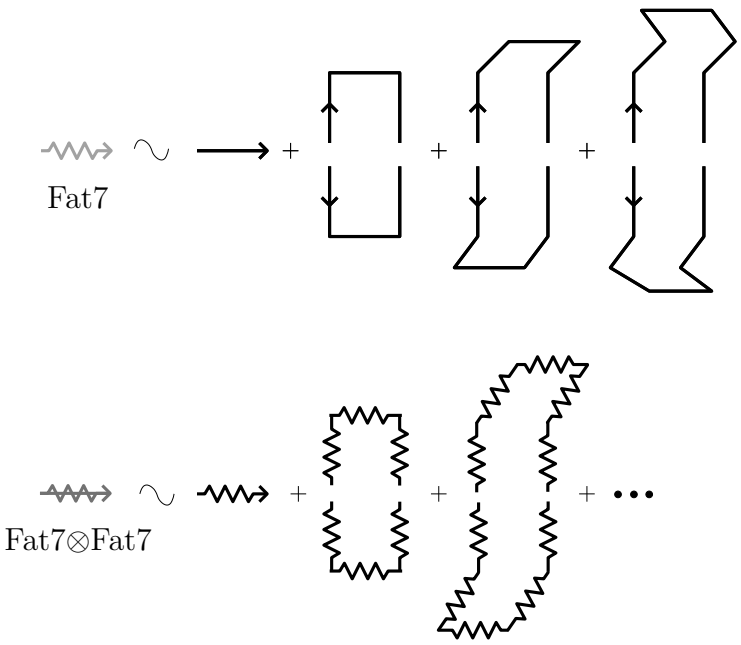

Figure 3.3: A schematic of Fat7 smearing (2.26b), and the principle behind smeared-smearings: the original smeared links are used in the second smearing. The $\sim$ is because appropriate coefficients and sums over all directions of the path elements are not shown.

Increased smearing causes two problems in perturbation theory. The paths become much longer – combining a 7-link smearing like Fat7 with itself gives paths that are 7^2 links long — factorially more difficult to compute the analytic Feynman rules. The automated methods discussed in §2 can still be applied, so in principle this is not a problem. Smearing improves the form-factors [37]. The perturbative expansion of a complicated smearing which is a sum of many paths with many links would have many terms; potentially they could add up to large numbers and spoil perturbation theory. In a simulation the equivalent effect would be observed in correlations between links that could lead to large contributions. Re-unitarisation and SU(3) back projection reset the normalisation and cure the problems from $\sqrt{length}$ growth in correlations. By itself re-unitarisation does not

achieve very much; it is only when acting on long paths that its effects are seen. It is the combination of smearing and re-unitarisation that is very exciting for reducing taste-changing interactions.

The most obvious action to try is re-unitarised Fat7 smearing of the links (Fat7$_R$) to form improved links that can be used as the new parallel transporters in the usual Fat7 action, followed by another hit of re-unitarisation: Fat7$_R$⊗Fat7$_R$. This combines smearing of the side-links with re-unitarisation. The taste-changing coefficients from this action and its close $\mathcal{O}(a^2)$ improved cousin Fat7$_R$⊗Asqtad which involves only one re-unitarisation step are shown in table 3.2 where they can be compared to the perturbative HYP and the original Fat7 results. It is clear that there is a massive improvement, and that Fat$_R$⊗Fat7$_R$ is slightly better than HYP. The improvement can be traced to two things: re-unitarisation has no effect on the one-gluon vertex, but reduces the symmetric two-gluon vertex, and clever smearing which can improve all the form-factors especially the anti-symmetric two-gluon vertex which is also unaffected by re-unitarisation. The HYP results shown are for the perturbative values of the coefficients in the smearing, which are required for tree-level taste-changing to vanish, and not the non-perturbatively tuned ones [40], though there is little difference [44] in the pion splittings. These same actions can be compared by quenched simulation of pions. At $\beta = 5.93$ with Wilson glue and a fixed bare mass of 0.03 the splittings of the 16 different tastes of pion can be measured with respect to the lowest, taste singlet, Goldstone boson. The difference in the squared masses is a preferred measure which is less sensitive to the bare mass. The splittings are shown for several actions in figure 3.4. There is currently no intuition about which coefficients are the most important for taste-changing, but a reasonable measure of the total is the sum of the coefficients

Table 3.2: Perturbative coefficients for the currents (3.11) required to exactly eliminate one-loop taste-changing effects in units of α_s. Four different quark actions are shown; all use Wilson glue.

(a) Fat7$_R$⊗Fat7$_R$

ζ^2	$c_V^{(8)}$	$\tilde{c}_V^{(8)}$	$c_V^{(1)}$	$\tilde{c}_V^{(1)}$
1	0	0.085i	0	
2	0.145i	0.104i	0.105i	
3	0.045i	0.035i	0.033i	
4	0.021i	-	0.015i	

ζ^2	$c_A^{(8)}$	$\tilde{c}_A^{(8)}$	$c_A^{(1)}$	$\tilde{c}_A^{(1)}$
1	0.008i	0.018i	0.006i	
2	0.061i	0.048i	0.045i	
3	0.016i	0.030i	0.012i	
4	-	0.013i	-	

(b) HYP

ζ^2	$c_V^{(8)}$	$\tilde{c}_V^{(8)}$	$c_V^{(1)}$	$\tilde{c}_V^{(1)}$
1	0.153i	0.276i	0.112i	
2	0.210i	0.153i	0.154i	
3	0.127i	0.092i	0.093i	
4	0.086i	-	0.063i	

ζ^2	$c_A^{(8)}$	$\tilde{c}_A^{(8)}$	$c_A^{(1)}$	$\tilde{c}_A^{(1)}$
1	0.066i	0.120i	0.049i	
2	0.091i	0.076i	0.067i	
3	0.049i	0.086i	0.036i	
4	-	0.054i	-	

(c) Fat7

ζ^2	$c_V^{(8)}$	$\tilde{c}_V^{(8)}$	$c_V^{(1)}$	$\tilde{c}_V^{(1)}$
1	1.602i	0.851i	1.117i	
2	0.614i	0.397i	0.448i	
3	0.283i	0.193i	0.207i	
4	0.128i	-	0.094i	

ζ^2	$c_A^{(8)}$	$\tilde{c}_A^{(8)}$	$c_A^{(1)}$	$\tilde{c}_A^{(1)}$
1	0.066i	0.120i	0.049i	
2	0.091i	0.076i	0.067i	
3	0.049i	0.086i	0.036i	
4	-	0.054i	-	

(d) Fat7$_R$⊗Asqtad

ζ^2	$c_V^{(8)}$	$\tilde{c}_V^{(8)}$	$c_V^{(1)}$	$\tilde{c}_V^{(1)}$
1	0.147i	0.067i	0.107i	
2	0.192i	0.131i	0.141i	
3	0.067i	0.059i	0.049i	
4	0.035i	-	0.025i	

ζ^2	$c_A^{(8)}$	$\tilde{c}_A^{(8)}$	$c_A^{(1)}$	$\tilde{c}_A^{(1)}$
1	0.029i	0.054i	0.021i	
2	0.054i	0.045i	0.041i	
3	0.013i	0.023i	0.010i	
4	-	0.011i	-	

$\sum_\zeta |c|^2$, which is also shown on the plot.

3.3 Conclusion

There is a procedure for explicitly removing perturbative taste-changing interactions order-by-order by adding explicit counter-terms. One-loop taste-changing

can be reduced below the level of 2-loop effects by a combination of well-smeared links and re-unitarisation, whilst still retaining the essential $\mathcal{O}(a^2)$-accuracy required for high-precision lattice simulations of the QCD sector of the standard model. Taste-changing in staggered quarks is understood and well-explained by perturbation theory. Quenched simulations are underway for Fat7$_R\otimes$Asqtad, and are expected to be very similar to Fat7$_{SU(3)}\otimes$Asqtad. The most highly improved quark action is now the Fat7$_R\otimes$Asqtad action which has $3\times$ smaller taste-changing than Improved Staggered, comparable to HYP.

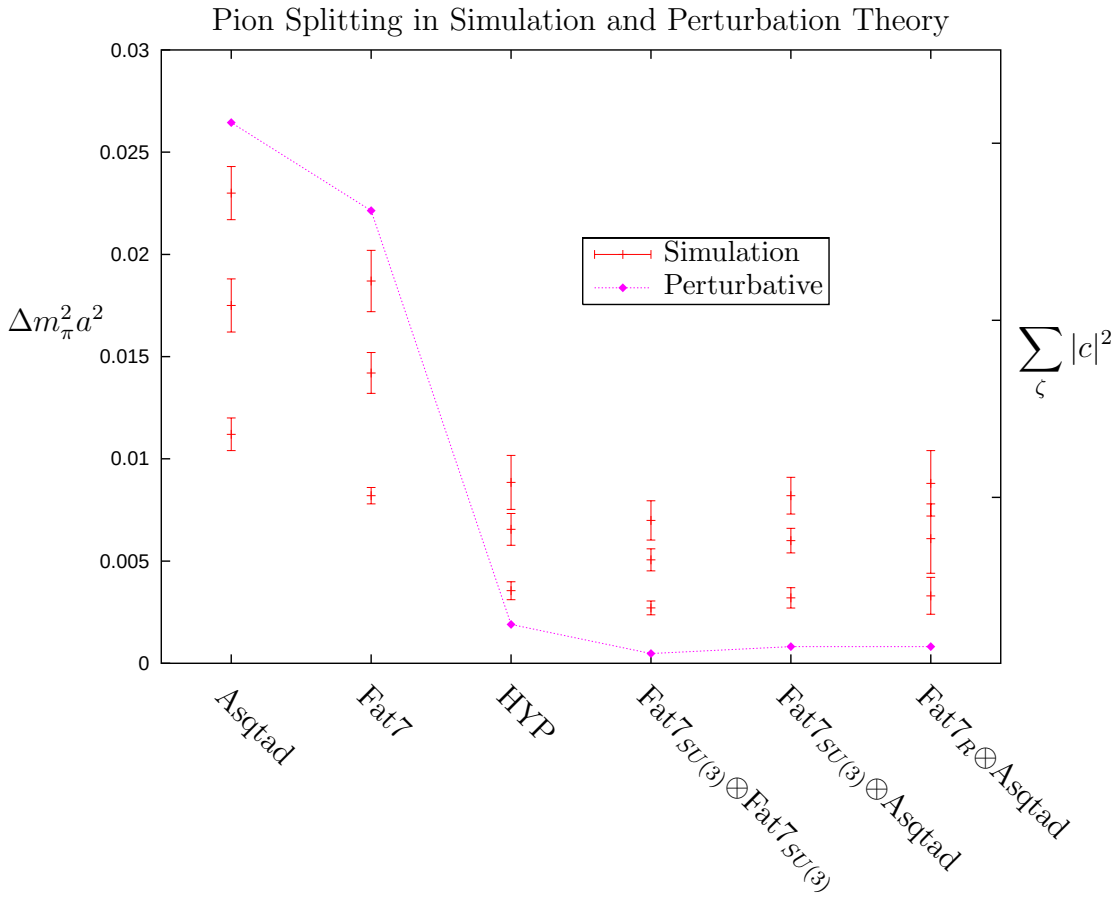

Figure 3.4: Quenched, $m_0 = 0.03$, $\beta = 5.93$ splittings of m_π^2 for the 1-, 2- and 3-link tasteful mesons above the Goldstone pion for various quark actions with Wilson glue. On a different scale a measure of the one-loop perturbative taste-changing effects, $\sum_\zeta |c|^2$ is also shown which qualitatively explains the non-perturbative pion splittings; verifying that taste-changing can be understood as an $\mathcal{O}(a^2\alpha_s^2)$ *perturbative* process. The proposed action Fat7$_R\otimes$Asqtad, shown on the right, has scaling violations due to taste-changing interactions about twice as small as the previous action, Asqtad, shown on the left.

CHAPTER 4

STRANGE QUARK MASS

The mass of the strange quark, along with the masses of the other quarks and the coupling constant are fundamental parameters of the Standard Model. The strange quark mass is input for various phenomenological studies, including the important CP-violating quantity ϵ'/ϵ [46] where it severely limits the theoretical precision. It is also an important input to QCD factorisation; particularly for the theoretical explanations of the 96 B-decay modes being studied at the B-factories for new physics, CKM angle γ, Hadronic flavour-changing neutral currents and CP-violations [47, 48].

This determination comes from a breakthrough in unquenching in Lattice QCD. Improved staggered quarks [7] have small renormalisations [40, 45] and are relatively quick. The use of improved staggered quarks has allowed simulations with 2 dynamical quarks and one heavier dynamical strange quark at a wide range of valence and sea quark masses down to approximately four times lighter than ever before. Despite the increased realism the u, d masses are still too heavy and a partially quenched chiral extrapolation is performed to correct for this. The data is now clearly in the chiral regime and therefore the answer quoted involves no separate estimation of chiral or unquenching errors for the first time.

The simulation data of the MILC collaboration [12] is used; staggered quarks corrected to $\mathcal{O}(\alpha_s a^2, a^4)$ [7] and one-loop Symanzik improved gluons with Tadpole improvement [10]. Two sets of configurations were used, a "coarse" set with lattice spacings of $a \approx 1/8$fm and sea quark masses of $am_u = am_d = 0.007, 0.01, 0.02$ with $am_s = 0.05$ and a "fine" set at $a \approx 1/11$fm with sea quark masses of $am_u = am_d = 0.0062, 0.0124$ and $am_s = 0.031$. The valence masses ranged from m_s down to

$m_s/10$. The continuum strange quark mass is then determined from:

$$m_{\rm s}^{\overline{\rm MS}}(\mu) = \frac{(am_s)_0}{a}\left(1 + \alpha_V(q^*)\, Z_m^{(2)}(a\mu, (am_s)_0) + \mathcal{O}(\alpha^2)\right), \tag{4.1}$$

where the bracket is Z_m, the mass renormalisation that connects the bare lattice mass and the $\overline{\rm MS}$ mass, and $(am_s)_0$ is the *a posteriori* tuned bare strange mass in lattice units. Many configurations of gluon and fermion fields are generated according to the probability distribution e^{-S}. Meson correlators are related to experimental measurements by fitting the excitation spectrum in lattice units and extracting the scale a required for agreement. The lattice unit spacing a was determined from the Υ–Υ' mass difference that is approximately independent of the quark masses, including the b-mass. The result agrees with that from f_π and f_K at the light scale, at the heavy scale with several other splittings in the Υ-system, the 1P-1S Ψ splitting and in the Baryonic sector by $3M_\Xi - M_N$. These all agree at the 3% level which is much smaller than the perturbative or extrapolation errors, and is the first time a systematic study of all of these scales has been performed [2]. The coupling constant was set by 3rd order expressions for the logarithms of small Wilson loops §5, lattice quantities which are very ultraviolet, and run to an optimal scale q^*.

To correct for using the wrong bare input light quark masses $(am_{u,d})$ and (am_s) in the simulation leading-order chiral perturbation theory [49] can be used. However this does not fit the data well because the chiral expansion parameter for strange quarks,

$$x_s \equiv \frac{\chi_s}{(4\pi f_\pi)^2} \equiv \frac{2\mu m_s}{(4\pi f_\pi)^2}, \tag{4.2}$$

is approximately 0.33 in the normalisation of [49] where $f_\pi = 93.3$ MeV. The simulations are sufficiently close to the correct strange mass that chiral perturbation theory is both unnecessary and poorly convergent for the m_s dependence

and linear interpolation is used instead. Only the u and d quarks are treated as light in this chiral scheme and therefore there are a different set of chiral parameters for strange quantities. For π's the leading-chiral fit parameters needed are $\mu m_{u,d}, f, L_{4,5,6,8}$ [49] where L_i are the Gasser-Leutwyler Low-Energy-Constants, and to describe the Kaon $\mu_s m_s, f_s, L_{4s,5s,6s,8s}$ are used. The leading parameters μ_s and f_s should differ from the corresponding pion parameters by amounts of order $x_s^2 \approx 5 - 10\%$, while the others should differ by $x_s \approx 20 - 30\%$. The leading pion parameters should be within $x_s/3 \approx 10\%$ of their lowest order values if chiral perturbation theory works.

The differences in form factors between the coarse and fine lattices as a function of the bare light quark masses were used to determine the $\mathcal{O}(a^2)$ corrections which were 2-3%. The fine set is mid-way between the coarse set and the continuum, so the corrections and an error were applied to the fine set to extrapolate to the continuum, where the final chiral fit was made with lightly constraining Bayesian priors [50]. A simultaneous fit of m_π^2, m_K^2, f_π and f_K as functions of $(am_{u,d}^{\rm val})$ and $(am_{u,d}^{\rm sea})$ was performed. The fitting functions were of the form:

$$m_{ab}^2 = m^2 \begin{pmatrix} 1 + \delta_{m^2} \\ +c_f(x_a + x_b)^2 + c_{2f}(2x_l)^2 \\ +c_{3f}(x_a + x_b)(2x_l) \end{pmatrix}, \tag{4.3}$$

where a, b are the valence quarks, l are the light sea quarks, and δ_{m^2} is the complete partially quenched Chiral perturbation correction which is first order in x_i [49]. The higher order coefficients should be $\mathcal{O}(1)$ or less. An analogous expansion was used for the form-factors. Using light quark masses less than $m_s/2$ keeps corrections of order $x_{u,d}^2$ smaller than 1-5% and within the domain of χPT. Finite-volume errors in the δ_{m^2} were included roughly and estimated to be 1% for the smallest

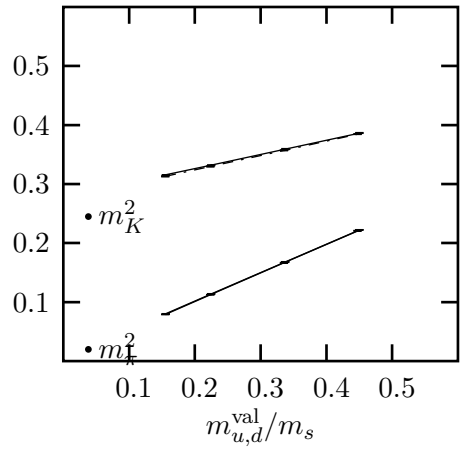

Figure 4.1: Chiral fits of m_π^2 and m_K^2 versus $m_{u,d}$ (all in GeV) on the fine lattice *before* interpolation in m_s. The valence and sea quark s-quark masses are $am_s = 0.031$ (16% too high).

masses. The individual runs at different masses were only approximately tuned to the same a^{-1} so r_1 [51, 52] was used to make small corrections between the masses. The chiral scaling corrections to the static quark potential which affect r_1 are expected to decrease with r^2 and are less than 0.5% between the coarse and fine lattices, so are not needed at this accuracy. Non-analytic $\mathcal{O}(a^2)$ errors from the logarithms in staggered chiral perturbation theory were included by an additional overall 1.5% error in f_π.

The fit for m_K^2 and m_π^2 on the fine lattice is shown in figure 4.1. With the fit results the lattice data can be extrapolated in both the valence and sea light-quark masses. The correct values are determined by m_π^2 for $(am_{u,d})$ and $2m_K^2 - m_\pi^2$ for the strange. The strange quark was decoupled from the chiral perturbation theory that went into the fit by design, so a linear interpolation in the strange mass was performed for each physical quantity. A correction of $\mathcal{O}(x_s) \approx \frac{1}{3}$ in the interpolation was included to assess the error. The final results with the corrected

Table 4.1: Selected parameters from Bayesian partially quenched χPT-fits to the finer set of lattice simulation data after interpolation in m_s. The first error combines statistical, $\mathcal{O}(a^2)$ and fit errors and the second is from the interpolation in m_s.

Fine	$a \approx 1/11$ fm	
$am_{u,d}$	0.00106	(2)(1)
am_s	0.0274	(6)(12)
$\chi_{u,d}$	0.018	(1)
χ_s	0.419	(42)
f_π/expt	1.015	(24)(2)
f_K/expt	0.991	(22)(8)

light quark masses are in table 4.1. The Gasser-Leutwyler parameters came out in agreement with phenomenological values; these and results for f_π will be presented elsewhere [53]. QCD is an asymptotic theory so the quarks do not appear as free particles at low energies. To define their mass the conventional choice is the modified Minimal Subtraction ($\overline{\text{MS}}$) scheme at a scale of 2 GeV. The tuned bare lattice mass is converted to an $\overline{\text{MS}}$ mass by computing the renormalisation $Z_m^{(2)}$. This is done by connecting the bare quark-mass to the pole-mass in lattice perturbation theory, and using the pole mass to $\overline{\text{MS}}$ mass relation [54] at one loop.

$$Z_m^{(2)}(a\mu, am_0) = \left(b(am_0) - \frac{4}{3\pi} - \frac{2}{\pi}\ln(a\mu) \right), \tag{4.4}$$

where $b(am) = 0.52574 - 0.4866(am)^2$ which is correct to 0.1% up to $(am) = 0.1$ for the original improved staggered quarks [7], and $\gamma_0 = \frac{2}{\pi}$ is the universal one-loop anomalous mass dimension. There is a choice for the scale μ at which to match the lattice to $\overline{\text{MS}}$; afterall the $\overline{\text{MS}}$mass can be run very accurately at three loops [55]. One choice is $\mu = \mu^*(a)$ such that $m_{\overline{\text{MS}}}(\mu^*(a))$ has the same a dependence as m_{lat}:

the evolution should be as close as possible

$$\frac{d}{d\ln a} m_{\overline{\rm MS}}(\mu^*(a)) = \frac{d}{d\ln a} m_{lat} \left[1 + \mathcal{O}\left(\alpha_V^3\left(q^*(\mu^*)\right), (ma)^2\alpha_V^2\right)\right], \tag{4.5}$$

$$\implies m_{\overline{\rm MS}}(\mu^*(a)) = m_{lat}\left[1 + \mathcal{O}(\alpha_V^2)\right]. \tag{4.6}$$

This implies matching at $\mu^* = 1.17/a = 2.67(3)$ GeV for $a^{-1}_{fine} = 2.271(28)$ GeV which gives $q^* = 2.25/a$, set by a second order method [36], §2.5, and for which $\alpha_V(q^*) = 0.227(4)$ on the fine lattice. Matching directly at 2 GeV shifts the final answer by less than one MeV, with similar errors. The final value for the strange quark mass is then

$$m_s^{\overline{\rm MS}}(2{\rm GeV}) = 75\ (5)^{sim.}(5)^{PT}{\rm MeV}, \tag{4.7}$$

where the simulation error comes mainly from strange quark mass interpolation (4 MeV) and a^{-1}, and the second from perturbation theory; dominated by $\mathcal{O}(\alpha_V^2)$, which is 6%. On the coarser lattice, α_s is bigger, and the unknown two-loop lattice quark mass renormalisation is a larger effect. For comparison the value there is 73(5)(11) MeV.

4.1 Comparison to previous determinations

There is a long history of sum rule determinations of the strange quark mass. The current status [56,57] is broad agreement between results from Scalar and Pseudo-Scalar spectral functions and particularly accurate results from SU(3) breaking in τ hadronic decays. These methods are very sensitive to $|V_{us}|$ which is not very well known. Using the Particle Data Group average the strange quark mass is at 105±20 MeV, but the unitarity constrained CKM matrix fit for $|V_{us}|$ gives results about 1σ higher. These values agree with quenched lattice [58] results but several

more recent $n_f = 2$ unquenched results are lower. This is the first time $n_f = 3$ simulations have been possible.

4.2 Conclusion

The use of Improved Staggered quarks has enabled the first exploration of chiral logarithms in the light mesons with all three light quarks dynamical. Essential features are their significantly reduced cost and great scaling properties which have allowed simulations to generate hundreds of configurations with sea u and d quarks with masses down to 1/7th that of the strange quark and valence quarks to 1/10th; approximately four times lighter than ever before. The limiting factor for this lattice determination of the strange quark mass in the $\overline{\rm MS}$ scheme is no longer unquenching, or having the correct number of light quarks, volume dependence or taste-changing effects but the unknown perturbative mass renormalisation. The simulation error can be easily improved by reducing the interpolation error in the dynamical strange quark lattice mass. The final value of $m_s^{\overline{\rm MS}}(2{\rm GeV})$=75(8) MeV has a complete error that is comparable and slightly smaller than sum rules, but the central value is lower than given by sum rules which agree with the unphysical quenched results. Adding two light flavours reduces the strange quark mass determined from lattice QCD from about 100-110 MeV quenched to 85-90 MeV. This is the first determination with three light flavours for which a full chiral extrapolation has been performed. The fit agrees with the phenomenological Gasser-Leutwyler parameters but finds a small additional reduction for three light flavours in the central value for the strange quark mass in the continuum limit. QCD factorisation fits to B-physics also favour a slightly lower strange quark mass [48]. The two-loop lattice multiplicative quark mass renormalisation calculation is already

underway and results are expected this Autumn [59]. The three-loop errors that would remain after that would be only 1.5%, 1 MeV, at the scale used for this determination.

CHAPTER 5

$\alpha_{\overline{\rm MS}}(M_Z)$

There are two steps to determining the strong coupling constant from lattice simulations. First an accurate unquenched simulation with three light dynamical quarks must be carefully tuned to reproduce the spectrum of the Standard Model, or at least those gold-plated quantities that must be correct with "no excuses" [2], of which §4 is a part. These quantities must have well understood and controlled extrapolation to the chiral limit ($a \to 0$) and to the correct light quark masses, and should cover the widest possible range of scales from the light-light mesons through the heavy-light to heavy-heavy mesons and baryonic observables to show that the simulation has correctly reproduced all the physics. Secondly an appropriate short-distance quantity should be measured and converted to the scheme and scale of choice with perturbation theory. This method is dominated by perturbative uncertainties rather than statistical or chiral extrapolation errors but currently has the smallest errors of any method of setting $\alpha_{\overline{\rm MS}}(M_Z)$ [4, 60, 61]. Other lattice techniques have been used allowing a comparison of systematics but so far very few fully extrapolated 2+1 simulations have been done; other techniques are typically statistics bound and proven with only 2 dynamical light quarks. Ideally α_s's from several lattice actions should be computed in each technique in order to compare the effects of different discretisations; here four are compared.

This work focuses on the contribution from perturbation theory which itself consists of two steps. A range of short-distance quantities need to be calculated to high-order in lattice perturbation theory. The choice of short-distance is so that the quantities have the least IR sensitivity to e.g. condensates, have a large scale q^* associated with them and hence should be well described by perturbation

theory. Agreement between several short-distance quantities with a range of scales would demonstrate that α_s was correctly running between those scales and provide a check over the contribution from condensates [60]. The traditional selection was the logarithm of the plaquette, here this is extended to several small Wilson loops up to 2×2 and to carefully selected combinations with good behaviour known as Creutz Ratios [62] in §5.2. The other perturbative calculation is to compute the relation between the lattice coupling $\alpha_{\rm lat}$ which is a poor expansion parameter vis. §2.5 and the conventional but unphysical scheme of $\overline{\rm MS}$ by way of a coupling that is physically relevant on the lattice, namely α_V. Fortunately the conversion between the $\overline{\rm MS}$ and the α_V (Potential) scheme has already been computed and checked at the requisite order [63, 64], leaving the non-trivial calculation of the connection between the lattice regulator and some other scheme at two loops. The lattice scheme depends on the precise details of the lattice action, particularly its approach to the UV cutoff and therefore the connection must be calculated for every action of interest; this is presented in §5.1. It is a necessary precursor to using any results of lattice perturbation theory expanded in some coupling α_s because an accurate method of setting the value of α_s is needed.

5.1 Background Field Matching

In Abbott's background field gauge (2.41) the action retains *explicit* gauge invariance at the quantum level [21]. This severely limits possible renormalisations and this is the reason that it is the prefered method for relating coupling constants, at least at this order. The quantum fields A, ψ, c do not need renormalising even at higher orders because they occur only in loops. The usual wavefunction renormalisations, $\sqrt{Z}$, cancel between the two renormalised fields in the vertices,

and the $1/Z$'s from the propagator that connects them. In field theory a vertex $g_0^m A_0^n \to (Z_g^m g^m)(Z_A^{n/2} A^n)$ so at least two vertex renormalisations must be calculated — eg the two point and the three point must be used to extract $\sqrt{Z_A}$ and Z_g (though typically ghost vertices are chosen). There are only three renormalisations of interest in the background field formalism:

$$g_0 \equiv \mathcal{Z}_g g, \quad B_0 \equiv \mathcal{Z}_B^{1/2} B, \quad \xi_0 = \mathcal{Z}_\xi \xi, \tag{5.1}$$

the coupling, background field and the gauge parameter. The gauge parameter for the quantum coupling must be renormalised because the longitudinal part of the gauge field propagator is not renormalised. These three are not all independent as the renormalisation of the field strength F is

$$(F^a_{\mu\nu}) = Z_B^{1/2} \left[\partial_\mu B^a_\nu - \partial_\nu B^a_\mu + i g Z_g Z_B^{1/2} f^a_{bc} B^b_\mu B^c_\nu \right], \tag{5.2}$$

and F is only gauge-covariant if $\mathcal{Z}_g = \mathcal{Z}_B^{-1/2}$. This statement was also proved on the lattice [19]. This means that calculating the renormalisation of only one n-point function is required. The two-point background field correlator at finite external momentum method of Abbot [21], is selected as being the simplest program for the matching calculation. Weinberg [65] suggests that the four-point vertex at all zero external momentum is easier but on the lattice there are a tremendous number of diagrams and there is no IR cutoff. In principal this could be handled in the analytic approach but for the numerical diagrammatic approach this is a disaster. Furthermore even more lattice vertices are required – including up to B^4A^4 and B^2A^6 which would be very very large §2.2.5.

Following the pioneering work of Lüscher and Weisz [19,20] for the unimproved Wilson gluon action, the idea is to calculate $d_1(s)$ and $d_2(s)$ from

$$\alpha_{\overline{\rm MS}}(s/a) = \alpha_{\rm lat} + d_1(s)\alpha^2_{\rm lat} + d_2(s)\alpha^3_{\rm lat} + \ldots. \tag{5.3}$$

Defining renormalisation constants between the $\overline{\rm MS}$ and lattice schemes

$$g_0 \equiv Z_g(g_0, \mu a) g, \quad \xi_0 = Z_\xi \xi. \tag{5.4}$$

Expanding

$$\frac{g^2}{g_0^2} = Z_g^{-2} = 1 + d_1(s)\frac{g_0^2}{4\pi} + d_2(s)\frac{g_0^4}{(4\pi)^2} + \ldots \tag{5.5}$$

where the coefficients $d_{1,2}(s)$ are independent of the gauge parameter. To calculate them consider the two-point functions for background and quantum fields

$$\Gamma^B_{\overline{\rm MS}}(p,-p)^{ab}_{\mu\nu} = -\delta^{ab}\Big(\delta_{\mu\nu}p^2 - p_\mu p_\nu\Big)\Big[1 - \nu_{\overline{\rm MS}}(p)\Big]\frac{1}{g^2} \tag{5.6}$$

$$\Gamma^A_{\overline{\rm MS}}(p,-p)^{ab}_{\mu\nu} = -\delta^{ab}\Bigg\{\Big(\delta_{\mu\nu}p^2 - p_\mu p_\nu\Big)\Big[1 - \omega_{\overline{\rm MS}}(p)\Big] + \frac{1}{\xi}p_\mu p_\nu\Bigg\}. \tag{5.7}$$

The tensor structure comes from the symmetries of the theory and the appropriate Ward identity. Note the longitudinal component. The lattice versions are

$$\sum_\mu \Gamma^B_{\rm lat}(p,-p)^{ab}_{\mu\mu} = -\delta^{ab}3\hat{p}^2\Big[1 - \nu_{\rm lat}(p)\Big]\frac{1}{g_0^2} + \mathcal{O}(a) \tag{5.8}$$

$$\sum_\mu \Gamma^A_{\rm lat}(p,-p)^{ab}_{\mu\mu} = -\delta^{ab}\hat{p}^2\Big\{3\Big[1 - \omega_{\rm lat}(p)\Big] + \frac{1}{\xi_0}\Big\} + \mathcal{O}(a), \tag{5.9}$$

where $\hat{p} = \frac{2}{a}\sin(ap_\mu/2)$. Dropping lattice artifacts the two-point lattice function can be expanded to two loops as

$$\begin{aligned}\nu_{\rm lat}(p,a,g_0) &= g_0^2\,\nu^{(1)}_{\rm lat}\Big(\xi_0 - Z^{(1)}_\xi g_0^2\xi_0\Big) + g_0^4\,\nu^{(2)}_{\rm lat}(\xi_0) \\ &= g_0^2\,\nu^{(1)}_{\rm lat}(\xi_0) + g_0^4\,\nu^{(2)}_{\rm lat}(\xi_0) - g_0^4\,\xi_0\,Z^{{\rm lat},(1)}_\xi \frac{\partial \nu^{(1)}_{\rm lat}}{\partial \xi_0}\bigg|_{\xi=\xi_0},\end{aligned} \tag{5.10}$$

including the gauge parameter renormalisation. It would be convenient to work in Landau gauge $\xi_0 = 0$ because this is invariant under renormalisation, but unfortunately background field gauge has vertices proportional to $1/\xi_0$ so this is not possible. The $\overline{\rm MS}$ version of (5.10) is

$$\nu_{\overline{\rm MS}}(p,\mu,g) = g^2\,\nu^{(1)}_{\overline{\rm MS}}(\xi_0) + g^4\,\nu^{(2)}_{\overline{\rm MS}}(\xi_0) - g^4\,\xi_0\,Z^{\overline{\rm MS},(1)}_\xi \frac{\partial \nu^{(1)}_{\overline{\rm MS}}}{\partial \xi_0}\bigg|_{\xi=\xi_0}. \tag{5.11}$$

Then

$$\frac{g^2}{g_0^2} = \frac{1-\nu_{\rm lat}(p,a,g_0)}{1-\nu_{\overline{\rm MS}}(p,\mu,g)} \tag{5.12}$$

but where the coupling parameter g of $\nu_{\overline{\rm MS}}(p,\mu,g)$ depends implicitly on the lattice one through (5.4). Expanding (5.12) self-consistently in g_0^2 using (5.4), (5.10) and (5.11):

$$\begin{aligned} Z_g^{-2} = 1 &+ \left\{ \nu_{\rm lat}^{(1)} - \nu_{\overline{\rm MS}}^{(1)} \right\}_{\xi=\xi_0}^{\mu=s/a} g_0^2 \\ &+ \left\{ \nu_{\rm lat}^{(2)} - \nu_{\overline{\rm MS}}^{(2)} + \xi_0 \left[Z_\xi^{\overline{\rm MS},(1)} - Z_\xi^{{\rm lat},(1)} \right] \frac{\partial \nu^{(1)}}{\partial \xi} \right\}_{\xi=\xi_0}^{\mu=s/a} g_0^4 \\ &+ \left\{ \left(\nu_{\rm lat}^{(1)} - \nu_{\overline{\rm MS}}^{(1)} \right)^2 \right\}_{\xi=\xi_0}^{\mu=s/a} g_0^4. \end{aligned} \tag{5.13}$$

The fact that the gauge parameter dependence of $\nu^{(1)}$ is universal because $d_1(s)$ must be gauge independent follows from differentiating

$$d_1(s) = -4\pi \left\{ \nu_{\overline{\rm MS}}^{(1)}(p) - \nu_{\rm lat}^{(1)}(p) \right\}_{\mu=s/a}^{\xi=\xi_0} \tag{5.14}$$

and therefore

$$d_2(s) = d_1(s)^2 - 4\pi \left\{ \nu_{\rm lat}^{(2)} - \nu_{\overline{\rm MS}}^{(2)} + \xi_0 \mathcal{Z}_\xi^{(1)} \frac{\partial \nu^{(1)}}{\partial \xi} \right\}_{\xi=\xi_0}^{\mu=s/a} \tag{5.15}$$

where the fact that $Z_\xi = Z_A^{-1}$, and using (5.7), (5.9) gives

$$\mathcal{Z}_\xi^{(1)} = \left\{ \omega_{\rm lat}^{(1)}(p) - \omega_{\overline{\rm MS}}^{(1)}(p) \right\}_{\xi=\xi_0}, \tag{5.16}$$

which is a simple one-loop calculation of the gluon two-point function subtracted from the well known continuum $\overline{\rm MS}$ value.

To summarise; the lattice computations necessary are the one-loop gluon self-energy and the two-loop background-field two-point function. However, the one-loop background-field self-energy must be done for a general gauge parameter in

at least one scheme but the other calculations can set $\xi_0 = 1$ for Feynman gauge, which is more convenient in the continuum, and for unimproved lattice calculations.

The one-loop $\overline{\rm MS}$ calculations of $\nu^{(1)}(\xi)$ and $\omega^{(1)}(\xi)$ are standard and well known and $\nu^{(2)}_{\rm gluonic}$ was done a long time ago by Ellis [66]. The divergent piece, β_1, was done before that but the constant piece of $\nu^{(2)}_{n_f}$ which is more difficult has only been done by the Lattice authors of [67] and subsequently checked for this project. The results for $\overline{\rm MS}$ necessary for two-loop matching with the lattice are:

$$\begin{aligned}\nu^{(1)}_{\overline{\rm MS}}(p,\xi) = \frac{N}{16\pi^2}&\left[-\frac{11}{3}\ln\frac{p^2}{\mu^2} + \frac{205}{36} + \frac{3\xi}{2} + \frac{\xi^2}{4}\right] \\ &+ \frac{N_f}{16\pi^2}\left[\frac{2}{3}\ln\frac{p^2}{\mu^2} - \frac{10}{9}\right],\end{aligned} \tag{5.17}$$

$$\begin{aligned}\omega^{(1)}_{\overline{\rm MS}}(p,\xi) = \frac{N}{16\pi^2}&\left[\left(-\frac{13}{6} + \frac{\xi}{2}\right)\ln\frac{p^2}{\mu^2} + \frac{97}{36} + \frac{\xi}{2} + \frac{\xi^2}{4}\right] \\ &+ \frac{N_f}{16\pi^2}\left[\frac{2}{3}\ln\frac{p^2}{\mu^2} - \frac{10}{9}\right],\end{aligned} \tag{5.18}$$

$$\begin{aligned}\nu^{(2)}_{\overline{\rm MS}}(p,\xi=1) = \frac{1}{(16\pi^2)^2}\Bigg\{&N^2\left[-8\ln\frac{p^2}{\mu^2} + \frac{577}{18} - 6\zeta(3)\right] \\ &+ N_f\left[N\left(3\ln\frac{p^2}{\mu^2} - \frac{401}{36}\right) - \frac{1}{N}\left(\ln\frac{p^2}{\mu^2} - \frac{55}{12} + 4\zeta(3)\right)\right]\Bigg\}.\end{aligned} \tag{5.19}$$

5.1.1 A three-loop result: β_2

A further benefit of this calculation is to determine β_2 for the lattice β-function. Although β_2 is a three-loop non-universal quantity its value can be determined in the lattice scheme by using the known three-loop value in the $\overline{\rm MS}$ scheme and the *two*-loop calculation at hand. The value obtained can be used to examine the corrections to asymptotic scaling far from the critical point where lattice simulations are performed. On the lattice the renormalisation group β-function is written as

$$\beta^{\rm L}(g_0) \equiv -a\frac{dg_0}{da}\Big|_{g_r,\mu} = -b_0^{\rm L}g_0^3 - b_1^{\rm L}g_0^5 - b_2^{\rm L}g_0^7 - \ldots, \tag{5.20}$$

where g_r is the renormalised coupling and μ is the subtraction point. It establishes how the bare coupling and the cutoff a must simultaneously vary to keep the renormalised quantities fixed. In the $\overline{\text{MS}}$ scheme the renormalised β-function is defined by

$$\beta(g_r) \equiv \mu \frac{dg_r}{d\mu}\Big|_{g_0,a} = -b_0 g_r^3 - b_1 g_r^5 - b_2 g_r^7 - \ldots, \tag{5.21}$$

which is renormalisation scheme-dependent but independent of the regularisation. Using (5.4): $g_0 = Z_g(g_0, a\mu) g_r$ where

$$Z_g^2(g_0, a\mu) = 1 + L_0(a\mu) g_0^2 + L_1(a\mu) g_0^4 + \mathcal{O}(g_0^6), \tag{5.22a}$$

$$L_0(a\mu) = 2\beta_0 \ln a\mu + l_0 \tag{5.22b}$$

$$L_1(a\mu) = 2\beta_1 \ln a\mu + l_1, \tag{5.22c}$$

from dimensional arguments, and omitting lattice artifacts. The coefficients of the logarithms are set by differentiating with respect to the lattice spacing

$$\beta^{\text{L}}(g_0) = \frac{g_0}{Z_g(g_0, \mu a)} \left(\frac{\partial Z_g(g_0, \mu a)}{\partial g_0} \beta^{\text{L}}(g_0) - a \frac{\partial Z_g(g_0, \mu a)}{\partial a} \right), \tag{5.23}$$

and requiring that the *beta*-function be finite, that is independent of $\ln(\mu a)$. This also precludes any higher powers of the logarithms from appearing in (5.22b) and (5.22c). Differentiating with respect to the scale μ instead gives

$$0 = \beta(g_r) Z_g(g_0, \mu a) + g_r \mu \frac{\partial Z_g(g_0, \mu a)}{\partial \mu}, \tag{5.24}$$

and combining the two gives

$$\beta^{\text{L}}(g_0) = \frac{\beta(g_r(g_0))\ Z_g(g_0, \mu a)}{1 - \frac{\partial \ln Z_g}{\partial \ln g_0}}, \tag{5.25}$$

which relates the coefficients in (5.20) to (5.21). In particular

$$\begin{aligned} b_0^{\mathrm{L}} &= b_0 \\ b_1^{\mathrm{L}} &= b_1 \\ b_2^{\mathrm{L}} &= b_2 + b_0 l_1 - b_1 l_0. \end{aligned} \tag{5.26}$$

The constants l_0, l_1 are that part of the coefficients in (5.22a) that are independent of μ and a, and happen to be the quantities of interest for the $\alpha_{\mathrm{lat}} \leftrightarrow \alpha_{\overline{\mathrm{MS}}}$ calculation of the previous section; this is of course not an accident. The first two relations establish the well-known result that β_0 and β_1 are universal and independent of the renormalisation scheme. By using the third relation the much simpler two-loop constant is required to determine β_2 rather than the three-loop computation suggested by (5.23). The values of b_i in the $\overline{\mathrm{MS}}$ scheme for SU(3) are well known [68]:

$$b_0 = \frac{1}{(4\pi)^2}\left[11 - \frac{2}{3}n_f\right] \tag{5.27}$$

$$b_1 = \frac{1}{(4\pi)^4}\left[102 - \frac{38}{3}n_f\right] \tag{5.28}$$

$$b_2 = \frac{1}{(4\pi)^6}\left[\frac{2857}{2} - \frac{5033}{18}n_f + \frac{325}{54}n_f^2\right]. \tag{5.29}$$

The beta-function can be integrated through the renormalisation-group equation:

$$\left(-a\frac{\partial}{\partial a} + \beta^{\mathrm{L}}(g_0)\frac{\partial}{\partial g_0}\right)\Lambda_{\mathrm{L}} = 0, \tag{5.30}$$

where Λ_{L} is the renormalisation-group invariant mass in the lattice regularisation. The following is the particular solution

$$a\Lambda_{\mathrm{L}} = \exp\left[-\int^{g_0}\frac{dg}{\beta_{\mathrm{L}}(g)}\right]. \tag{5.31}$$

Consequently the asymptotic relation

$$a\Lambda_{\mathrm{L}} = \exp\left(-\frac{1}{2b_0 g_0^2}\right)\left(b_0 g_0^2\right)^{-\frac{b_1}{2b_0^2}}\left[1 + q\ g_0^2 + \mathcal{O}(g_0^4)\right], \tag{5.32}$$

is obtained which describes how the lattice cut-off $\Lambda_{\rm L}$ changes with the bare coupling. The linear correction q to the two-loop approximation of $\Lambda_{\rm L}$ is important in order to verify that the scaling in the continuum limit is well-behaved, and shows the onset of strong coupling in QCD. The non-universal, scheme dependent coefficient q, is made from the coefficients of the β-function:

$$q = \frac{b_1^2 - b_0 b_2^{\rm L}}{2b_0^3}, \tag{5.33}$$

and should be small.

5.1.2 Lattice Calculation

At one loop order the diagrams are given by figure 5.1, and the integral has the form:

$$\Gamma^{A,B}_{\rm lat}\Big|_{\mathcal{O}(g_0^2)} = \int_{-\pi}^{\pi} \left\{ \frac{F(k,p)}{P(k)} + \frac{G(k,p)}{P(k+p/2)\,P(k-p/2)} + H(k,p) \right\} \frac{d^4k}{(2\pi)^4} \tag{5.34}$$

setting $a = 1$ from now on. The function $F(k,p)$ comes from the tadpole vertex, $G(k,p)$ from the rainbow diagrams, and $H(k,p)$ from the zero-loop "lattice counter-term" diagram. $P(k)$ is the inverse gluon propagator. Useful information for extracting the form of the total in (5.34) was derived from (5.23) by substituting (5.22) — the coefficients of the logarithms. These results are very useful for the lattice calculation — constraining the curvature of $\nu^{(1)}$ and $\nu^{(2)}$ in $\ln(pa)$ to known values from previous $\overline{\rm MS}$ calculations, and at second order ensuring that total double logarithm vanishes. The leading logarithm at each order is shared between the continuum and the lattice, but furthermore because the lattice Feynman rules are identical to the continuum in the IR, they are the same for *each* diagram when done in the same gauge. The form of the total near the continuum limit

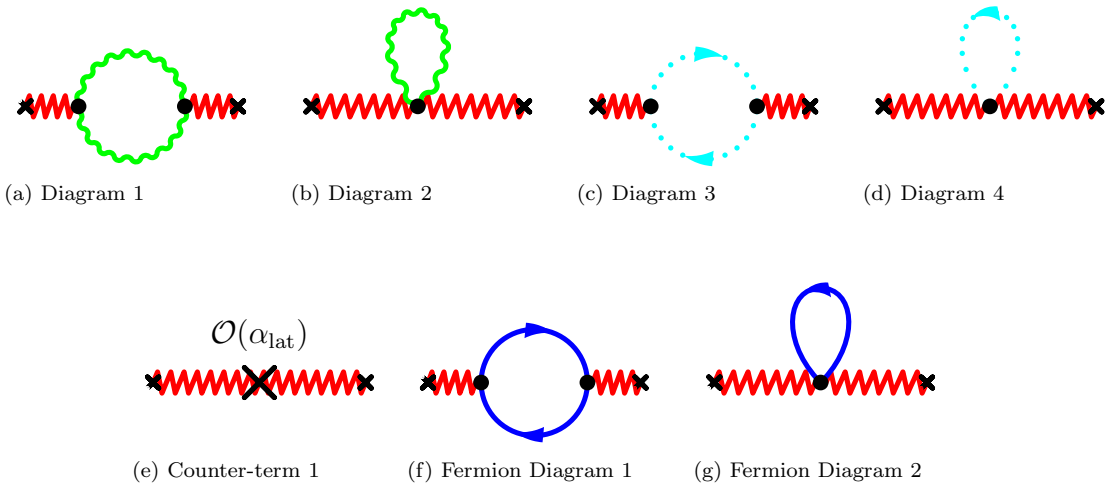

(a) Diagram 1 (b) Diagram 2 (c) Diagram 3 (d) Diagram 4

(e) Counter-term 1 (f) Fermion Diagram 1 (g) Fermion Diagram 2

Figure 5.1: One loop Background field diagrams. Figure (e) is a one-loop counter-term from $\mathcal{O}(\alpha_{\rm lat})$ corrections in the action (2.6).

$p \to 0$ is therefore

$$\Gamma^B_{\rm lat}\Big|_{\mathcal{O}(g_0^2)} = \hat{p}^2 \nu^{(1)}_{\rm lat}(p) = C_{\text{Quad Div.}} + p^2 \left(C_{\rm const} + b_0 \ln p^2\right) + \mathcal{O}(p^4, p^4 \ln p^2). \quad (5.35)$$

The lattice calculation has artifacts to all orders n in $(ap)^{2n} \ln^m[(ap)^2]$ for $m = \{0, 1\}$ (up to the leading logarithm), where p is the external background momentum. Unfortunately this means that deviations from the pure behaviour grow as ap is increased, which is where the integrals are easier. The quadratic divergence vanishes independently for pure glue, ghost and quark diagrams independently, which is a useful check. Afterwards the all important constant $C_{\rm const}$ can be extracted by subtracting the quadratic divergence in the integrand and forming

$$\frac{\nu^{(1)}_{\rm lat}(p) - \nu^{(1)}_{\rm lat}(0)}{4 \sin^2 P/2} = \left(C_{\rm const} + b_0 \ln p^2\right) + \mathcal{O}(p^2, p^2 \ln p^2), \quad (5.36)$$

for many different $p_\mu = (P, 0, 0, 0)$ in the range $P \in \{0.001 \to 1\}$ and fitting to (5.36). The numerical derivative in (5.36) and the fact that p is being used as the IR regulator shows that the integral has several widely varying scales in it. This means that for small p the statistical `VEGAS` errors are much larger as it has a more difficult time adapting to the integrand. For larger p the lattice artifacts come into play and grow to dominate the desired behaviour so there is a window of opportunity in the middle around $p \sim 0.1$ which controls the overall error obtainable for $C_{\rm const}$ using the numerical evaluation approach The extrapolation is performed using Bayesian techniques [50] with priors for the artifacts up to $p^{10} \ln p^2$ that are of order $C_{\rm const}$ and b_0 as appropriate.

The computation is easily extended to include fermions. Interestingly from the diagrams in figure 5.1 it is immediately obvious that the gluon action has no affect on the fermionic result at one-loop, and that the result is identical to the fermionic

contribution to $\omega^{(1)}_{\rm lat}$, the gluon self-energy. To complete the necessary one-loop calculations the gluonic part of $\omega^{(1)}_{\rm lat}(p)$ can be evaluated in exactly the same way, but where the logarithmic coefficient is slightly different. The final results are:

$$\omega^{(1)}_{\rm lat}(p,\xi=1) = -\frac{5}{16\pi^2}\ln p^2 + C_\omega + n_f\left[\frac{1}{24\pi^2}\ln p^2 + C_{n_f}\right], \tag{5.37a}$$

$$\nu^{(1)}_{\rm lat}(p,\xi=1) = -\frac{11}{16\pi^2}\ln p^2 + C_{\nu^{(1)}} + n_f\left[\frac{1}{24\pi^2}\ln p^2 + C_{n_f}\right], \tag{5.37b}$$

Using the known relationship between the $\overline{\rm MS}$ and potential schemes [63, 64]:

$$\alpha_{\overline{\rm MS}}\left(e^{-\frac{5}{6}}q\right) = \alpha_V(q)\left[1 + 0.63662\alpha_V(q) + (-0.73440 + 0.14110n_f)\alpha_V^2(q)\right], \tag{5.38}$$

and (5.13) to relate $\alpha_{\rm lat}$ to $\alpha_{\overline{\rm MS}}$ the relationship between $\alpha_{\rm lat}$ and α_V is then

$$\alpha_{\rm lat} = \alpha_V(q)\left[1 - v_1(q)\,\alpha_V(q) - v_2(q)\,\alpha_V^2(q)\right] + \mathcal{O}(\alpha_V^4), \tag{5.39a}$$

where

$$v_1(q) = \beta_0 \ln\left(\frac{\pi}{aq}\right)^2 + v_{1,0}, \tag{5.39b}$$

$$v_2(q) = \beta_1 \ln\left(\frac{\pi}{aq}\right)^2 - \left[v_1(q)\right]^2 + v_{2,0}, \tag{5.39c}$$

for $\beta_0 = (4\pi)b_0 = \frac{1}{4\pi}(11 - \frac{2}{3}n_f)$ and $\beta_1 = (4\pi)^2 b_1$. The one-loop constant pieces $C_\omega, C_{\nu^{(1)}}$ and $v_{1,0}$ are given in table 5.1.

However, the bulk of the work is in the two-loop calculation for $v_{2,0}$. The number of diagrams is much greater; $35+23n_f$, though the number in the continuum is only $10 + 4n_f$. They are shown in figures 5.2 and 5.3. The form in the continuum limit now has a double logarithm:

$$\begin{aligned}\hat{p}^2\nu_i^{(2)}(p) = c_{0,i} + c_{1,i}\sum_\mu \frac{p_\mu^4}{p^2} + p^2\left\{c_{2,i}\left[\frac{\ln p^2}{(4\pi)^2}\right]^2 + c_{3,i}\frac{\ln p^2}{(4\pi)^2} + c_{4,i}\right\} \\ + \mathcal{O}(p^4, p^4\ln p^2, p^4\ln^2 p^2),\end{aligned} \tag{5.40}$$

Table 5.1: One-loop background field matching results for the constant pieces (5.37), (5.39b) for various lattice actions. Very accurate Wilson results were checked to lower precision and are copied from [69].

Action	C_ω	C_ν	C_{n_f}	$v_{1,0}$
Wilson	0.37019 (0)	0.609629 (0)	−0.013732194 (5)	4.70181 (0) −5.110 (0) $\times 10^{-2} n_f$
Naïve	−	−	−0.00966162 (51)	− +0.481 (64)$\times 10^{-4} n_f$
Asqtad	0.31185 (6)	0.519660 (13)	−0.00967497 (42)	3.57123 (17)−1.196 (53)$\times 10^{-4} n_f$

Figure 5.2: Two-loop Background field diagrams (pure glue). The square vertex in **B**ackground **D**iagram 9 (BD9) and BD16 is from the measure term §2.2.1. BCTX are lattice counter-term diagrams which involve vertices from the $\alpha_{\rm lat}$ expansion of the action at $\mathcal{O}(\alpha_{\rm lat})$ (cross) and $\mathcal{O}(\alpha_{\rm lat}^2)$ (double-cross) given in (2.6).

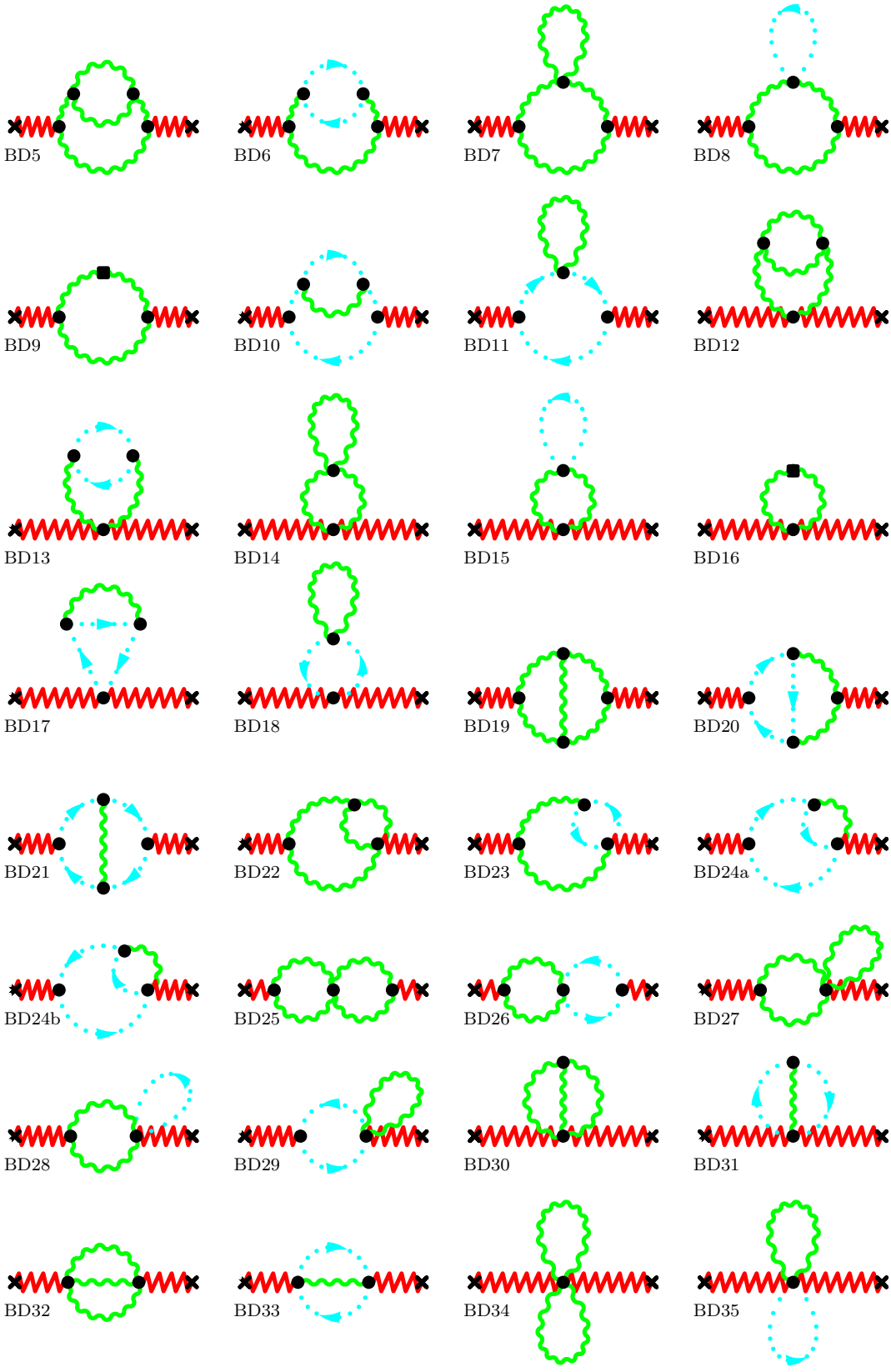
BD5
BD6
BD7
BD8
BD9
BD10
BD11
BD12
BD13
BD14
BD15
BD16
BD17
BD18
BD19
BD20
BD21
BD22
BD23
BD24a
BD24b
BD25
BD26
BD27
BD28
BD29
BD30
BD31
BD32
BD33
BD34
BD35

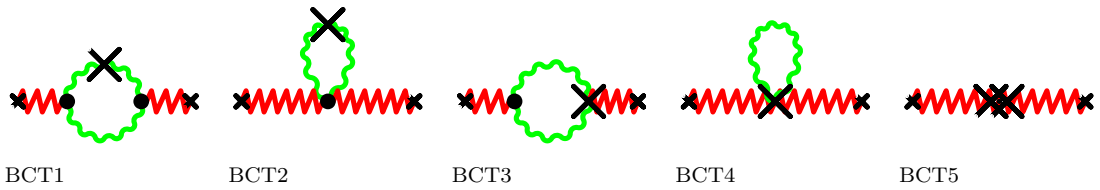

The lattice counter-term diagrams from (2.6). The double-cross in background counter-term diagram 5 is $\mathcal{O}(\alpha_{\rm lat}^2)$.

for the ith diagram. The double logarithms $c_{2,i}$ are shared with the continuum, the quadratic divergences $\sum_i c_{0,i}$ vanish independently for the sum of gluon, ghost and fermion diagrams, abd $\sum_i c_{1,i}$ vanishes because Lorentz invariance is restored in the continuum limit. The all important constant piece $\sum_i c_{4,i}$ can be extracted from a fit in a similar manner to (5.36). The coefficients have a simple dependence on N, the number of colours: $c_{n,i} = c_{n,i}^{(0)}/N^2 + c_{n,i}^{(1)} + c_{n,i}^{(2)}N^2 + n_f(c_{n,i}^{(-f)}/N + c_{n,i}^{(f)}N)$, but for simplicity results are given only for $N = 3$. An example of the fitting for gluon diagram 19 (figure 5.3), one of the noisest diagrams for the Asqtad action, is shown in figure 5.4, along with the fit parameters in table 5.2. Although the double logarithms are individually shared with the continuum, it is only the sum of the single logarithms, $\sum_i c_{3,i}$ on the lattice that is constrained to be β_1. Applying this constraint to the sum reduces the error in the constant by about a factor of $3-5$, and the final fit for the highly improved Asqtad action is shown in figure 5.5.

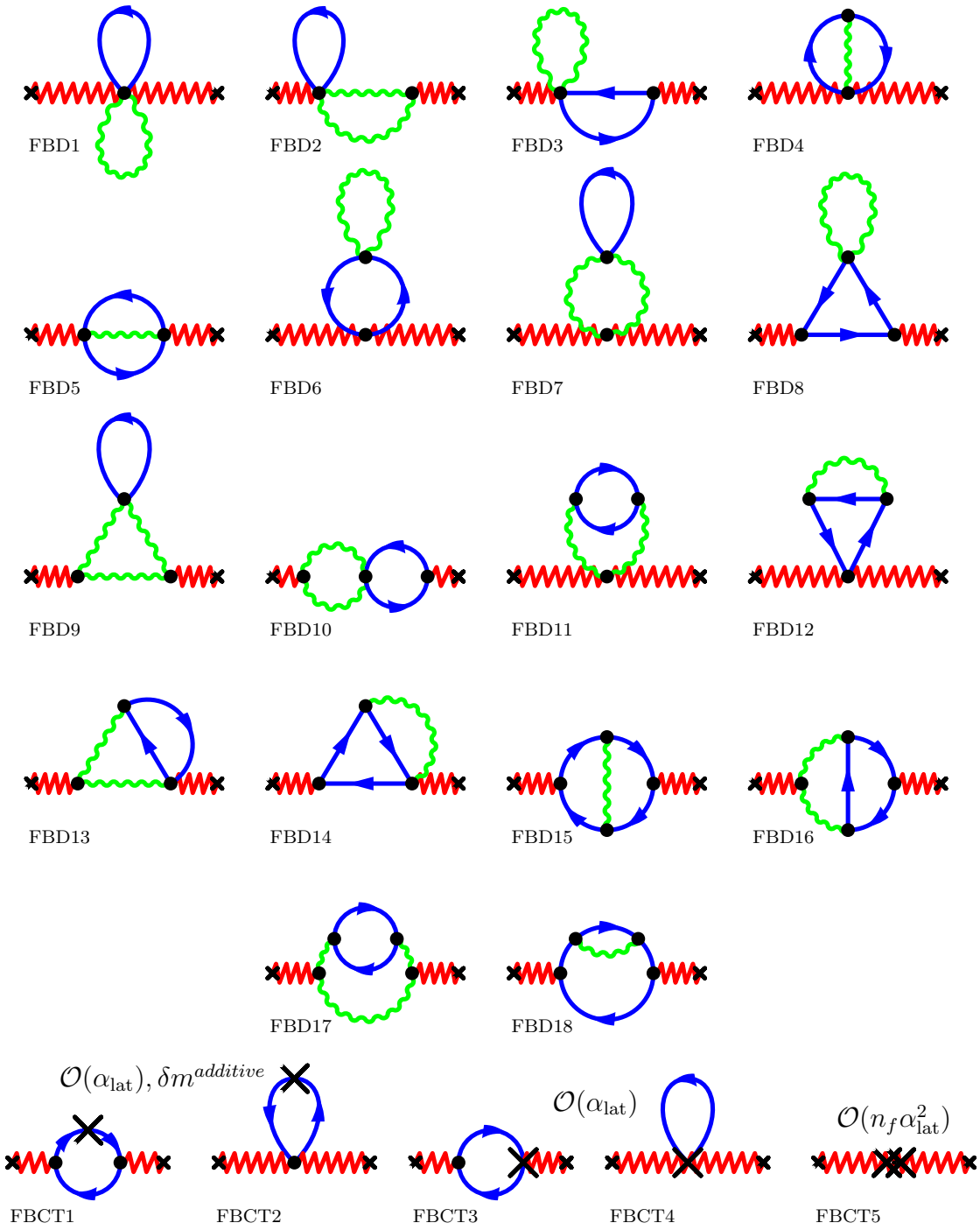

Figure 5.3: Two-loop **F**ermionic **B**ackground field **D**iagrams. The numbering scheme comes from [69]. After combining 7+11 and 9+17 everything is IR finite. 15-18 are the 4 continuum diagrams, and the last row are one- and two-loop lattice counter-term diagrams from (2.6).

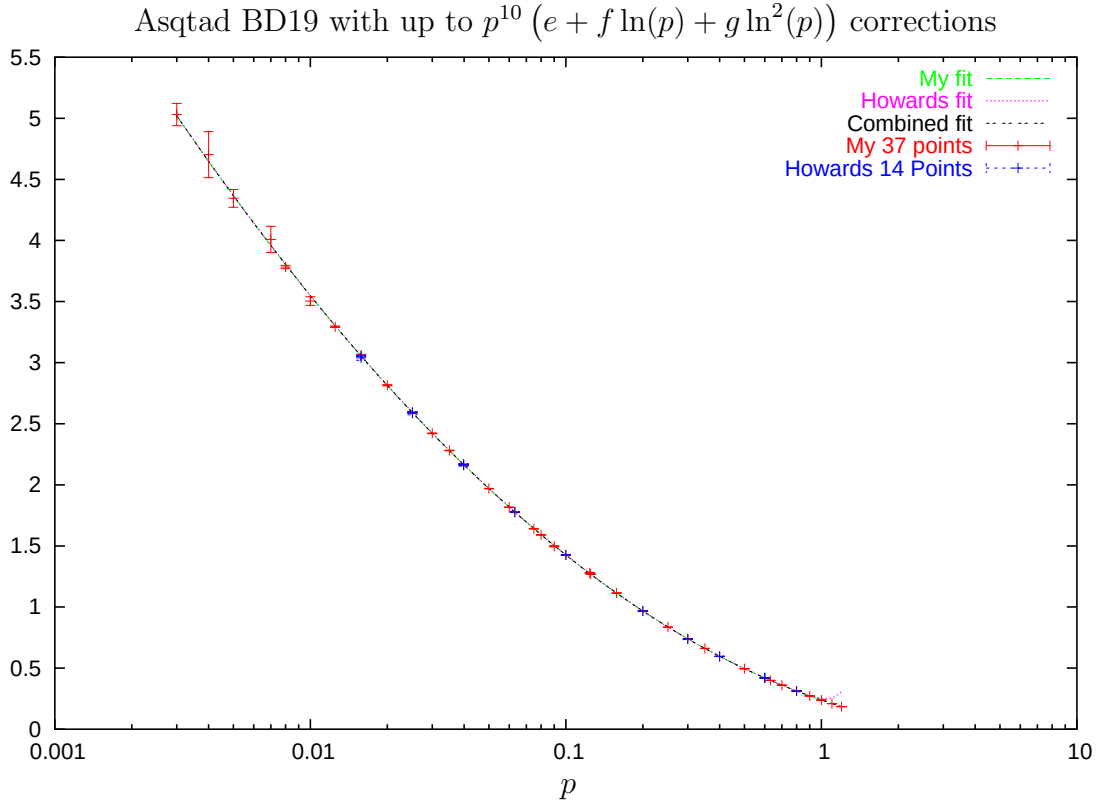

Figure 5.4: A sample fit for gluon diagram 19 in figure 5.3, one of the noisest, against the external momentum p in a semi-log plot. The curvature is the double logarithm with coefficient $3\frac{3}{8}$, and the constant, logarithm and artifacts are fit for. The two independent evaluations clearly agree and easily track the curve over almost three decades. Note that the errors increase at smaller p.

Table 5.2: The conservative fit parameters corresponding to the plot in figure 5.4 for diagram 19 in figure 5.3. The priors were $0 \pm \frac{1}{9}$ which corresponds to $1 \times \alpha_{\text{lat}}$ for all the lattice artifacts. The continuum coefficient c_2 was fixed to 3.375 but c_3 and c_4 started at 0 ± 3. The fit is insensitive to many of the lattice artifacts, particularly the double-logarithms and had a χ^2/d.o.f. of 0.42 from 37; equally good fits can be made only keeping terms to $\mathcal{O}(p^6)$.

	Constant	Log	Double-Log
Continuum	$0.205 \underset{c_4}{} \quad (5)$	$-0.1660 \underset{c_3}{} \quad (8)$	$3.375 \underset{c_2}{} \quad (10^{-9})$
p^2	$0.034 \quad (56)$	$-0.035 \quad (65)$	$0.032 \quad (43)$
p^4	$0.005 \quad (77)$	$-0.005 \quad (99)$	$0.002 \quad (100)$
p^6	$-0.004 \quad (80)$	$-0.005 \quad (100)$	$0.001 \quad (110)$
p^8	$-0.007 \quad (81)$	$0.004 \quad (100)$	$0.006 \quad (110)$
p^{10}	$0.005 \quad (56)$	$-0.001 \quad (79)$	$-0.020 \quad (73)$

New diagram by diagram results for the continuum coefficients are shown in table 5.3 for the one-loop improved Symanzik gluon action and the n_f dependence in table 5.4 for improved staggered, and in table 5.5 for unimproved Wilson glue with Naïve quarks. The vanishing of the total quadratic divergence is one important check that is satisfied to better than one part in a thousand. Another important check is that the coefficient of the single logarithm correctly matches β_1. The results for this for the most expensive action, Asqtad, are much less than one sigma, and accurate to better than 6%. The fermionic result for staggered fermions, which must be divided by 16, explicitly shows that staggered fermions have exactly 16 on-shell quarks per flavour at two-loop order. Previous results for Wilson glue [20], Wilson quarks [67] and Clover quarks [70] were reproduced at some lower accuracy as an additional check of the codes. Fitting the results for each diagram but constraining the total logarithm to β_1 the final conversion formula to the coupling α_V is (5.39). The final result of this section is table 5.6, where the last line alone constitutes about 5 GHz-CPU-years each for the two independent evaluations. Constraining the logarithm is worth an additional factor of 2-3 in the error for the constant, and so two columns are shown: an individual fit to each diagram and the global fit, denoted "MFit". For Wilson quarks [67] was checked, but unfortunately there is a discrepancy over c_4 for FBD14 and FBD16, that significantly affects the result. Until this is satisfactorily resolved it is not clear whose calculation is in error. The same principal author extended the calculation to Clover fermions in [70] which was also checked to a few % accuracy for $c_{SW} = 1$ and was found to be in agreement.

The values of $\beta_2 = (4\pi)^3 b_2$ for the bare lattice scheme and q, the linear correction to asymptotic scaling can be determined from $b_2^L = b_2^{\overline{\rm MS}} + b_0 l_1 - b_1 l_0$, using

$d_1(1) = -l_0$ and $d_2(1) = d_1(1)^2 - l_1$. The results in table 5.7 show once again that the bare lattice coupling is not a great choice of scheme, and that Clover fermions with unimproved glue have alarmingly large c_{SW}^2 contributions.

Table 5.3: The final fit parameters (5.40) for the gluonic two-loop background field diagrams in figure 5.2 for the one-loop Symanzik improved gluon action. The columns denoted "MFit" are huge 200+ degree-of-freedom fits to all of the data simultaneously with conservative priors ($\chi^2 < 1$), to their left is an individual agressive fit tuned for each diagram.

Asqtad	$c_0 \times \frac{(4\pi)^2}{9}$	$c_2 \times \frac{1}{9}$	$c_3 \times \frac{(4\pi)^2}{9}$	$c_3 \times \frac{(4\pi)^2}{9}$ Mfit	$c_4 \times \frac{(4\pi)^2}{9}$	$c_4 \times \frac{(4\pi)^2}{9}$ Mfit
BD5	0.1187 (9)	15/4	−0.09189 (101)	−0.09165 (54)	0.09134 (660)	0.09231 (310)
BD6	0.1396 (2)	5/12	−0.02609 (73)	−0.02672 (29)	0.07631 (469)	0.07183 (160)
BD7	3.3654 (43)		−0.19739 (119)	−0.19643 (60)	0.89513 (766)	0.90234 (340)
BD10	−0.0192 (3)	1/6	−0.00807 (59)	−0.00768 (27)	0.01321 (389)	0.01575 (150)
BD11	−0.2695 (3)		−0.00714 (19)	−0.00708 (10)	0.01666 (138)	0.01705 (66)
BD12	−0.1036 (48)				−0.02633 (15)	−0.02624 (10)
BD13	−0.1252 (2)				0.01486 (2)	0.01487 (1)
BD14	−0.9218 (51)				0.43865 (20)	0.43870 (17)
BD17	0.0474 (1)					
BD18	0.1347 (4)					
BD19	0.3864 (150)	27/8	−0.16599 (75)	−0.16574 (39)	0.20522 (498)	0.20746 (220)
BD20	−0.0040 (1)	-1/4	0.00616 (45)	0.00650 (21)	−0.01011 (305)	−0.00785 (120)
BD21	−0.0259 (0)	1/24	−0.00440 (18)	−0.00430 (10)	0.00676 (128)	0.00743 (60)
BD22	−0.7963 (43)	-9/8	−0.07652 (201)	−0.07824 (110)	0.36786 (1086)	0.36007 (560)
BD23	−0.0246 (1)	-5/24	0.01597 (54)	0.01563 (29)	−0.04477 (359)	−0.04706 (160)
BD24	0.0452 (90)	-1/6	0.00646 (111)	0.00778 (76)	−0.02987 (612)	−0.02414 (400)
BD25	0.1187 (1)	-6	0.24104 (54)	0.24088 (33)	−0.37400 (407)	−0.37528 (200)
BD27	−5.1098 (66)		0.23284 (62)	0.23241 (41)	−0.99849 (507)	−1.00214 (290)
BD29	0.2695 (0)		0.00717 (6)	0.00710 (2)	−0.01658 (44)	−0.01711 (13)
BD30	−2.3985 (25)				−0.05893 (9)	−0.05881 (4)
BD31	0.1738 (0)					
BD32	2.7727 (81)		0.019 (0)	0.01899 (0)	0.06403 (406)	0.06188 (300)
BD33	−0.1936 (6)				0.00624 (13)	0.00642 (7)
BD34	2.5629 (41)				0.29171 (73)	0.29126 (61)
BD35	−0.1349 (4)					
Sum	0.0080 (229)	0	−0.05096 (322)	$-\frac{1}{2\pi^2}$	Sum 0.92890 (2012)	0.92872 (401)
|Sum|	20.2617				CT −0.42037 (75)	−0.42037 (75)
					Final 0.50853 (2014)	0.50835 (408)

Table 5.4: The final fit parameters (5.40) for the fermionic two-loop background field diagrams in figure 5.3 for the one-loop Symanzik improved gluon and improved staggered quark action (Asqtad).

Asqtad	$c_0 \times \frac{(4\pi)^2}{9}$	$c_2 \times \frac{1}{9}$	$c_3 \times \frac{(4\pi)^2}{9}$	$c_3 \times \frac{(4\pi)^2}{9}$ Mfit	$c_4 \times \frac{(4\pi)^2}{9}$	$c_4 \times \frac{(4\pi)^2}{9}$ Mfit
FD1	9.255 (36)				−0.00267 (1)	−0.00267 (1)
FD2	13.769 (26)				−0.00383 (2)	−0.00384 (1)
FD3	−32.347 (16)		−0.0676 (6)	−0.06792 (6)	0.00978 (71)	0.00918 (37)
FD4	−11.921 (12)				−0.00056 (0)	−0.00056 (0)
FD5	6.285 (6)				−0.00180 (2)	−0.00181 (2)
FD6	−14.936 (3)				−0.00033 (0)	−0.00033 (0)
FD7+11	8.385 (13)				−0.00457 (0)	−0.00457 (0)
FD8	28.884 (45)		0.0566 (2)	0.05653 (2)	−0.01388 (14)	−0.01381 (10)
FD10	4.313 (6)		0.0115 (0)	0.01155 (0)	−0.00212 (4)	−0.00213 (2)
FD12	6.203 (37)				0.00020 (0)	0.00019 (0)
FD13	1.504 (11)				0.00098 (4)	0.00093 (3)
FD14	9.771 (8)		0.0244 (4)	0.02475 (5)	−0.00527 (21)	−0.00507 (27)
FD15	−0.343 (3)	1/27	−0.0031 (1)	−0.00305 (1)	0.00035 (6)	0.00033 (6)
FD16	6.298 (7)	4/3	−0.0251 (4)	−0.02485 (3)	−0.00137 (24)	−0.00123 (19)
FD9+17	−21.325 (15)	-5/3	0.0608 (9)	0.06115 (9)	−0.01610 (49)	−0.01595 (49)
FD18	−13.892 (41)	8/27	−0.0393 (10)	−0.03986 (9)	0.00810 (52)	0.00780 (51)
Sum	−0.096 (90)	0	0.0183 (16)	$\frac{26}{9(4\pi)^2}$	Sum −0.03310 (107)	−0.03352 (17)
|Sum|	189.432				CT −0.00550 (0)	−0.00550 (0)
					Final −0.03860 (107)	−0.03902 (17)

Table 5.5: The final fit parameters (5.40) for the fermionic two-loop background field diagrams in figure 5.3 for unimproved Wilson gluon action with Naïve quarks.

Naïve	$c_0 \times \frac{(4\pi)^2}{9}$	$c_2 \times \frac{1}{9}$	$c_3 \times \frac{(4\pi)^2}{9}$	$c_3 \times \frac{(4\pi)^2}{9}$ Mfit	$c_4 \times \frac{(4\pi)^2}{9}$	$c_4 \times \frac{(4\pi)^2}{9}$ Mfit
FD1	9.255 (36)				−0.00267 (1)	−0.00267 (1)
FD2	13.769 (26)				−0.00383 (2)	−0.00384 (1)
FD3	−32.347 (16)		−0.0676 (6)	−0.06792 (6)	0.00978 (71)	0.00918 (37)
FD4	−11.921 (12)				−0.00056 (0)	−0.00056 (0)
FD5	6.285 (6)				−0.00180 (2)	−0.00181 (2)
FD6	−14.936 (3)				−0.00033 (0)	−0.00033 (0)
FD7+11	8.385 (13)				−0.00457 (0)	−0.00457 (0)
FD8	28.884 (45)		0.0566 (2)	0.05653 (2)	−0.01388 (14)	−0.01381 (10)
FD10	4.313 (6)		0.0115 (0)	0.01155 (0)	−0.00212 (4)	−0.00213 (2)
FD12	6.203 (37)				0.00020 (0)	0.00019 (0)
FD13	1.504 (11)				0.00098 (4)	0.00093 (3)
FD14	9.771 (8)		0.0244 (4)	0.02475 (5)	−0.00527 (21)	−0.00507 (27)
FD15	−0.343 (3)	1/27	−0.0031 (1)	−0.00305 (1)	0.00035 (6)	0.00033 (6)
FD16	6.298 (7)	4/3	−0.0251 (4)	−0.02485 (3)	−0.00137 (24)	−0.00123 (19)
FD9+17	−21.325 (15)	-5/3	0.0608 (9)	0.06115 (9)	−0.01610 (49)	−0.01595 (49)
FD18	−13.892 (41)	8/27	−0.0393 (10)	−0.03986 (9)	0.00810 (52)	0.00780 (51)
Sum	−0.096 (90)	0	0.0183 (16)	$\frac{26}{9(4\pi)^2}$	Sum −0.03310 (107)	−0.03352 (17)
|Sum|	189.432				CT −0.00550 (0)	−0.00550 (0)
					Final −0.03860 (107)	−0.03902 (17)

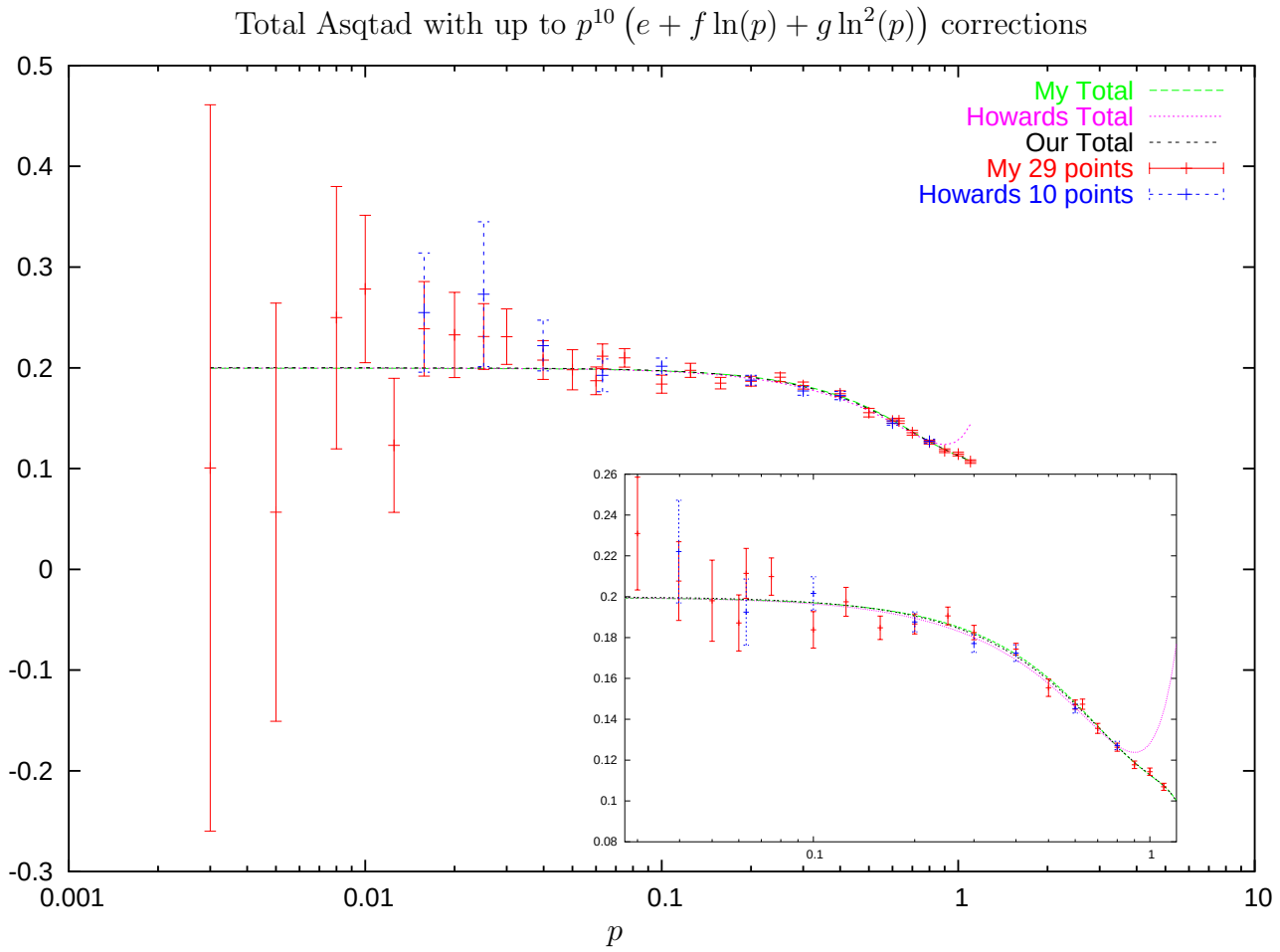

Figure 5.5: The final fit for the constant in $\nu^{(2)}_{\rm lat} = \sum_i c_{4,i} + \beta_1 \ln p$, after the known logarithm, β_1 was subtracted out, shown over the complete range of external momenta calculated for the Asqtad action. Inset shows that data for $p \sim 0.1$ controls the quality of the final fit, and the agreement between the two independent evaluations.

Table 5.6: $\alpha_{\rm lat} \to \alpha_V$ matching to two-loop order for several actions (5.39). The Wilson result uses the impressive accuracy of [67] but differs for two diagrams. The Clover result is from [71], is additional to the Wilson value, and was checked to lower accuracy. The Asqtad action result shown is the first improved gluon action matching calculation.

Action	$v_{1,0}$	$v_{1,0}^{n_f}$	$v_{2,0}$	$v_{2,0}^{n_f}$
Naïve	4.70181	4.81 (64) $\times 10^{-5}$	9.52806	−0.5440 (65)
Wilson	4.70181	5.110423 (6) $\times 10^{-2}$	9.52806	−0.67697 (81)
Clover		6.3419 c_{SW}^1 $\times 10^{-2}$		−0.0245 c_{SW}^1
		37.5024 c_{SW}^2 $\times 10^{-2}$		2.0266 c_{SW}^2
				0.0749 c_{SW}^3
				0.0164 c_{SW}^4
Asqtad	3.57123 (17)	−1.196 (53) $\times 10^{-4}$	5.382 (39)	−1.0511 (51)

Table 5.7: Results for the non-universal three-loop scheme dependent coefficient β_2 for all the actions. The linear correction to asymptotic scaling of the Λ-parameter, (5.32) is also shown for three flavours. The Clover results are shown as a power series in c_{SW} which should be *added* to the Wilson numbers. The correction to asymptotic scaling is quite pronounced in the three lattice actions with unimproved glue, and Clover fermions have an extremely large c_{SW}^2 contribution. The numerical values for SU(3) in the $\overline{\rm MS}$ and potential (V) schemes are shown for comparison.

Scheme	$\beta_2\vert_{n_f=0}$	$\beta_2^{n_f}$	$\beta_2^{n_f^2}$	$q\vert_{n_f=3}$
$\overline{\rm MS}$	0.7199	−0.1409	0.0030	−0.0074
V	0.0011	−0.0002	0.0000	−0.0672
Naïve	−3.1747	0.2286 (57)	−0.0183 (3)	0.2237 (1)
Wilson	−3.1747	0.3120 (7)	−0.2130 (7)	0.2063 (1)
c_{SW}^1		0.0624 (1)	−0.0064 (1)	−0.0101 (1)
c_{SW}^2		−2.0162 (1)	0.1376 (1)	0.3731 (1)
c_{SW}^3		−0.0655 (1)	0.0040 (1)	0.0125 (1)
c_{SW}^4		−0.0144 (1)	0.0009 (1)	0.0027 (0)
Asqtad	−0.284 (32)	0.5436 (45)	−0.0452 (3)	−0.0551 (20)

5.2 Fruit Loops

In principle these are the simplest calculations for lattice perturbation theory: Wilson loops have a large $q^* \sim \pi/a$ and are dominated by UV physics for which the Feynman rules regulate themselves, have IR divergences only a small set of 2PI diagrams contributing to insertions of one-loop propagators that are easily removed, §2.4, and no external quark lines. The simplest Wilson loop, the plaquette is the only lattice quantity that has been computed to three-loops by the diagrammatic method, even that was only for the most unimproved action and there are more than 150 diagrams at third order. A trick can be used to significantly reduce the work required by approximately halving the number of diagrams and removing one of the propagators [72]. This is a very useful step for the unimproved actions which have diagonal propagators in Feynman gauge but incredibly useful for improved glue where the additional sum over Lorentz indices would be very expensive. The trick is to convert the expectation of a simple observable like the plaquette which is *already* in the action to the calculation of its susceptibility in the usual manner from Statistical Mechanics. Schematically for an action containing $\beta\Box$ and other things S' in the action S:

$$\langle \Box \rangle = \frac{1}{Z} \int \mathcal{D}U \; \Box \; e^{-\beta\Box - S'} \tag{5.41}$$

$$= 1 + \frac{1}{6}\frac{1}{V}\frac{\partial \ln Z}{\partial \beta}, \tag{5.42}$$

where Z is the partition function and $\ln Z$ is the sum of 1PI vacuum bubbles. For the unimproved action where the plaquette *is* the gluon action and the only term with an explicit β, the derivative with respect to its coefficient in the action can

be with respect to the coupling $\beta = \frac{6}{g^2}$:

$$S_G^{\text{Unimp.}} = \beta \sum_x (1 - \frac{1}{3} \operatorname{Re} \operatorname{Tr} \square), \tag{5.43}$$

which can be therefore be done *after* expanding (5.42) in powers of α_s and integrating. The additional 1 is to compensate for the $\beta \times V$ in (5.43) and the factor of $\frac{1}{6}$ is because there are actually six plaquettes in the action in different orientations, but the expectation of only one is required. This was the technique used in the two previous papers [72,69]. However for the improved action which has rectangle and corner-cube paths also multiplied by β, or for expectations of other Wilson loops not present in either action the method needs to be generalised and the derivative should actually be done with respect to the coefficient when evaluating the diagram. Consider the generating functional

$$Z[J] = \int \mathcal{D}U \, \mathcal{D}\psi \; e^{-S[U,\psi] - J\phi}. \tag{5.44}$$

By analogy to Statistical Mechanics the derivative of the Free Energy is the susceptibility:

$$\langle \phi \rangle = -\frac{1}{V} \left. \frac{d \ln Z[J]}{dJ} \right|_{J=c} \tag{5.45}$$

where c should be the coefficient of ϕ in the action, possibly zero. The more general method of (5.45) reduces to that used in the unimproved action (5.42) only in a funny gauge to compensate for the fact that the gauge-fixing term is not multiplied by β. The susceptibility (5.45) can be calculated order by order in α_s by expanding $\ln Z$ and evaluating vacuum bubble Feynman diagrams. The new derivative is effectively putting the extra propagator back into the integrand, but saving the cost of having to multiply its 16 entries by different combinations of other vertices and summing. The derivative can be very efficiently implemented via

the technique of automatic differentiation [73], or by simple numerical differencing over an interval of $10^{-\{3,4\}}$. Except for the largest vertices, most of the computer time spent in integrating is actually on evaluating the sum over Lorentz indices and *not* on evaluating the vertices themselves, §2, and the cost of an automatic derivative is negligible. The fermionic contribution is in the form of quark loops but the formalism and implementation are not affected. The calculation is IR finite after appropriate grouping of diagrams and thus can be done in the infinite volume limit. Spherical transforms §2.3 are only helpful for subtracted diagrams. The first order calculation is done with the direct method (2.8) and the second order can easily be done by both direct and susceptibility methods and in various gauges as a check of correctness. The third order calculation is more difficult and takes about 22 GHz-CPU-days each for the pure gluonic and for the fermionic loops for the most highly improved action available – that used by the "MILC" collaboration and for a fixed number of integration points the time taken is roughly independent of the loop being calculated over the range used – 1x1, 1x2, 1x3 and 2x2. The error increases somewhat as the area of the loop is increased. For the final expansion in the preferred coupling, α_V, however the error is dominated by the more difficult background field scheme-matching calculation. The results for the expectation of different Wilson loops of size $R \times T$ are calculated in terms of the bare lattice coupling $\alpha_{\rm lat}$:

$$\langle W(R,T)\rangle = 1 - w_0\,\alpha_{\rm lat} - w_1\,\alpha_{\rm lat}^2 - w_2\,\alpha_{\rm lat}^3 + \mathcal{O}(\alpha_{\rm lat}^4). \tag{5.46}$$

The one- and two-loop diagrams contributing to w_0 and w_1 are shown in figures 5.6 and 5.7. New results for each diagram's contribution to w_2 and for a variety of actions at third order are shown for SU(3) for the diagrams in figure 5.8 in table 5.8 with the fermionic n_f dependence in figure 5.9 and table 5.9. However the seri are

rather divergent. The plaquette is not a physical quantity as it has no continuum analogue and is therefore not expected to have a well-behaved expansion. However, large Wilson loops are related to δm, the mass generated in the lattice formulation of heavy quark effective theory, HQET. In weak-coupling perturbation theory the potential between static-quarks falls like $1/r$ in their separation r, the expectation value of large Wilson loops decreases exponentially with the perimeter of the loops, specifically:

$$W(R,T) = \exp\left(ig \oint_{R,T} A \cdot dx\right) \tag{5.47}$$

$$\langle W(R,T)\rangle \sim e^{-2\,\delta m\,(R+T)}, \tag{5.48}$$

so a better behaved expansion than (5.46) should be

$$-\frac{\ln\langle W(R,T)\rangle}{2(R+T)} = \frac{w_0}{2(R+T)}\alpha_{\rm lat}\left[1 + a_1\,\alpha_{\rm lat} + a_2\,\alpha_{\rm lat}^2 + \mathcal{O}(\alpha_{\rm lat}^3)\right], \tag{5.49}$$

where w_0 is expected to be $\mathcal{O}(1)\times 2(R+T)$. The final result of this section converts to the renormalised coupling $\alpha_V(q^*)$, evaluated at the Brodsky-Lepage-Mackenzie scale q^* [6] appropriate for each operator

$$-\frac{\ln\langle W(R,T)\rangle}{2(R+T)} = \frac{w_0}{2(R+T)}\alpha_V\left[1 + r_1\,\alpha_V + r_2\,\alpha_V^2 + \mathcal{O}(\alpha_V^3)\right]. \tag{5.50}$$

Each perturbative coefficient is split into gluonic and fermionic components:

$$\begin{aligned} w_i &\equiv w_{i,g} + \sum_{j=1}^{i} w_{i,f}^{(j)} n_f^j \\ a_i &\equiv a_{i,g} + \sum_{j=1}^{i} a_{i,f}^{(j)} n_f^j \\ r_i &\equiv r_{i,g} + \sum_{j=1}^{i} r_{i,f}^{(j)} n_f^j, \end{aligned} \tag{5.51}$$

so that the three-loop coefficients, w_2, a_2 and r_2, which can have two fermion loops, have a n_f^2 contribution, while the two-loop coefficients have only n_f pieces. For

staggered quarks the perturbation theory is done unstaggered and quark loops are divided by 16 so that n_f is the number of light quarks simulated, §2.2.2. These have been checked by independent evaluation using two separate implementations of the Feynman rule generators, momentum routings and diagram evaluations, in two different languages with compilers from different vendors. The 1×1 plaquette for unimproved glue was also checked diagram by diagram using the direct methods against the first calculation [72] which is effectively a test of gauge invariance and of the susceptibility method. The fermionic part was checked for several (m, R) values against the Wilson quark totals in [69]. The gauge invariance of the Asqtad plaquette was explicitly tested by evaluating at $\xi = 1$ and $\xi = 2$.

Final results for the coefficients w_i, a_i and r_i are given in table 5.10. The last expansion (5.50) has coefficients r_1 and r_2 that depend on q^* and require knowing the matching between two schemes, $\alpha_{\rm lat}(\alpha_V)$ to two-loops that is worked out in table 5.6 from §5.1. Values are also given for the two Creutz ratios [62] that can be made from the four Wilson loops. Creutz ratios are certain combinations of Wilson loops designed to access the behaviour of the Wilson loops that is sub-leading to the perimeter and capture the string tension which comes proportional to the area. Creutz ratios of large Wilson loops are expected to be better behaved and are at a lower scale $q^* \sim 1.15$ compared to $q^* \sim 3$ for the Wilson loops; thereby allowing a determination of α_s over a larger range.

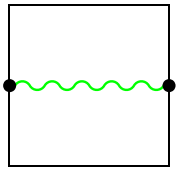

Figure 5.6: One-loop Feynman diagram for the expectation of a Wilson loop.

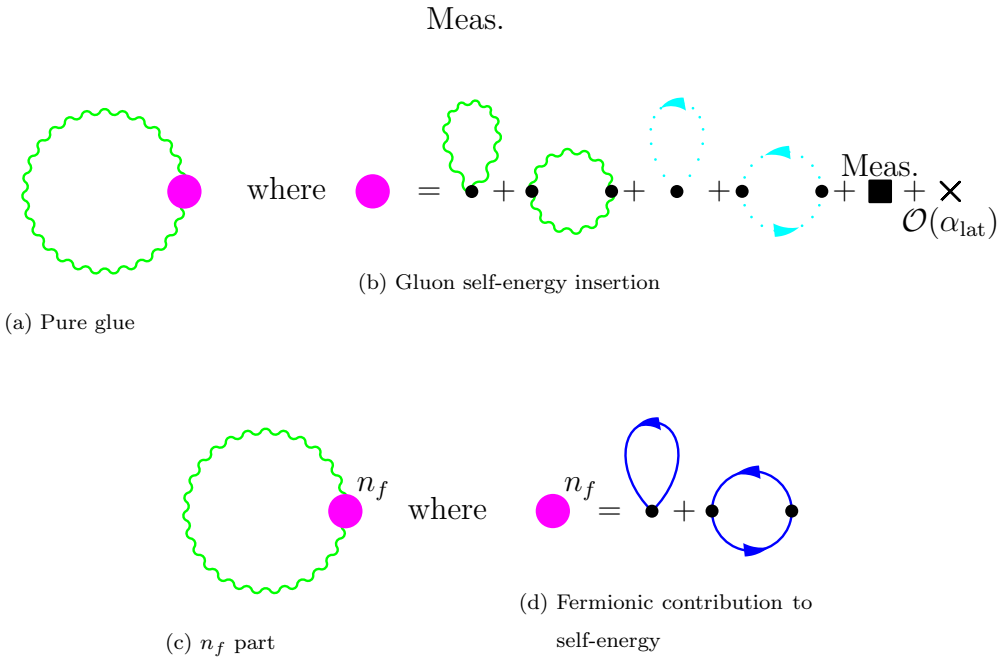

(a) Pure glue

(b) Gluon self-energy insertion

(c) n_f part

(d) Fermionic contribution to self-energy

Figure 5.7: The two loop Feynman diagrams for the expectation of a Wilson loop, evaluated from derivatives of vacuum bubbles using the susceptibilty method (5.45). The magenta vertex defines the amputated one-loop gluon propagator. The square vertex comes from the measure, and the cross from $\mathcal{O}(\alpha_{\rm lat})$ "lattice counter-terms" in the action. This contribution is drawn and evaluated separately from the 1PI insertion at higher orders where it is expedient to keep all the counter-terms together in order to keep the N_{colour} factors straight and to distinguish different $\mathcal{O}(\alpha_{\rm lat})$-improved actions.

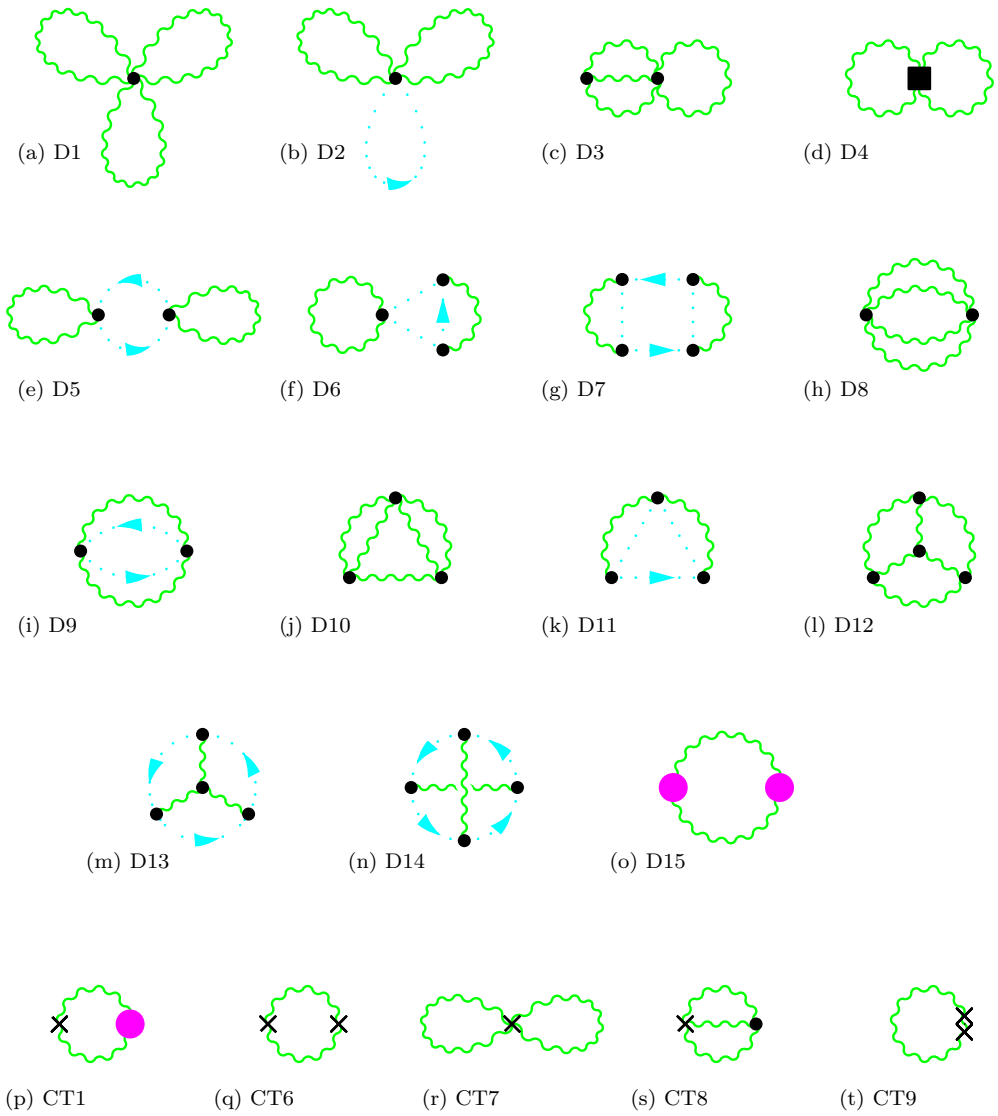

Figure 5.8: The three-loop pure glue Feynman diagrams for the expectation of a Wilson loop, evaluated from derivatives of vacuum bubbles using the susceptibilty method (5.45). The magenta vertex is the amputated one-loop gluon propagator of figure 5.7. The diagram numbering is consistent with [72]. The lattice counter-terms are shown separately. The square vertex g^4A^4 comes from the measure, and the cross, [double-cross] from $\mathcal{O}(\alpha_{\rm lat}^{[2]})$ terms in the action.

Table 5.8: The diagram by diagram results for the gluonic loops of figure 5.8 in $\alpha_{\rm lat}^3$ for Wilson loops of various sizes for both improved (one-loop Symanzik glue) and unimproved Wilson-glue actions, evaluated using the susceptibility method.

Asqtad	1x1	1x2	1x3	2x2
D1	0.7116 (63)	−21.4081 (211)	−71.7507 (837)	–114.6867 (3224)
D2	0.2476 (1)	0.5752 (2)	0.9113 (4)	1.3245 (7)
D3	10.2236 (80)	35.4147 (355)	59.9474 (1212)	102.4075 (1640)
D4	0.2475 (1)	0.5750 (1)	0.9112 (3)	1.3245 (5)
D5	0.2474 (1)	0.5747 (2)	0.9107 (4)	1.3231 (6)
D6	0.1409 (1)	0.3397 (2)	0.5475 (6)	0.8175 (10)
D7	0.0097 (1)	0.0280 (2)	0.0489 (4)	0.0794 (7)
D8	−2.9711 (31)	−11.3644 (213)	−19.0987 (301)	−28.7640 (843)
D9	0.0958 (0)	0.2268 (1)	0.3627 (2)	0.5289 (3)
D10	−0.0129 (17)	1.9599 (94)	4.0012 (375)	3.4002 (976)
D11	0.0559 (1)	0.1416 (2)	0.2323 (8)	0.3506 (14)
D12	−0.3323 (5)	−1.8326 (28)	−3.6707 (78)	−6.4475 (129)
D13	0.0184 (1)	0.0600 (3)	0.1079 (8)	0.1797 (13)
D14	0.0041 (0)	0.0121 (1)	0.0213 (3)	0.0358 (4)
D15	−16.3955 (146)	−13.0171 (533)	15.3298 (910)	21.3372 (688)
Sum	−7.7095 (181)	−7.7146 (714)	−11.1878 (1799)	−16.7894 (3904)
CT	−6.2354 (127)	−4.2333 (154)	8.2513 (276)	19.4253 (458)
Total	−13.9448 (221)	−11.9478 (730)	−2.9365 (1820)	2.6359 (3930)

Wilson	1x1	1x2	1x3	2x2
D1	Impressive precision using the direct method of (5.42) is available per diagram in [72]	−4.4756 (945)	−83.7436 (5622)	–136.5500 (5217)
D2		1.0453 (3)	1.5897 (6)	2.1859 (9)
D3		44.4779 (511)	75.6335 (1516)	126.2558 (2180)
D4		1.0451 (2)	1.5894 (4)	2.1857 (7)
D5		1.0449 (3)	1.5889 (6)	2.1845 (9)
D6		0.6908 (5)	1.0665 (8)	1.5042 (13)
D7		0.1011 (3)	0.1633 (5)	0.2443 (8)
D8		−13.0181 (119)	−21.7845 (250)	−31.8266 (383)
D9		0.4093 (2)	0.6280 (3)	0.8666 (4)
D10		−0.7459 (172)	−0.7419 (388)	−4.8948 (532)
D11		0.2420 (4)	0.3830 (8)	0.5462 (14)
D12		−1.3422 (31)	−2.7779 (66)	−4.8190 (153)
D13		0.0830 (5)	0.1442 (10)	0.2331 (14)
D14		0.0183 (1)	0.0301 (2)	0.0493 (5)
D15		−49.9866 (367)	20.4958 (1002)	41.2504 (1092)
Total	−26.6442 (0)	−20.4108 (1155)	−5.8798 (5927)	−0.5845 (5799)

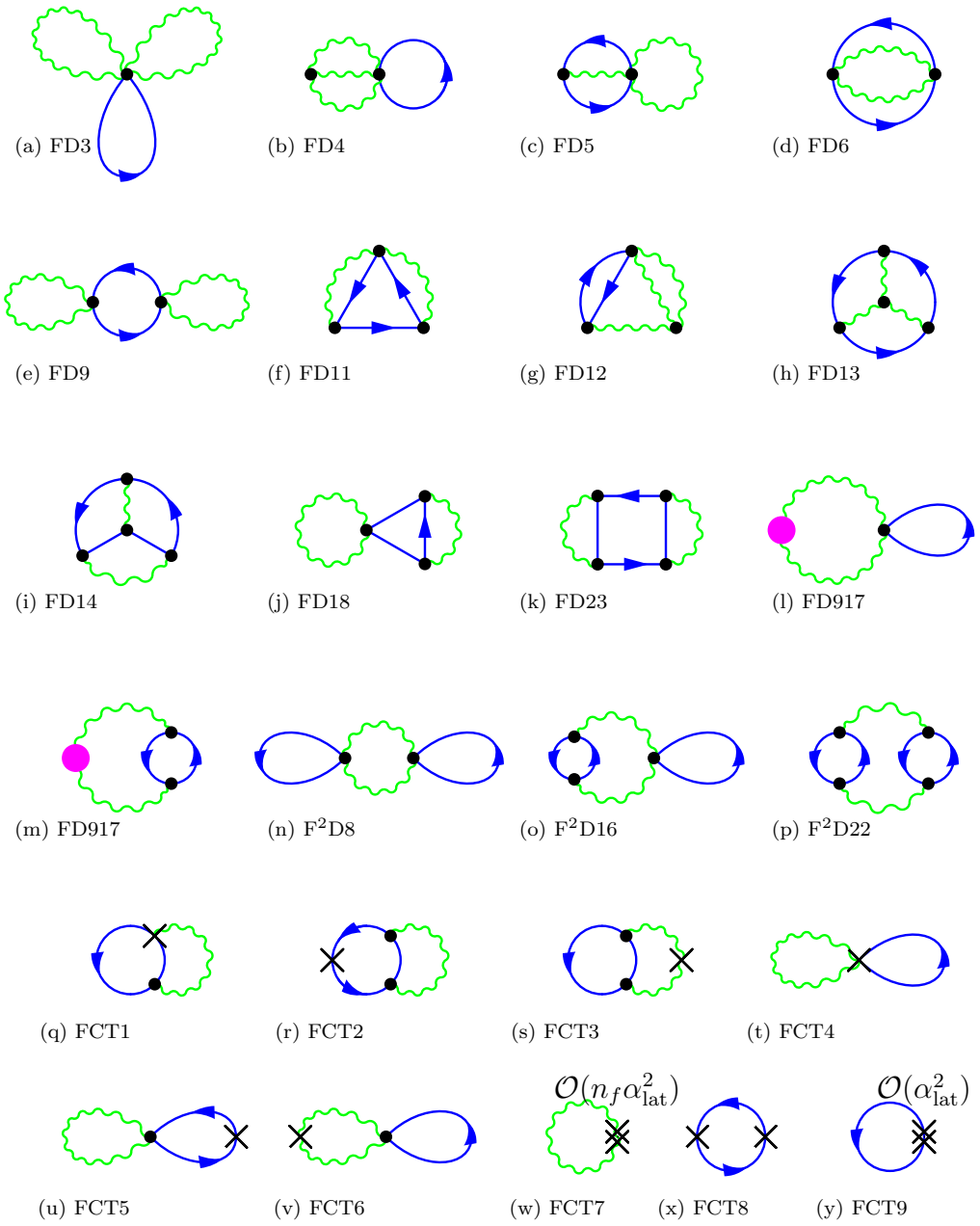

Figure 5.9: The three-loop fermionic Feynman diagrams for the expectation of a Wilson loop, evaluated from derivatives of vacuum bubbles using the susceptibilty method (5.45). The diagram numbering is consistent with [69] except this D917=D7+D10+D15+D19+D25 and this D97=D17+D20+D21+D24+D26. The notation F^{2}DX indicates that diagram X is propotional to n_f^2 rather than n_f, and CT indicates lattice counter-term. FCT8 and FCT9 are identically zero.

Table 5.9: The diagram by diagram results for massless fermionic loops in $\alpha_{\rm lat}^3$ for Wilson loops of various sizes, evaluated using the susceptibilty method for several quark actions.

Asqtad	1x1 n_f	1x2 n_f	1x3 n_f	2x2 n_f
FD3	−0.66546 (51)	−0.90979 (109)	−1.03305 (478)	−1.44227 (368)
FD4	−0.10305 (36)	−0.40063 (140)	−0.68761 (336)	−0.91568 (397)
FD5	0.35629 (55)	0.79112 (147)	1.26189 (345)	1.90793 (606)
FD6	0.00092 (4)	−0.00665 (10)	−0.01911 (22)	−0.06436 (34)
FD9	0.55935 (15)	0.99634 (35)	1.38242 (71)	1.93121 (115)
FD11	−0.02948 (14)	−0.09123 (64)	−0.16299 (173)	−0.29059 (325)
FD12	−0.04009 (10)	−0.14015 (34)	−0.27276 (121)	−0.40875 (182)
FD13	−0.02537 (3)	−0.09174 (129)	−0.18750 (110)	−0.34226 (257)
FD14	−0.00003 (0)	0.00038 (5)	0.00116 (23)	0.00323 (31)
FD18	−0.30946 (17)	−0.66116 (142)	−1.03447 (110)	−1.64528 (186)
FD23	0.02973 (11)	0.09841 (33)	0.17967 (80)	0.33720 (141)
FD97	0.80171 (22)	1.13189 (84)	1.31003 (225)	1.49010 (292)
FD917	0.53873 (74)	0.63139 (250)	0.12568 (154)	−0.26257 (359)
Sum	1.11379 (117)	1.34818 (409)	0.86334 (784)	0.29791 (1072)
FCT	0.8168 (13)	1.49769 (5)	2.0262 (11)	2.8299 (18)
Total	1.9306 (14)	2.84587 (41)	2.8895 (79)	3.1278 (109)
n_f^2	1x1 n_f^2	1x2 n_f^2	1x3 n_f^2	2x2 n_f^2
F^2D8	−0.01184 (1)	−0.01234 (1)	−0.01175 (2)	−0.01313 (1)
F^2D16	−0.00903 (1)	−0.01382 (2)	−0.01492 (3)	−0.02317 (5)
F^2D22	−0.00701 (1)	−0.01748 (3)	−0.02803 (2)	−0.04132 (4)
Total	−0.02788 (2)	−0.04364 (4)	−0.05471 (4)	−0.07762 (7)

Naïve	1x1 n_f	1x2 n_f	1x3 n_f	2x2 n_f
FD3	−0.27570 (2)	−0.43561 (14)	−0.66248 (26)	−0.91059 (40)
FD5	0.26585 (3)	0.27580 (24)	0.46036 (42)	0.85649 (60)
FD6	0.04156 (2)	0.07178 (17)	0.11061 (27)	0.13080 (40)
FD9	0.44103 (3)	0.69663 (23)	1.05985 (39)	1.45754 (61)
FD11	−0.06428 (7)	−0.03809 (57)	−0.07636 (117)	−0.18358 (235)
FD13	−0.12767 (10)	−0.14518 (145)	−0.26453 (174)	−0.59218 (474)
FD14	−0.00365 (2)	−0.00520 (11)	−0.00803 (24)	−0.00890 (36)
FD18	−0.42537 (10)	−0.44041 (89)	−0.73928 (167)	−1.37198 (265)
FD23	0.10456 (20)	0.09878 (100)	0.16404 (153)	0.40855 (229)
FD917	2.02176 (28)	2.64231 (166)	2.07192 (341)	2.10076 (490)
Total	1.97808 (38)	2.72082 (267)	2.11612 (466)	1.88690 (809)
n_f^2	1x1 n_f^2	1x2 n_f^2	1x3 n_f^2	2x2 n_f^2
F^2D22	−0.01696 (1)	−0.03608 (3)	−0.05585 (4)	−0.06959 (7)
Total	−0.01696 (1)	−0.03608 (3)	−0.05585 (4)	−0.06959 (7)

Table 5.9: (Continued)

FD27 is FCT2 where the lattice counter-term is a 1-loop additive mass insertion [70] to keep the quarks massless at $\mathcal{O}(\alpha_s)$, similarly FD28 comes from FCT5. Missing diagrams/blanks are zero.

Wilson	1x1 n_f	1x2 n_f	1x3 n_f	2x2 n_f
FD3	−0.27040 (13)	−0.42723 (173)	−0.64869 (289)	−0.89310 (420)
FD5	0.13405 (10)	0.05824 (95)	0.15748 (162)	0.39371 (232)
FD6	−0.00508 (9)	−0.02048 (68)	−0.03905 (114)	−0.07488 (165)
FD9	−2.35545 (43)	−3.72031 (293)	−5.65688 (486)	−7.77404 (589)
FD11	0.00083 (15)	0.03944 (168)	0.05494 (483)	0.07318 (614)
FD13	−0.21356 (12)	−0.39101 (125)	−0.69714 (255)	−1.15022 (427)
FD14	−0.00725 (4)	−0.00868 (20)	−0.01062 (42)	−0.00789 (63)
FD18	0.38050 (35)	−0.11307 (271)	−0.00548 (459)	0.46628 (620)
FD23	−0.00803 (38)	−0.03961 (88)	−0.05753 (153)	−0.09669 (186)
FD27	2.92959 (34)	0.51722 (165)	0.49581 (305)	−0.11365 (594)
FD28	−0.31245 (31)	4.62785 (84)	7.03873 (141)	9.67733 (194)
FD917	2.29139 (131)	3.00481 (307)	2.44468 (718)	2.40851 (987)
Total	2.56414 (156)	3.52717 (619)	3.07623 (1233)	2.90854 (1718)
n_f^2	1x1 n_f^2	1x2 n_f^2	1x3 n_f^2	2x2 n_f^2
F^{2}D22	−0.02211 (7)	−0.04674 (13)	−0.07030 (20)	−0.09561 (26)
Total	−0.02211 (7)	−0.04674 (13)	−0.07030 (20)	−0.09561 (26)

The Clover plaquette is the Wilson plaquette plus a series in c_{SW}^n.

Clover	1x1 $c_{SW}^1 n_f$	1x1 $c_{SW}^2 n_f$	1x1 $c_{SW}^3 n_f$	1x1 $c_{SW}^4 n_f$
FD5	0.0458 (2)	−1.8982 (2)		
FD6		2.0927 (6)		
FD11	0.0512 (7)	0.1006 (3)	−0.0060 (1)	
FD12	0.0005 (2)	0.0649 (4)		
FD13	0.0307 (2)	0.0257 (1)	0.0125 (0)	
FD14	0.0009 (0)	−0.0051 (0)	0.0001 (0)	0.0013 (0)
FD18	0.6237 (6)	0.6280 (4)		
FD23	0.0017 (6)	−0.0727 (4)	−0.0368 (1)	0.0329 (0)
FD28	−0.3507 (5)	0.3550 (4)		
δm^{csw}FD27	−0.7824 (4)			
δm^{csw}FD28	0.0837 (3)	0.0936 (1)	−0.0948 (1)	
$\delta m^{c_{sw}^2}$FD27		−0.3256 (2)		
$\delta m^{c_{sw}^2}$FD28		0.0348 (1)	0.0390 (1)	−0.0394 (0)
FD917	−0.0703 (9)	2.0155 (7)		
Total	−0.3653 (16)	3.1093 (12)	−0.0860 (2)	−0.0052 (1)
n_f^2	1x1 $n_f^2 c_{SW}^1$	1x1 $n_f^2 c_{SW}^2$	1x1 $n_f^2 c_{SW}^3$	1x1 $n_f^2 c_{SW}^4$
F^{2}D22		0.0028 (0)	0.0029 (0)	−0.0310 (0)
Total	0.0000 (0)	0.0028 (0)	0.0029 (0)	−0.0310 (0)

Table 5.10: The final results to third order for Wilson loops and Creutz ratios for several actions.

(a) Naïve Quarks, Wilson glue

R	T	w_0	$w_{1,g}$	$w_{1,f}^{(1)}$	$w_{2,g}$	$w_{2,f}^{(1)}$	$w_{2,f}^{(2)}$
1	1	4.1887902 (0)	5.3553 (4)	−0.25789 (2)	27.16 (3)	−1.9781 (4)	0.01695 (1)
1	2	7.2235734 (49)	0.6078 (18)	−0.49640 (15)	20.34 (7)	−2.7185 (26)	0.03606 (3)
1	3	10.0714895 (108)	−12.1870 (63)	−0.72975 (25)	5.66 (32)	−2.1169 (46)	0.05586 (4)
2	2	11.4715348 (129)	−19.0434 (83)	−0.86561 (31)	0.01 (35)	−1.8837 (79)	0.06957 (7)

R	T		$a_{1,g}$	$a_{1,f}^{(1)}$	$a_{2,g}$	$a_{2,f}^{(1)}$	$a_{2,f}^{(2)}$
1	1		3.3729 (1)	−0.06157 (5)	17.688 (7)	−0.7301 (1)	0.004047 (2)
1	2		3.6959 (3)	−0.06872 (21)	20.817 (10)	−0.8727 (4)	0.004992 (4)
1	3		3.8257 (6)	−0.07246 (25)	22.187 (32)	−0.9399 (5)	0.005546 (4)
2	2		4.0757 (7)	−0.07546 (27)	24.823 (31)	−1.0298 (8)	0.006065 (6)

R	T	aq^*	w_0	$r_{1,g}$	$r_{1,f}^{(1)}$	$r_{2,g}$	$r_{2,f}^{(1)}$	$r_{2,f}^{(2)}$
1	1	3.40		−1.1906 (1)	−0.07000 (1)	−1.697 (7)	0.3832 (65)	0.005157 (2)
1	2	3.07		−1.0463 (3)	−0.06632 (2)	−1.306 (10)	0.3217 (65)	0.004668 (4)
1	3	3.01		−0.9510 (6)	−0.06797 (3)	−1.128 (32)	0.2946 (65)	0.004916 (4)
2	2	2.65		−0.9240 (7)	−0.05745 (3)	−0.684 (31)	0.2627 (65)	0.003671 (6)
$\ln \frac{1\text{x}1\ 2\text{x}2}{(1\text{x}2)^2}$		1.09	1.2132	−0.3831 (42)	0.00454 (3)	−0.962 (198)	0.1745 (73)	0.000285 (17)
$\ln \frac{1\text{x}3}{2\text{x}2}$		1.06	−1.4001	−0.7293 (14)	0.01820 (4)	−1.134 (22)	0.1555 (71)	0.000708 (24)

Table 5.10: (Continued)

(b) Wilson Quarks, Wilson glue

R	T	w_0	$w_{1,g}$	$w_{1,f}^{(1)}$	$w_{2,g}$	$w_{2,f}^{(1)}$	$w_{2,f}^{(2)}$
1	1	4.1887902 (0)	5.3553 (4)	−0.2919 (1)	27.16 (3)	−2.5642 (15)	0.02210 (1)
1	2	7.2235734 (49)	0.6078 (18)	−0.5562 (8)	20.34 (7)	−3.5283 (60)	0.04673 (1)
1	3	10.0714895 (108)	−12.1870 (63)	−0.8025 (15)	5.66 (32)	−3.0747 (122)	0.07026 (2)
2	2	11.4715348 (129)	−19.0434 (83)	−0.9944 (18)	0.01 (35)	−2.9087 (170)	0.09553 (3)

R	T		$a_{1,g}$	$a_{1,f}^{(1)}$	$a_{2,g}$	$a_{2,f}^{(1)}$	$a_{2,f}^{(2)}$
1	1		3.3729 (1)	−0.06969 (2)	17.688 (7)	−0.9041 (4)	0.005277 (15)
1	2		3.6959 (3)	−0.07700 (10)	20.817 (10)	−1.0446 (11)	0.006469 (17)
1	3		3.8257 (6)	−0.07968 (15)	22.187 (32)	−1.1078 (19)	0.006976 (19)
2	2		4.0757 (7)	−0.08668 (16)	24.823 (31)	−1.2480 (23)	0.008327 (22)

R	T	aq^*	w_0	$r_{1,g}$	$r_{1,f}^{(1)}$	$r_{2,g}$	$r_{2,f}^{(1)}$	$r_{2,f}^{(2)}$
1	1	3.40		−1.1906 (1)	−0.02697 (3)	−1.697 (7)	0.295 (1)	0.00115 (1)
1	2	3.07		−1.0463 (3)	−0.02345 (11)	−1.306 (10)	0.254 (1)	0.00109 (1)
1	3	3.01		−0.9510 (6)	−0.02404 (15)	−1.029 (31)	0.231 (1)	0.00120 (2)
2	2	2.65		−0.9239 (7)	−0.01751 (16)	−0.597 (31)	0.195 (2)	0.00112 (2)
$\ln \frac{1\text{x}1\ 2\text{x}2}{(1\text{x}2)^2}$		1.09	1.2133	−0.3831 (42)	0.02009 (24)	−0.962 (198)	0.119 (7)	−0.00022 (8)
$\ln \frac{1\text{x}3}{2\text{x}2}$		1.06	−1.4001	−0.7293 (14)	0.02932 (21)	−1.134 (22)	0.163 (4)	−0.00012 (7)

Table 5.10: (Continued)

(c) Clover Quarks, Wilson glue

R T	w_0	$w_{1,g}$	$w_{1,f}^{(1)}$	$w_{2,g}$	$w_{2,f}^{(1)}$	$w_{2,f}^{(2)}$
1 1	4.1887902 (0)	5.3553 (4)	−0.29175 (9)	27.16 (3)	−2.5642 (15)	0.02210 (1)
c_{SW}^1			0.008425 (20)		−0.3653 (16)	0
c_{SW}^2			−0.251095 (1)		3.1093 (12)	0.00283 (2)
c_{SW}^3					−0.0860 (2)	0.00294 (2)
c_{SW}^4					−0.0052 (1)	−0.03098 (2)
R T		$a_{1,g}$	$a_{1,f}^{(1)}$	$a_{2,g}$	$a_{2,f}^{(1)}$	$a_{2,f}^{(2)}$
1 1		3.3729 (0)	−0.069651 (21)	17.688 (7)	−0.90391 (37)	0.005277 (15)
c_{SW}^1			0.002011 (5)		−0.07879 (38)	0
c_{SW}^2			−0.059945 (2)		0.49120 (29)	0.000675 (1)
c_{SW}^3					−0.02053 (5)	0.000703 (1)
c_{SW}^4					−0.00125 (1)	−0.007395 (0)
R T	aq^*	$r_{1,g}$	$r_{1,f}^{(1)}$	$r_{2,g}$	$r_{2,f}^{(1)}$	$r_{2,f}^{(2)}$
1 1	3.40	−1.1906 (1)	−0.02693 (2)	−1.697 (7)	0.29436 (95)	0.00115 (1)
c_{SW}^1			−0.06141 (5)		0.07836 (38)	0.00359 (0)
c_{SW}^2			0.31508 (0)		−1.88128 (29)	−0.02088 (1)
c_{SW}^3					−0.09541 (5)	−0.03775 (1)
c_{SW}^4					−0.01768 (2)	0.08828 (0)

Table 5.10: (Continued)

(d) Improved Staggered Quarks, One-loop Symanzik Improved glue

R	T	w_0	$w_{1,g}$	$w_{1,f}^{(1)}$	$w_{2,g}$	$w_{2,f}^{(1)}$	$w_{2,f}^{(2)}$
1	1	3.0683952 (5)	3.5586 (2)	−0.27884 (3)	13.94 (2)	−1.9306 (11)	0.02786 (1)
1	2	5.5511969 (120)	1.4221 (18)	−0.46709 (10)	11.93 (6)	−2.8466 (39)	0.04361 (2)
1	3	7.8765310 (373)	−6.1317 (60)	−0.61619 (9)	2.99 (15)	−2.8925 (76)	0.05474 (4)
2	2	9.1997545 (499)	−10.8301 (93)	−0.80669 (14)	−2.79 (30)	−3.1318 (106)	0.07763 (6)

R	T		$a_{1,g}$	$a_{1,f}^{(1)}$	$a_{2,g}$	$a_{2,f}^{(1)}$	$a_{2,f}^{(2)}$
1	1		2.6939 (1)	−0.09087 (11)	11.241 (5)	−0.9080 (4)	0.009079 (4)
1	2		3.0318 (3)	−0.08414 (18)	13.843 (10)	−0.9799 (7)	0.007857 (4)
1	3		3.1598 (8)	−0.07823 (12)	14.927 (20)	−0.9834 (10)	0.006949 (5)
2	2		3.4227 (10)	−0.08769 (15)	17.078 (33)	−1.1471 (12)	0.008438 (7)

R	T	aq^*	w_0	$r_{1,g}$	$r_{1,f}^{(1)}$	$r_{2,g}$	$r_{2,f}^{(1)}$	$r_{2,f}^{(2)}$
1	1	3.325		−0.7753 (2)	−0.096934 (12)	−0.722 (39)	0.7737 (51)	0.010217 (4)
1	2	2.998		−1.6202 (4)	−0.079130 (19)	−0.407 (40)	0.6870 (52)	0.007038 (4)
1	3	2.934		−0.5335 (8)	−0.070713 (13)	−0.245 (44)	0.6487 (52)	0.005842 (8)
2	2	2.582		−0.4934 (10)	−0.066670 (16)	−0.030 (51)	0.6016 (53)	0.005205 (11)
$\ln \frac{1x1\ 2x2}{(1x2)^2}$		1.20	1.1658	−0.0143 (51)	−0.028476 (26)	−1.43 (18)	0.4518 (62)	−0.000374 (27)
$\ln \frac{1x3}{2x2}$		1.21	−1.3233	−0.2687 (25)	−0.041732 (38)	−1.56 (12)	0.5425 (57)	−0.001686 (17)

5.3 Final Story

The results of this chapter consist of a handful of numbers which represent ∼6 GHz-CPU-years of computing for 139 Feynman diagrams evaluated using four of the most common actions available, two of which are improved. These are the first multi-loop results for Asqtad, the most highly improved action available. A first determination of 1×2, 1×3 and 2×2 Wilson loops at third order is presented. The background field method used to match the lattice actions to the α_V scheme at third order was checked for Wilson and Clover fermions with Wilson glue and new results for Naïve quarks with Wilson glue and improved staggered fermions with one-loop Symanzik improved glue were calculated. Unfortunately our two mostly-independent calculations significantly disagree with a previous calculation using the analytic approach on two diagrams for Wilson quarks. These two are among the most difficult to do using the analytic approach and many subtractions have to be applied to isolate the coefficients of the logarithm and double-logarithm and to extract the constant. There was no gauge-invariance test done for the original calculation and this is now being done. Until this matter is resolved a confident prediction of $\alpha_{\overline{\rm MS}}(m_Z)$ is not appropriate. All the necessary pieces for that calculation have been presented though. If the non-fermionic result can be trusted however then the convergence of quenched determinations can be examined. There has been a discrepancy between determinations using Wilson quarks and staggered quarks for the valence phenomenology, that is clearly resolved by the third order perturbation theory in figure 5.10. As quenched simulations are manifestly unphysical it is not very informative to calculate $\alpha_{\overline{\rm MS}}(m_Z)$ from this data. It is important to note that each order in perturbation theory has errors that are of the next order in size and the two formalisms converge as the next-order contribution shrinks in

Table 5.11: Simulation results for the Wilson loops and Creutz Ratios with the Asqtad action at a^{-1}_{fine}=2.271(28) GeV, and $m_u = m_d = m_s/5$, are used to set the value of $\alpha_V(q^*)$ from the perturbative expression at 1-, 2- and 3-loops. This is then run to the scale $3.325/a_{fine}$, the q^* of the plaquette, for comparison. The first error, (P), comes from errors in the perturbative coefficients, statistical errors in the simulation, and running to $3.325/a$. The second error, (T), is an estimate of truncation of fourth order terms in the expression. This is the maximum of that derived from the differences between the results at each order (the Wilson loops) and $\pm 1\alpha_V^4$ (the Creutz ratios). The final goal is $\alpha_{\overline{\rm MS}}(m_Z)$ which is also shown with an error, (A), from a^{-1}. The Creutz ratios are much more convergent.

		Simulation	1st Order	2nd Order	3rd Order							
	aq^*	Result	$\alpha_V(3.325/a)$	$\alpha_V(3.325/a)$	α_V	P	T	$\alpha_{\overline{\rm MS}}(m_Z)$	P	T	A
ln 1x1	3.325	0.59487 (1)	0.1693	0.2219	0.1981	(4)	(108)	0.1143	(1)	(33)	(3)
ln 1x2	2.998	0.35979 (2)	0.1787	0.2207	0.1988	(4)	(114)	0.1145	(1)	(35)	(3)
ln 1x3	2.934	0.22166 (2)	0.1842	0.2205	0.1994	(4)	(123)	0.1147	(1)	(37)	(3)
ln 2x2	2.582	0.15346 (1)	0.1881	0.2227	0.2000	(5)	(149)	0.1149	(1)	(44)	(3)
ln $\frac{\text{1x1 2x2}}{(\text{1x2})^2}$	1.20		0.1992	0.2031	0.2041	(25)	(40)	0.1161	(8)	(12)	(3)
ln $\frac{\text{1x3}}{\text{2x2}}$	1.21		0.1904	0.2071	0.2062	(44)	(25)	0.1168	(7)	(13)	(3)

the way expected for a well-behaved perturbative quantity.

The coefficient of $n_f\alpha_V^3$ in the logarithm of the Wilson loops for the Asqtad action, 0.7, is distressingly large because of the n_f. This could be the sign of more taste-changing that was exactly cured only for one-loop computations, bad "luck", or a sign that perturbation theory is breaking down if there are large $\mathcal{O}(1)n_f^2\alpha_V^4$ terms. The simulation results can aid this determination and currently it appears from table 5.11 that there are large contributions from the fermionic sector at fourth order because the Wilson loops do not converge very well. This could be also be due to the fact that at these high scales of order the lattice cutoff that the lattice loops are no longer logarithmic, which is assumed in the q^* analysis. The Creutz ratios which are at a lower scale are much better behaved. The final value for $\alpha_{\overline{\rm MS}}(m_Z)$ for the determinations in table 5.11 is 0.1164(12), which agrees very well with the current world average over nine completely different methods of determining the coupling $\alpha_{\overline{\rm MS}}(m_Z)$=0.1172(20) [4].

Adding a fourth order of perturbative results is in principle possible, but likely to be prohibitively difficult with the current level of computing. Although the Wilson loops at fourth order are probably well within reach they can be studied using the High Beta and numerical Stochastic approaches to lattice perturbation theory far easier than in the diagrammatic approach. In general the high-beta simulation method of doing perturbation theory finds a good signal at one higher order than for which the corresponding perturbation theory is known. If increased precision were required the high-beta method plus third order diagrammatic results would probably be the technique of choice. Additionally the α_V scheme is only well-defined up to third order, so a new well-motivated scheme suitable for lattice scales would have to be selected.

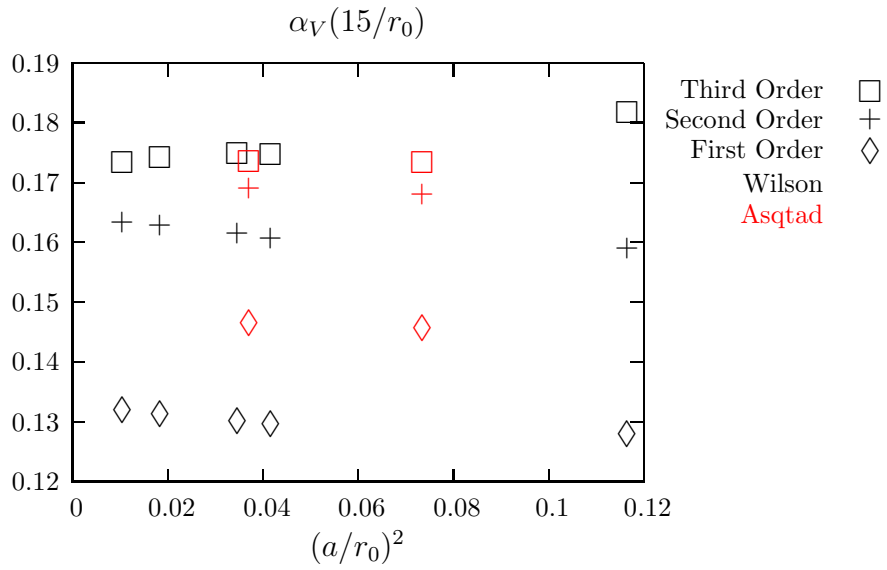

Figure 5.10: For a long time the values of α from unimproved Wilson glue (in black) and improved glue (in red) did not agree very well; this plot shows how each order of perturbation theory improves the convergence of the two discretisations. Note that the scaling is much better for the one-loop Symanzik improved glue as expected. The quenched approximation is so unphysical that it is not worth running these coupling determinations to $\alpha_{\overline{\rm MS}}(m_Z)$.

CHAPTER 6

CONCLUSION

The future of lattice QCD is very exciting. A new era of accurate predictions relevant to experiment is dawning. Simulations are unquenched with three dynamical light quarks with masses that are sufficiently close to being physical that chiral perturbation theory is both relevant and applicable. Results are available that have no estimated errors or systematic uncertainties due to quenching, the correct number of light quarks or chiral extrapolations for the first time. However to fully realise this potential perturbative results at two-loops are needed for various operators, matrix elements and action-parameters, particularly for heavy-quarks. Perturbation theory in lattice QCD has had an important rôle in enabling these new simulations by improving the action and will continue to make a leading contribution to the results.

Automated methods for doing lattice perturbation theory are necessary to cope with the massive complexity, many actions and different operators. These methods have been applied to the first two and three loop results for improved actions that have non-diagonal propagators. Two-loop renormalisations of IR sensitive quantities have been shown to be feasible using these techniques for improved actions in moderate CPU time even without optimisation. A new approach to lattice perturbation theory has been developed here and applied to several important physics problems.

Any perturbation theory calculation expands results in a coupling, α_s, so a way of evaluating it is probably the most important perturbative calculation required. This can now be done for lattice simulations using four Wilson loops that have been evaluated to three-loops for the first time. It is important to check that

different implementations of lattice QCD which manifest as different actions and particularly approaches to the quark discretisation agree, so these results are given for the four most common light-quark actions in use. It has once again been shown how important it is to tadpole improve the action and to choose an appropriate scheme for the coupling as the bare $\alpha_{\rm lat}$ is a poor expansion parameter. These simple steps significantly improve the convergence of lattice perturbation theory.

Taste-changing effects which are one of the biggest drawbacks of using staggered quarks can be investigated perturbatively and removed systematically. A new staggered quark action has been proposed that was predicted to have much smaller taste errors by a one-loop perturbative calculation and has demonstrated in simulation quenched pion splittings that are indeed about three times reduced.

The bare strange quark mass can be determined using partially quenched chiral perturbation theory from about 0.5 Tflop-years of simulations at a wide variety of valence and sea-quark masses, to an impressive accuracy of a few MeV. The quark mass renormalisation calculated in one-loop perturbation theory is a small correction but the unknown error from the two-loop contribution vastly dominates the overall accuracy. Lattice determinations of the strange quark mass decrease as the number of light quark flavours is increased from zero to three and the final value is 75(8) MeV. This is in agreement with sum rule determinations only at the one sigma level and worryingly low compared to the sum rule constraints. The two-loop calculation is an important project on the list, calculating for heavy-quarks as well would similarly help the determination of m_c and m_b.

There is a clear need for lattice perturbation theory calculations to improve and renormalise the actions and currents, and also to compare to the continuum. The HPQCD collaboration has an ambitious perturbative program that involves many

one and two-loop expansions, some of which have never been attempted before on the lattice. The techniques developed here have been shown to be a reliable and relatively painless method for the evaluation of the necessary integrals.

APPENDIX A

TWISTED BOUNDARY CONDITIONS

Consider an infinite lattice periodic in steps of L in certain directions and "twisted" in the rest. The gauge fields on this lattice are identified with the set of fields $U_\mu(x) \in \mathrm{SU}(N)$, $x/a \in \mathbb{Z}^4$, $\mu = 0, \ldots 3$, which are twisted periodic thus

$$U_\mu(x + L\hat{\nu}) = \Omega_\nu U_\mu(x) \Omega_\nu^\dagger \tag{A.1}$$

for ν in the twisted directions. We keep the discussion general in anticipation of introducing doubly and triply-twisted fields later. Note the difference with Lüscher [13] of replacing $^{-1} \rightarrow ^\dagger$ to account for the change in definition $U = e^{gA} \rightarrow e^{igA}$. The twist matrices Ω_ν are constant, gauge field independent elements of $\mathrm{SU}(N)$, which satisfy the algebra

$$\Omega_1 \Omega_2 = z_3 \Omega_2 \Omega_1, \qquad z = e^{2\pi i/N}. \tag{A.2}$$

This condition comes from considering the two orders of applying (A.1) to $U_1(L+1, L+1)$ whilst relating it back to $U_1(1,1)$.

$$\begin{aligned} U_1(L+1,L+1) &= \Omega_1 U_1(1,L+1)\Omega_1^\dagger \\ &= \Omega_1\Omega_2 U_1(1,1)\Omega_2^\dagger\Omega_1^\dagger \end{aligned} \quad \text{and} \quad \begin{aligned} U_1(L+1,L+1) &= \Omega_2 U_1(L+1,1)\Omega_2^\dagger \\ &= \Omega_2\Omega_1 U_1(1,1)\Omega_1^\dagger\Omega_2^\dagger \end{aligned}$$

$$\begin{aligned} \Omega_1\Omega_2 U_1 \left(\Omega_1\Omega_2\right)^\dagger &= \Omega_2\Omega_1 U_1 \left(\Omega_2\Omega_1\right)^\dagger \\ \left(\Omega_2\Omega_1\right)^\dagger \Omega_1\Omega_2 U_1 &= U_1 \left(\Omega_2\Omega_1\right)^\dagger \Omega_1\Omega_2. \end{aligned} \tag{A.3}$$

where the unitary property of SU, ($\Omega^\dagger = \Omega^{-1}$) has been used. (A.3) shows that $(\Omega_2\Omega_1)^\dagger\Omega_1\Omega_2$ commutes with all $\mathrm{SU}(N)$ elements and is therefore an element of the centre group of $\mathrm{SU}(N)$, $\mathbb{Z}(N)$. Then for $z_i \in \mathbb{Z}_3$

$$\begin{aligned} (\Omega_2\Omega_1)^\dagger\Omega_1\Omega_2 &= z_i \\ \Omega_1\Omega_2 &= z_i\Omega_2\Omega_1, \end{aligned} \tag{A.4}$$

and z_i is chosen to be $z = e^{2\pi i/N}$ in order to get a twist. The corresponding gauge group $\mathcal{G}_\Omega$ consists of all fields $\Lambda(x) \in \mathrm{SU}(N)$ with

$$\Lambda(x + L\hat{\nu}) = \Omega_\nu \Lambda(x) \Omega_\nu^\dagger. \tag{A.5}$$

The twist algebra (A.2) insures the self-consistency of the twisted fields in the sense that it provides a unique extension of $U_\mu(0 \leq x \leq L)$ to all points in the twisted directions of the lattice and by extension of the periodic boundary conditions to the entire lattice. Whilst an explicit representation of the actual twist matrices is not needed for perturbation theory they are required for simulations and are readily available in the literature [74]. Some useful notes from Lüscher on Ω's are:

- Twist matrices are fixed up to unitary transformations only.
- Irreducibility; any matrix which commutes with Ω_1 and Ω_2 is a multiple of the identity.
- $\Omega_\nu^N = (-1)^{N-1}\mathbb{I}_N$, i.e. $\Omega_\nu^3 = 1$ for QCD.

Lüscher [13] shows that the toron manifold is trivial and one may do straightforward expansion of the $U = e^{igA}$ in powers of g as before in (2.10); gauge fix (2.19) and derive the ghost vertices, with the usual measure terms from $\mathcal{D}A \leftrightarrow \mathcal{D}U$. The only change is the colour-momentum phase factor that replace the colour or adjoint colour factors.

A.1 Gluon Twisted Colour

The gauge field A satisfies

$$A_\mu(x)^\dagger = A_\mu(x), \qquad \mathrm{Tr}\ A_\mu(x) = 0. \tag{A.6}$$

Taylor expanding $U = e^{igA}$ and applying (A.1) term by term implies that A must also satisfy the same boundary conditions as for the link field:

$$A_\mu(x + L\hat{\nu}) = \Omega_\nu A_\mu(x)\Omega_\nu^\dagger. \tag{A.7}$$

Now A can be expanded into plane waves by Fourier decomposition, replacing (2.11) with

$$A_\mu(x) \equiv \frac{1}{NL^3T}\sum_k \Gamma_k\, e^{ikx} e^{ik_\mu a_\mu/2} A_\mu(k), \tag{A.8}$$

where the complex momentum-dependent phase Γ_k replaces the usual Gell-Mann matrix T^C_{ab}. Applying this decomposition to (A.7) implies that

$$\frac{1}{NL^3T}\sum_k e^{ikx} e^{ik_\nu L} e^{ik_\mu a/2} A_\mu(k) = \frac{1}{NL^3T}\sum_k \Omega_\nu \Gamma_k \Omega_\nu^\dagger e^{ikx} e^{ik_\mu a/2} A_\mu(k), \tag{A.9}$$

which directly leads to the eigenvalue equation

$$\Omega_\nu \Gamma_k \Omega_\nu^\dagger = e^{ik_\nu L}\Gamma_k. \tag{A.10}$$

This is solved by twice left multiplying by Ω_ν and right-multiplying by $\Omega_\nu^\dagger$ giving

$$\begin{aligned} \Omega_\nu\Omega_\nu\Omega_\nu\Gamma_k\Omega_\nu^\dagger\Omega_\nu^\dagger\Omega_\nu^\dagger &= e^{ip_\nu L}\Omega_\nu\Omega_\nu\Gamma_k\Omega_\nu^\dagger\Omega_\nu^\dagger, \\ \Gamma_k &= e^{i3p_\nu L}\Gamma_k, \end{aligned} \tag{A.11}$$

which quantises the momenta in the twisted directions ν as

$$k_\nu = \frac{2\pi}{NL} n_\nu \quad \text{equivalently} \quad \frac{2\pi}{L} m_\nu + \frac{2\pi}{NL} n'_\nu. \tag{A.12}$$

In terms of the colour factor the n_ν are only defined modulo N so an equivalent representation is a regular periodic piece (m_ν) plus a small twisted correction n'_ν. The apparent increase in the box size to $3L$ for the twisted momenta reduces finite volume Ewald image-in-the-walls errors.

One can now solve the eigenvalue equation up to an arbitrary phase with the *ansatz* $\Gamma_k = \Omega_1^\alpha \Omega_2^\beta$.

$$\begin{aligned}
\Omega_1 \Gamma_k \Omega_1^\dagger &= z^{n_1} \Gamma_k \\
\Omega_1 \Omega_1^\alpha \Omega_2^\beta \Omega_1^\dagger &= z^{n_1} \Gamma_k \\
z^\beta \Omega_1^\alpha \Omega_2^\beta &= z^{n_1} \Gamma_k \qquad\qquad \Omega_2 \Omega_1^\dagger = z \Omega_1^\dagger \Omega_2 \\
\beta &= n_1 \\
&\text{and} \\
\Omega_2 \Gamma_k \Omega_2^\dagger &= z^{n_2} \Gamma_k \\
\Omega_2 \Omega_1^\alpha \Omega_2^\beta \Omega_2^\dagger &= z^{n_2} \Gamma_k \\
z^{-\alpha} \Omega_1^\alpha \Omega_2^\beta &= z^{n_2} \Gamma_k \\
\alpha &= -n_2 \\
\Gamma_k &= \Omega_1^{-n_2} \Omega_2^{n_1} \times \text{phase}
\end{aligned} \tag{A.13}$$

The traceless requirement on $A_\mu(x)$ eliminates the zero mode of the extra twisted momenta, $n_1' = n_2' = 0$, leaving the expected eight adjoint colour degrees of freedom $n_1, n_2 = 0, 1, 2$ in SU(3). The properties of the Γ_k independent of the choice of phase are

$$\begin{aligned}
\Gamma_k &\in \mathrm{SU}(N) \\
\Gamma_{k'} &= \Gamma_k \qquad \text{if } k_\perp' = k_\perp \pmod N, \\
\Gamma_k &= \mathbb{I} \qquad \text{if } k_\perp = 0 \pmod N, \\
\mathrm{Tr}\ \Gamma_k &= 0 \qquad \text{unless } k_\perp = 0 \pmod N,
\end{aligned} \tag{A.14}$$

$$\mathrm{Tr}\ \Gamma_{k'}^\dagger \Gamma_k = \begin{cases} N & \text{iff } k_\perp' = k_\perp \pmod N, \\ 0 & \text{else} \end{cases}, \tag{A.15}$$

where $k_\perp$ is the twisted momentum components rather than the periodic ones. The remaining two are the most important properties from a perturbation theory point of view; the relation of $\Gamma_k^\dagger$ to Γ_{-k} and the composition rule. These are however dependent on the phase that is chosen. This phase is a function of the twisted component of the momenta, $f(k) = f(n_1, n_2)$:

$$\begin{aligned}
\Gamma_k^\dagger &= \Omega_1^{n_2}\Omega_2^{-n_1} f^*(n_1,n_2) && \Omega^{\dagger n_1} = \Omega^{-n_1} \\
&= \Omega_2^{-n_1-1} z^{-n_2}\Omega_1^{n_2}\Omega_2 f^*(n_1,n_2) && \Omega_2 \text{ through } n_2\Omega_1\text{'s} \\
&= z^{-2n_2n_2}\Omega_1^{n_2}\Omega_2^{2n_1} f^*(n_1,n_2) && \times 2n_2 \\
&= z^{n_1n_2}\Omega_1^{n_2}\Omega_2^{-n_1} f^*(n_1,n_2) && \Omega^2 = \Omega^{-1} \\
&= \Gamma_{-k}\, z^{n_1n_2}\frac{f^*(n_1,n_2)}{f(-n_1,-n_2)} && \text{(A.16)}
\end{aligned}$$

In the case of [13, 15], (where $f(k) = z^{\frac{1}{2}(n_1+n_2)(n_1+n_2-1)}$), this dagger phase, $d(k)$, is

$$\begin{aligned}
d(k) &= z^{n_1n_2}\frac{f^*(n_1,n_2)}{f(-n_1,-n_2)} \\
&= z^{n_1n_2} z^{-\frac{1}{2}(n_1+n_2)(n_1+n_2-1)} z^{-\frac{1}{2}(n_1+n_2)(n_1+n_2+1)} \\
&= z^{-\frac{1}{2}(2n_1^2+2n_2^2+2n_1n_2)} \\
&\equiv z^{-(k,k)/2} && \text{(A.17)}
\end{aligned}$$

whereas if $f(n_1, n_2) = z^{-n_1n_2}$ then $d(k) = 1$. For the composition rule

$$\begin{aligned}
\Gamma_{k'}\Gamma_k &= \Omega_1^{-n_2'}\Omega_2^{n_1'}\Omega_1^{-n_2}\Omega_2^{n_1} f(k) f(k') \\
&= z^{-n_1'}\Omega_1^{-n_2'}\Omega_1\Omega_2^{n_1'}\Omega_1^{-n_1-1}\Omega_2^{n_1} f(k) f(k') && \Omega_2\Omega_1 = \Omega_1\Omega_2 z^{-1} \\
&= z^{-2n_1'n_2}\Omega_1^{-n_2'}\Omega_1^{2n_2}\Omega_2^{n_1'}\cancel{\Omega_1^{-3n_2}}\Omega_1^{n_1} f(k) f(k') \\
&= \Omega_1^{-n_2'-n_2}\Omega_2^{n_1'+n_1} f(k) f(k') \\
&= \Gamma_{k+k'} z^{n_1'n_2}\frac{f(k)f(k')}{f(k+k')}. && \text{(A.18)}
\end{aligned}$$

The composition phase, $z(k',k)$, is then

$$\begin{aligned} z(k',k) &= z^{n_1' n_2} \frac{f(k)f(k')}{f(k+k')} \\ &= z^{-n_1 n_2' - n_1 n_1' - n_2 n_2'} \qquad \text{for} \quad [13,15] \\ &\equiv z^{\frac{1}{2}(\langle k',k\rangle - (k',k))} \qquad (A.19) \\ \text{or} \quad &= z^{n_1 n_2' - n_1' n_2} \equiv z^{-\langle k',k\rangle}. \qquad (A.20) \end{aligned}$$

The bracket notation is from [13]:

$$\begin{aligned} (k',k) &= n_1' n_1 + n_2 n_2' + \big(n_1 + n_2\big)\,(n_1' + n_2') \\ \langle k',k\rangle &= n_1' n_2 - n_1 n_2'. \end{aligned} \qquad (A.21)$$

The implementor has the choice of phase $f(k)$ for which the consequences of three are tabulated here:

Table A.1: Three possible cases for the phases in twisted algebra.

Case	$f(k)$ $\Gamma_k = f(k)\Omega_1^{-n_2}\Omega_2^{n_1}$	$d(k) = z(k,k)$ $\Gamma_k^\dagger = d(k)\Gamma_{-k}$	$z(k',k)$ $\Gamma_{k'}\Gamma_k = z(k',k)\Gamma_{k+k'}$	Notes
(1)	1	$z^{n_1 n_2}$	$z^{n_1' n_2}$	
(2)	$z^{-n_1 n_2}$	1	$z^{-\langle k',k\rangle}$	$\Gamma_k^\dagger = \Gamma_{-k}$
(3)	$z^{\frac{1}{2}(n_1+n_2)(n_1+n_2-1)}$	$z^{-\frac{1}{2}(k,k)}$	$z^{\frac{1}{2}(\langle k',k\rangle - (k',k))}$	$[13,15]$

Snippe says in [15] that the choice in [13] of $z^{\frac{1}{2}(n_1+n_2)(n_1+n_2-1)}$, case (3) in table A.1, is "convenient," but it appears that case (2) is in fact musch more effecient as explained below. Twisted vertex colour factors involve only phases and do not require explicit representations because the traces can be done in advance

using

$$\frac{1}{N}\text{Tr }\Gamma^\dagger_{k'}\Gamma_k = \begin{cases} 1 & \text{iff } k'_\perp = k_\perp \pmod N \\ 0 & \text{otherwise,} \end{cases} \tag{A.22}$$

Though for case (2) this means that Tr $\Gamma^\dagger_k\Gamma_k =$ Tr $\Gamma_{-k}\Gamma_k = N$, killing the additional phase factor. This therefore eliminates the last composition in high-point vertices Tr $[\Gamma_{k_1}\Gamma_{k_2}\cdots\Gamma_{k_6}]\,\delta(\sum_{i=1}^6 k_i) \sim$ Tr $\Gamma_{k_1}\Gamma_{-k_1=k_2+\ldots+k_6} = Nz(k_1, k_2+\ldots+k_6) = N$ thereby saving in expression complexity and computation time. The 6-pt gluon vertex has 60 independent colour factors even after removing those identical by virtue of cyclic permutation and inversion as detailed in (2.16) or (3.17) of [13].

A.2 Triple Twist

So far we have discussed doubly twisted manifolds. To introduce a third twist we note that the Ω are irreducible, and must satisfy (A.3) in three directions. This is automatic if we use

$$\Omega_3 = \Omega_1\Omega_1\Omega_2 \tag{A.23}$$

and make the same *ansatz* as before. Obviously the same results will be obtained from the conditions in the 1 and 2 directions. So we only need to determine the 3rd constraint

$$\begin{aligned} \Omega_3\Gamma_k\Omega_3^\dagger &= z^{n_3}\Gamma_k \\ \Omega_3\Omega_1^{-n_2}\Omega_2^{n_1}\Omega_3^\dagger &= z^{n_3}\Gamma_k \\ \Omega_1\Omega_1\Omega_2\Omega_1^{-n_2}\Omega_2^{n_1}\Omega_3^\dagger &= z^{n_3}\Gamma_k \\ z^{2n_1+n_2}\Gamma_k &= z^{n_3}\Gamma_k \\ n_3 = n_2 + 2n_1 &= n_2 - n_1. \end{aligned} \tag{A.24}$$

This constraint reduces the apparent $N^3 = 27$ additional momenta degrees of freedom in the new effective $(NL)^3 \times T$ lattice to the 8 expected to replace the $N^2 - 1 = 8$ colours in a propagator. The gluon propagator comes from

$$S + S_{\text{gf}} = -\frac{1}{2} \sum_{x,\mu,\nu} \text{Tr} \left\{ A_\mu(x) \left[\delta_{\mu\nu} \Delta^{(2)} - \left(1 - \frac{1}{\alpha}\right) \Delta^+_\mu \Delta^-_\mu \right] A_\nu(x) \right\}, \quad \text{(A.25)}$$

which can be Fourier transformed and expanded using $A = A^\dagger$ as

$$S + S_{\text{gf}} = \frac{1}{2} \sum_{x,\mu,\nu} \left\{ \left(\frac{1}{3L^3T} \right)^2 \times \right. \quad \text{(A.26)}$$
$$\left. \sum_{k',k} \text{Tr} \left(\Gamma^\dagger_{k'} \Gamma_k \right) e^{ix(k-k')} A^*_\mu(k') A_\nu(k) \cdot 2 \cdot \left[\delta_{\mu\nu} \hat{k}^2 - \left(1 - \frac{1}{\alpha}\right) \hat{k}'_\mu \hat{k}_\nu \right] \right\}.$$

Now $\sum_x e^{i(k-k')x} = L^3T \delta_{k_\parallel, k'_\parallel}$, $\text{Tr} \left(\Gamma^\dagger_k \Gamma_k \right) = N$ and $A^*(k) = z(k,k) A(-k)$. The inverse of the kernel is the gluon propagator

$$\langle \underline{A_\mu(-k)} A_\nu(k) \rangle = NL^3T \, D_{\mu\nu}(k) \chi_k \frac{1}{2} z^{-1}(k,k). \quad \text{(A.27)}$$

The twisted volume that will appear everywhere is NL^3T and eventually cancels against r appropriate volume factors in an r-loop sum over all modes in perturbation theory. For each external *integral* over discretized momenta in a finite box the volume factor is $N/(2\pi)^4$ – like the 2π rule in regular QFT (see §A.5). The additional twisted factor χ is the zero-momentum rejector:

$$\chi_k = \begin{cases} 0 & \text{if } k_\perp = 0 \pmod N, \\ 1 & \text{otherwise.} \end{cases} \quad \text{(A.28)}$$

where $k_\perp = 0 \pmod N$ is $n_1, n_2 = 0 \pmod N$, with the additional constraint in triple twist of $n_3 = n_2 - n_1 \pmod N$. Note when choosing a phase that case (2) has $z(k,k) = z^{-\langle k,k \rangle} = 1$, and thus the propagator is modified by a constant *real* factor of one-half after the momentum rejection step which can be pre-computed. This is still necessary for propagators carrying $k_1 + k_2$ momentum for example, as

it does not follow that the sum of two non-zero mode momenta is not a zero-mode. The factor of 2 in (A.26) is usually cancelled by Tr $T^a T^a = \frac{1}{2}$. The external $\frac{1}{2}$ reflects the forward or backward flowing nature of gluons. Quarks and Ghosts for example do not have this factor as they are directional. Finally the function $D_{\mu\nu}$ is the usual

$$D_{\mu\nu} = \frac{1}{\hat{k}^2}\left[\delta_{\mu\nu} - (1-\xi)\frac{\hat{k}_\mu \hat{k}_\nu}{\hat{k}^2}\right], \tag{A.29}$$

where $\hat{k}^2 = \sum_\mu 4\sin^2\left(\frac{k_\mu}{2}\right) = 8 - 2\sum_\mu \cos(k_\mu)$.

A.3 Quark Twisted Colour

We use the standard Wilson action for brevity and to adequately define all the signs. Using Euclidean space and dropping the traditional subscript ($S_E \to S$) we define the action in the path integral as e^{-S}:

$$\begin{aligned} S = \sum_{\forall x,\mu}\Big\{ & (M+4r)\overline{\Psi}(x)\Psi(x) \\ & - \frac{1}{2}\overline{\Psi}(x)\left[(r-\gamma_\mu)U_\mu(x)\Psi(x+\hat{\mu}) + (r+\gamma_\mu)U_\mu^\dagger(x-\hat{\mu})\Psi(x-\hat{\mu})\right]\Big\} \end{aligned} \tag{A.30}$$

$$\begin{aligned} \{\gamma_\mu, \gamma_\nu\} &= 2\delta_{\mu\nu}\mathbb{I} \\ \gamma_\mu^\dagger &= \gamma_\mu \end{aligned} \tag{A.31}$$

Explicit representations of the Euclidean γ's are in the appendix of [75]. However note that the U's are written differently in [75], which results in a different sign for all odd number of gluon vertices. We conform to the conventions in Rothe [14]. To formulate consistent twisted boundary conditions for quark fields one must introduce a smell group SU(N_S) in addition to the colour group SU(N_C), with $N_S = N_C = N$, as pointed out by Parisi [76]. The quark fields are then $N \times N$-

matrices Ψ_{sc} in smelly-colourful space. The regular quark sum is written

$$\sum_c \overline{\Psi}_c(x)\Psi_c(x) = \frac{1}{N_s}\sum_{c,s} \overline{\Psi}_{sc}(x)\Psi_{cs}(x) = \frac{1}{N_s}\mathrm{Tr}\ \overline{\Psi}(x)\Psi(x). \tag{A.32}$$

The $1/N$ is similar to (A.42) in origin, and cancels with the trace of Γ. An analogous condition to (A.1) can be formulated

$$\Psi(x + L\hat{\nu}) = \Omega_\nu \Psi(x)\Omega_\nu^\dagger \left[e^{i\frac{\pi}{N}}\right] \tag{A.33}$$

where the extra factor in square brackets can be used if anti-periodic boundary conditions for the quarks are desired:

$$\Psi(x + 3L\hat{\nu}) = \Omega_\nu^3 \Psi(c)\Omega_\nu^{\dagger 3} \left[e^{3i\pi}\right] = [-]\,\Psi(x). \tag{A.34}$$

Note that without this additional imposition the zero-mode for the quark momenta will *not* be eliminated as there is no analogous traceless condition on quark-fields. However, this may complicate the determination of $L \to \infty$ on-shell quantities such as the quark mass. The on-shell condition will be much more complicated in the absence of a $p = (iM, 0, 0, 0)$ mode and depend on L through the lowest-$|\vec{p}|$ mode as well as T through allowed quantised M. Boundary conditions put the following constraint on the momenta

$$\Gamma_p = [-]\, e^{ip3L}\Gamma_p \tag{A.35}$$

thus

$$p_i = \frac{2\pi}{3L}(n_i + \left[\tfrac{1}{2}\right]), \qquad n_1, n_2 \in \mathbb{Z}. \tag{A.36}$$

The derivation of Γ_p for quark momenta p in terms of $\Omega_1, \Omega_2, n_1, n_2$ follows the case of gluon momentum, k with the additional $\left[\frac{1}{2}\right]$ cancelling the extra phase in the anti-periodic case. Apart from spinor and flavour indices, $\Psi(p)$ is a scalar quantity

because the colour and smell group structure is absorbed in the Γ_p. Defining

$$\int\!\!\!\!\!\!\sum_p = \frac{1}{3L^3T}\sum_{p_\perp}\sum_{p_\parallel}, \tag{A.37}$$

the plane wave expansions

$$\begin{aligned}\Psi_\beta(x) &= \int\!\!\!\!\!\!\sum_p e^{ipx}\Gamma_p\widetilde{\Psi}_\beta(p)\\ \overline{\Psi}_\alpha(x) &= \int\!\!\!\!\!\!\sum_p e^{\mp ipx}\Gamma^\dagger_{\mp p}\widetilde{\overline{\Psi}}_\alpha(p),\end{aligned} \tag{A.38}$$

are then needed to derive the Feynman rules. Note that a choice of sign is given in the anti-quark field; this is in order to allow for Feynman rules with the convention of a leaving anti-quark (upper-sign), or those for which all fields are ingoing (lower-sign). The quark fields Ψ and $\overline{\Psi}$ are still 4-spinor valued and this is reflected by the spinor indices β and α. The composition for Γ's in table A.1 remain the same when fermionic fields are introduced. If anti-periodic boundary conditions are used then the definition for the n_1, n_2 is the modified (A.36) rather than (A.12), if triply-twisted boundaries are required then the modified χ is used for the propagators. Quark-loops must be divided by 3 in order to remove the smell and determine the n_f dependence. Staggered quarks loops evaluated with unstaggered perturbation theory have an additional factor of 16 that should also be divided out (§2.2.2).

A.4 Twisted Ghost Vertices

These Grassman fields are different from quarks because they carry an adjoint colour index $1\cdots N^2-1$ so behave like gluon "momenta–colour." In particular they must have the same boundary conditions as the glue. Their plane wave

expansions are analogous to (A.38). For reference:

$$\begin{aligned}
\Gamma_k\Gamma_{k'} &= z(k,k')\,\Gamma_{k+k'} && (k,k' \text{ is a gluon or ghost momentum}) \\
\Gamma_k\Gamma_p &= z(k,p)\,\Gamma_{k+p} && (k+p \text{ is a fermion momentum}) \\
\Gamma_p^\dagger\Gamma_{p'} &= z(p,p)\,z^{-1}(p,p')\,\Gamma_{p'-p} && (p'-p \text{ is a gluon or ghost momentum}).
\end{aligned} \tag{A.39}$$

The function z from table A.1 acts on n_1, n_2 which are defined from the twisted parts of $k|p$ as

$$k_\perp = \frac{2\pi}{3L}\,(n_1, n_2) \qquad \text{Gluon momenta } n_i \in \mathbb{Z} \tag{A.40}$$

$$p_\perp = \frac{2\pi}{3L}\left(n_1 + \left[\tfrac{1}{2}\right], n_2 + \left[\tfrac{1}{2}\right]\right) \qquad \text{Quark momenta } n_i \in \mathbb{Z} \tag{A.41}$$

From table A.1 the colour factor arising from a (directed) Grassman propagator is χ. The absence of the factor of half in comparison to gluons is due to the single derivative in the action which gives directed propagators. A more explicit algorithm than §2.2 for generating the gluon vertices may be found in [13], with the additional factor of i^r to correspond to the Hermitian Gell-Mann matrix convention here. The Clebsch-Gordon coefficients are now given by their (5.30)

$$C_r(k_1,\ldots,k_r) = \frac{1}{N}\Big\{\mathrm{Tr}\,\left(\Gamma_{k_1}\cdots\Gamma_{k_r}\right) + (-1)^r\,\mathrm{Tr}\,\left(\Gamma_{k_r}\cdots\Gamma_{k_1}\right)\Big\}. \tag{A.42}$$

The twisted colours can take advantage of the inversion and cyclic permutation properties of C_r just as the untwisted colour factors. There are therefore 3 independent C_4's, 12 C_5's and 60 C_6's. Only one each needs elucidating as a subroutine; the others may be obtained by suitable permutation. This can be automated in the Feynman diagram generating code in order to eliminate transcription errors. It is worth noting that the odd-point colour functions are anti-symmetric under inversion which implies that the vertex must also satisfy this property. This eliminates all odd-point vertices for the mean-link for example. For case (2) of the phase

choice in table A.1, applying momentum conservation and using $z(k_1, \text{-}k_1) = 1$ gives

$$\begin{aligned}
C_2(k_1,k_2) =& 2 && \text{Case (2) only}\\
C_3(k_1,k_2,k_3) =& z(k_2,k_3) - z(k_2,k_1)\\
C_4(k_1,k_2,k_3,k_4) =& z(k_2,k_3+k_4)z(k_3,k_4) + z(k_3,k_2+k_1)z(k_2,k_1)\\
C_5(k_1,k_2,k_3,k_4,k_5) =& z(k_2,k_3+k_4+k_5)z(k_3,k_4+k_5)z(k_4,k_5)\\
& - z(k_4,k_1+k_2+k_3)z(k_3,k_1+k_2)z(k_2,k_1),
\end{aligned} \tag{A.43}$$

which has already started to become complicated yet the choice of case (2) has removed two z's from each C and the expression for z is smaller anyway. For quarks

$$\begin{aligned}
\tilde{S_Q} =& \int_p \widetilde{\overline{\Psi}}(p)\, S_F^{-1}(p) \widetilde{\Psi}(p)\\
&+ \sum_{r=1}^{\infty} \frac{1}{r!} g_0^r \int_{p_1}\int_{p_2}\int_{k_1}\cdots\int_{k_r} \sum_{\mu_1}\cdots\sum_{\mu_r} \widetilde{A}_{\mu_1}(k_1)\ldots\widetilde{A}_{\mu_r}(k_r)\\
&\cdot \delta(\mp p_1 + p_2 + \sum_{i=1}^{r} k_i)\, \widetilde{\overline{\Psi}}(p_1)\, V_r^Q(p_1,p_2;k_1,\mu_1;\ldots;k_r,\mu_r)\, \widetilde{\Psi}(p_2).
\end{aligned} \tag{A.44}$$

The Feynman rules for the quark, ghost and lattice measure vertices are shown in figure A.1.

Figure A.1: The Feynman rules for lattice measure, ghost and quark vertices.

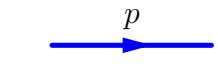

(a) Quark Propagator. (A.45) on page 128.

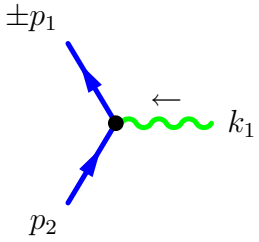

(b) One Gluon – Quark Vertex. (A.46) on page 128.

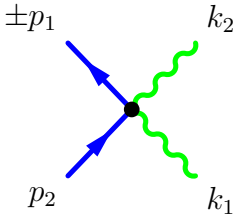

(c) Two Gluon – Quark Vertex. (A.47) on page 128.

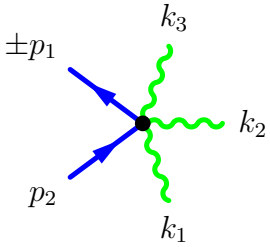

(d) Three Gluon – Quark Vertex. (A.48) on page 128.

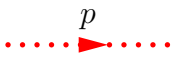

(e) Ghost Propagator. (A.49) on page 129.

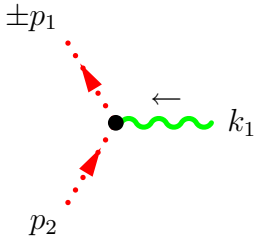

(f) One-Gluon – Ghost Vertex. (A.52) on page 130.

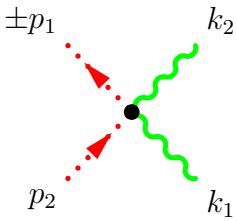

(g) Two-Gluon – Ghost Vertex. (A.53) on page 130.

None

(h) Three-Gluon – Ghost Vertex.

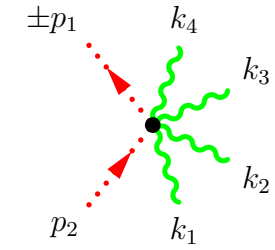

Figure A.1(Continued)

(i) Four-Gluon – Ghost Vertex. (A.54) on page 130.

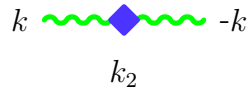

(j) Two-Gluon Measure Vertex. (A.61) on page 132.

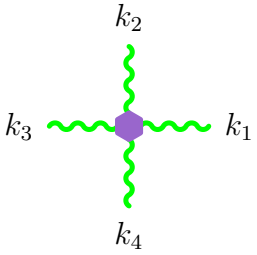

(k) Four-Gluon Measure Vertex. (A.65) on page 133.

Quark Propagator

$$S_F = \left\{ \frac{m_0 \mathbb{I} + \sum \left(-i\gamma_\mu \sin p_\mu + 2R\mathbb{I} \sin^2 \frac{p_\mu}{2} \right)}{\left(m_0 + 2R \sum \sin \frac{p_\mu}{2} \right)^2 + \sum \sin p_\mu^2} \right\}_{\alpha\beta} \cdot 1_{\text{Per.}}, \chi_{\text{A-Per.}} \tag{A.45}$$

The 4-spinor indices α and β come from the leaving and arriving quarks respectively. Quark traces always go backwards along the quark line with respect to the conventional arrow.

One Gluon – Quark vertex

$$V_1^Q(p_1, \alpha; p_2, \beta; k, \mu) = igz(k, p_2) \left\{ -\gamma_\mu \cos \frac{(p_2 \pm p_1)_\mu}{2} + iR\mathbb{I} \sin \frac{(p_2 \pm p_1)_\mu}{2} \right\}_{\alpha\beta} \tag{A.46}$$

The untwisted colour is T^C_{ab}, with the gluon $C = 1 \ldots N^2 - 1$, and the quarks have a (out), b (in) $\in \{1, 2, 3\}$.

Two Gluon – Quark vertex

$$\begin{aligned} V_2^Q = g^2 z(k_1 + k_2, p_2) \frac{\delta_{\mu\nu}}{2} \Bigg\{ & \Big[z(k_1, k_2) + z(k_1, k_2) \Big] \\ & \cdot \left(-\mathbb{I}R \cos \frac{(p_2 \pm p_1)}{2} + i\gamma_\mu \sin \frac{(p_2 \pm p_1)}{2} \right) \Bigg\}_{\alpha\beta} \end{aligned} \tag{A.47}$$

The improved quark vertices contain anti-symmetric colour parts, off-diagonal gluon emissions and $\gamma_\mu A_\nu$ parts. The untwisted colour is $\{T^C, T^D\}_{ab}$.

Three Gluon – Quark vertex

$$\begin{aligned} V_3^Q = & Ig^3 z(k_1 + k_2 + k_3, p_2) \frac{\delta_{\mu\nu\sigma}}{3!} \left(\gamma_\mu \cos \frac{(p_2 \pm p_1)_\mu}{2} - i \sin \frac{(p_2 \pm p_1)_\mu}{2} \right) \\ & \cdot \left\{ \Big[z(k_1, k_2 + k_3) z(k_2, k3) + z(k_3, k_2) z(k_2 + k_3, k_1) \Big] + 2 \text{ cyclic perms} \right\}_{\alpha\beta} \end{aligned} \tag{A.48}$$

and so on for the four-gluon quark vertices. Although for unimproved quarks the momentum dependence is the same for every permutation of the gluon lines for improved quarks this is not true. So for unimproved quarks such as Wilson ($R = 1$) or Naïve ($R = 0$) the vertex is independent of gluon momentum and can be evaluated once for each r-gluon vertex with the colour factor evaluated $r!$ times in permutation, while for improved the vastly more complicated vertex function has to be evaluated $r!$ ways too.

Ghost Propagator

$$S_F^{\text{Ghost}} = \frac{1}{\hat{k}^2}\delta_{\mu\nu}\,\chi \tag{A.49}$$

The twisted colour is χ as for the gluons, the untwisted δ_{AB}.

Ghost – Gluon Vertices

The untwisted colour factor for the r-gluon vertex is a product: $[t^a_{bc}]^r_{AB}$, where $t^a_{bc} = -if^a_{bc}$ is the adjoint which can be represented as a trace (from (A.32)) over a nested group of commutators of colour factors:

$$t^r \rightarrow \ \text{Tr}\left(\Gamma_{p_1}\Big[\Gamma_{k_1},\Big[\Gamma_{k_2},\ldots\big[\Gamma_{k_r},\Gamma_{p_2}\big]\Big]\Big]\right) \tag{A.50}$$

For convenience we can use $Z(k,p) = z(k,p) - z(p,k)$ which is the phase for the commutator of two Γ's. Following [14] we have

$$\begin{aligned}
S_{FP} &= -\sum_{A,B}\bar{c}^A\partial^{\text{L}}_\mu D_\mu c^B \\
D_\mu\left[\Phi\right] &= M^{-1}(\phi_\mu)\partial^{\text{R}}_\mu + i\Phi \\
\Phi_\mu &= gt^A_{BC}A^A_\mu \rightarrow g\mathbf{Z}(k)A_\mu(k) \\
M^{-1}(\phi) &= \frac{i\Phi}{1-e^{-i\Phi}} = 1 + \frac{i}{2}\Phi - \frac{1}{12}\Phi^2 - \frac{1}{720}\Phi^4 - \frac{1}{30240}\Phi^6 + \ldots
\end{aligned} \tag{A.51}$$

Here $\mathbf{Z}(k)$ is the k^{th} $(N^2-1)\times(N^2-1)$ (adjoint) matrix $Z^k_{k',k''} = Z(k,k')\delta(k+k'-k'')$. A useful identity is $\sum_x \chi_x \partial^{\mathrm{L}}_\mu \phi_x = -\sum_x (\partial^{\mathrm{R}}_\mu \chi_x)\phi_x$.

One Gluon – Ghost Vertex

$$V(p_1,A;p_2,B;k,\mu) = g\,Z(k,p_2)\,\left(\pm 2\sin\frac{p_1^\mu}{2}\cos\frac{p_2^\mu}{2}\right) \tag{A.52}$$

The corresponding untwisted colour would be if_{ABC}.

Two Gluon – Ghost Vertex

$$V_2(p_1,p_2;k_1,\mu;k_2,\nu) = \frac{g^2}{12}\delta_{\mu\nu}\Bigg\{\left(\pm 2\sin\frac{p_1^\mu}{2}2\sin\frac{p_2^\mu}{2}\right) \tag{A.53}$$
$$\cdot\Big[Z(k_1,k_2+p_2)Z(k_2,p_2)+Z(k_2,k_1+p_2)Z(k_1,p_2)\Big]\Bigg\}$$

The untwisted colour is $\left\{t^C,t^D\right\}_{AB}$. The twisted colour gets an additional trace compared to the untwisted colour by analogy to (A.32). There is no 3-gluon 2 ghost vertex.

Four Gluon – Two Ghost Vertex

$$V_4(p_1,p_2;k_1,\cdots,k_4) = \frac{g^4}{720}\delta_{\mu\nu\alpha\beta}\Bigg\{\left(\pm 2\sin\frac{p_1^\mu}{2}2\sin\frac{p_2^\mu}{2}\right) \tag{A.54}$$
$$\cdot\sum_{\sigma\in\mathbb{P}_4}\Big[Z(k_1,k_2+k_3+k_4+p_2)Z(k_2,k_3+k_4+p_2)Z(k_3,k_4+p_2)Z(k_4,p_2)\Big]\Bigg\}$$

The untwisted colour is $\left[\sum_{\sigma\in\mathbb{P}_4}\sigma\cdot(t^Ct^Dt^Et^F)\right]_{AB}$. There are 24 terms in $\mathbb{P}_4$, the permutation group of 4 elements.

Measure Terms

The measure term is also derived in [14]:

$$S_{\text{Measure}} = -\frac{1}{2}\ \text{Tr}\ \ln\left\{\frac{2(1-\cos\Phi)}{\Phi^2}\right\} = \frac{1}{24}\Phi^2+\frac{1}{2880}\Phi^4+\frac{1}{181440}\Phi^6+\ldots \tag{A.55}$$

This is expanded as before, though both twisted and untwisted colour are traced in the measure terms. The twisted colour has an additional normalisation factor of $1/N$. Some adjoint traces from appendix A of Pascual *QCD: Renormalistion for Practitioners* [77] are useful

$$\begin{aligned}
\left\{T^A, T^B\right\} &= \frac{1}{N}\delta_{AB} + d_{ABC}T^C \quad d \text{ real and totally symmetric} \\
\left[T^A, T^B\right] &= if_{ABC}T^C \quad f \text{ totally anti-symmetric} \\
\mathrm{Tr}_{\mathrm{Adj}}\, T^A T^B &= -\ \mathrm{Tr}\ f^A f^B = N\delta_{AB} \\
\mathrm{Tr}_{\mathrm{Adj}}\, T^A T^B T^C &= i\ \mathrm{Tr}\ f^A f^B f^C = i\frac{N}{2} f_{ABC} \\
\mathrm{Tr}_{\mathrm{Adj}}\, T^A T^B T^C T^D &= \ \mathrm{Tr}\ f^A f^B f^C f^D = \delta_{AB}\delta_{CD} + \delta_{AD}\delta_{BC} \\
&\qquad + \frac{N}{4}\left(d_{ABE}d_{CDE} - d_{ACE}d_{DBE} + d_{ADE}d_{BCE}\right)
\end{aligned} \tag{A.56}$$

Note that the d_{ABC} given in [14] is incorrect. An alternative source is the Particle Data Booklet [4].

2-pt Measure

The colour for the measure terms is the trace of the corresponding ghost twisted colour. Unfortunately this means that there is a spare index to be explicitly summed over using the following relation for phase choices (2) and (3) from table A.1

$$\sum_{q_\perp, q=0} z(ak_1 + bk_2, q) = N^2\delta_{ak_1+bk_2}, \quad \forall k_1, k_2, \tag{A.57}$$

Note that it is simpler to include the zero mode in the sum as the measure contains $Z(q, k_i) = 0$ if $q = 0$. Using the composition property $z(a, b + c) = z(a, b)z(a, c)$

both ways gives

$$\sum_{C,D} t^A_{CD} t^B_{DC} \to \frac{1}{N} \sum_{k_2,k_3} Z(k,k_2,k_3) Z(k_1,k_3,k_2) = \frac{1}{N} \sum_q Z(k,q) Z(\text{-}k,k+q)$$

$$= \frac{1}{N} \sum_q \left[z(k,q) - z(q,k) \right] \left[z(\text{-}k,k) z(\text{-}k,q) - z(k,\text{-}k) z(q,\text{-}k) \right] \quad \text{(A.58)}$$

$$= \frac{2}{N}\, z(\text{-}k,k) \left[N^2 - \frac{1}{2} \sum_q \Big\{ z(2q,k) + z(\text{-}2q,k) \Big\} \right] \quad \text{(A.59)}$$

$$= 2N\, z(\text{-}k,k) \left[1 - \delta_k \right]. \quad \text{(A.60)}$$

The contribution from δ_k is removed by the attached propagators leaving

$$V_2^{\text{Meas.}}(k,\mu;-k,\nu) = -\frac{1}{12} g^2 \Big[2N z(k,\text{-}k) \Big] \delta_{\mu\nu} \quad \text{(A.61)}$$

The untwisted colour is $N\delta_{AB}$.

4-pt Measure

The colour factor can be written

$$C_4^{\text{Meas.}} = \frac{1}{3} \sum_p Z(k_1,p) Z(k_2,k_1+p) Z(k_3,k_1+k_2+p) Z(k_4,p) z(k_4,\text{-}k_4) \quad \text{(A.62)}$$

where we have used conservation of momentum in the last Z. Specialising to case (2) for its anti-symmetry in the labels $z(k,p) = z(\text{-}p,k) = z(p,\text{-}k)$, expanding and

using the composition rule above gives

$$
\begin{aligned}
C_4^{\text{Meas.}} = \frac{1}{3}\sum_p \Big\{ & z(\text{-}k_2, k_1)\, z(\text{-}k_3, k_1{+}k_2) + z(k_2, k_1)\, z(k_3, k_1{+}k_2) \\
& + z(k_2, k_1)\, z(k_3, k_1{+}k_2)\, z(\text{-}2k_1{-}2k_4, p) - z(\text{-}k_2, k_1)\, z(\text{-}k_3, k_1{+}k_2)\, z(2k_1, p) \\
& + z(k_2, k_1)\, z(\text{-}k_3, k_1{+}k_2)\, z(\text{-}2k_3{-}2k_4, p) - z(\text{-}k_2, k_1)\, z(k_3, k_1{+}k_2)\, z(\text{-}2k_2, p) \\
& + z(k_2, k_1)\, z(\text{-}k_3, k_1{+}k_2)\, z(2k_2{+}2k_4, p) - z(\text{-}k_2, k_1)\, z(\text{-}k_3, k_1{+}k_2)\, z(2k_4, p) \\
& - z(\text{-}k_2, k_1)\, z(k_3, k_1{+}k_2)\, z(2k_3, p) + z(\text{-}k_2, k_1)\, z(\text{-}k_3, k_1{+}k_2)\, z(2k_1{+}2k_4, p) \\
& - z(k_2, k_1)\, z(\text{-}k_3, k_1{+}k_2)\, z(\text{-}2k_3, p) + z(\text{-}k_2, k_1)\, z(k_3, k_1{+}k_2)\, z(2k_3{+}2k_4, p) \\
& + z(\text{-}k_2, k_1)\, z(k_3, k_1{+}k_2)\, z(\text{-}2k_2{-}2k_4, p) - z(k_2, k_1)\, z(k_3, k_1{+}k_2)\, z(\text{-}2k_1, p) \\
& - z(k_2, k_1)\, z(k_3, k_1{+}k_2)\, z(\text{-}2k_4, p) - z(k_2, k_1)\, z(\text{-}k_3, k_1{+}k_2)\, z(2k_2, p) \Big\},
\end{aligned}
\tag{A.63}
$$

next the sum rule from (A.57) may be applied dropping terms such as δ_{k_1} which are already accounted for by the propagators:

$$
C_4^{\text{Meas.}}(k_1, k_2, k_3, k_4) = 3 \begin{cases} 2\Big[\delta_{k_1+k_2} + \delta_{k_1+k_3} + \delta_{k_2+k_3}\Big] \\ \quad + z(k_2, k_1) z(k_3, k_1{+}k_2) \\ \quad + \dfrac{1}{z(k_2, k_1) z(k_3, k_1{+}k_2)} \end{cases} \tag{A.64}
$$

The vertex is

$$
V_4^{\text{Meas.}}(k_1, k_2, k_3, k_4) = -\frac{1}{2880} g^4 \delta_{\mu\nu\rho\sigma} \sum_{\sigma \in \mathbb{P}_4} \Big(\sigma \cdot C_4^{\text{Meas.}}(k_1, k_2, k_3, k_4) \Big) \tag{A.65}
$$

The untwisted colour is $C_4^{\text{Meas.}} = \text{Tr}\left[t^A t^B t^C t^D\right]$ which was given in a reduced form in (A.56) with fewer internal summations.

A.5 Checking

In the large L limit twisted boundary conditions give the same perturbative answers as the untwisted boundaries. This can be realised by considering a cell of an r-loop integral – a small volume element $(\frac{2\pi}{L})^{4r}$ in untwisted k-space which contains one single lattice point. In twisted space this same volume will contain some number of twisted points $< N^{2r}$, after accounting for those which give no contribution. In the large L limit the momentum function part of the answer will factorise for all these points because the difference in momentum of these points goes to zero. The total colour factors must therefore also be the same. Thus the average over the extra twisted part of the momenta including the appropriate phase-space volume must equal that of the continuum. This average must be the same for all cells and all L however as the colour factors only use the momentum modulo N. This is a good way of checking the colour implementation. Some of the third order diagrams in the Wilson loop have sufficient propagators to reject more than 50% of the valid twisted-3 external momenta. Ron Horgan reports [78] that some `VEGAN` computations require an explicit sum over all the twisted leftovers n_i in each $2\pi/L$ momentum-space cell and cannot rely on randomness to converge but this is not necessarily always true.

A.6 Expectation Colour Factors

Many quantities of interest are expressed as the expectation of $\frac{1}{N}\mathrm{Re\ Tr}\ (\prod U)$. Twisted colours can use that N in (A.22), and use the same gluon colour functions for the expectation as for the action. The untwisted colour factor will need an extra overall $1/N$ from the expectation in comparison. The volume element for a D-

dimensional r-loop integral over either a finite or infinite lattice is $(d^D k)^r \Big/ (2\pi)^{Dr}$ for periodic boundary conditions and changes to $(N\, d^D k)^r \Big/ (2\pi)^{Dr}$ for finite twisted boundary conditions. An explicit sum over all modes is viable for 1-loop in the approach advocated here, but two and three loops are computationally intractable; however the volume factors would be: $1 \Big/ L^3 T$ and $1 \Big/ N L^3 T$ for periodic and twisted boundary conditions respectively, for each independent momentum on a lattice that was T lattice units in the time direction but L in the spatial directions.

APPENDIX B

AUTOMATICALLY GENERATED DIAGRAM CODE

The example diagram discussed in §2.3 can be automatically generated and the result is stored in an intermediate format. A back-end written for `C++` or some other language (there is partial support for LaTeX+`feynMP`) can be used to make compilable code. The following figures, B.1–B.4, illustrate the `C++` code. The macros, classes and functions in green need to be included from header files; hopefully their implementation is obvious. The basic idea is to keep the code as readable as possible, which is why all the variable names for the Feynman rules contain their type and the propagators names where they are going from and to. There is no reference to a particular action, and the code can be linked to any object file which implements the necassary vertices. The generated code in this case is compilable but the result would be assisted significantly by performing a linear transformation of the momenta because the routing is not particularly favourable (this could be automated) and because the Lorentz sum is not optimal. The same code can evaluate the diagram with finite, twisted or infinte momenta, or differentiate with respect to a parameter in the action (e.g. the quark mass) or one of the momenta (e.g. for a wavefunction renormalisation).

```
//1111111111111111111111111111111111111111111111111111111111111111111111111111
//1111111111111111111111111111111111111111111111111111111111111111111111111111
void diagram_1_gamma(Tr_data_cache& data)
{
  complex<double> answer=complex<double>(0.,0.);
  parallel_cout ≪ "Computing Trace for Diagram 1 ... "≪flush;
  for(int Z=MIN_VERT;Z<MAX_VERT;Z++) {
    for(int Y=MIN_VERT;Y<MAX_VERT;Y++) {
      for(int X=MIN_PROP;X<MAX_PROP;X++) {
        for(int W=MIN_PROP;W<MAX_PROP;W++) {
          for(int θ=1;θ<5;θ++) {
            for(int η=1;η<5;η++) {
              for(int χ=1;χ<5;χ++) {
                for(int ι=1;ι<5;ι++) {
                answer+=γ(Z,θ,η)×γ(Y,χ,ι)×γ(X,ι,θ)×γ(W,η,χ);
                }
              }
            }
          }
          if (abs(answer)≠0) {
            data.indices[data.number_to_do]=data.hash(Z, Y, X, W);
            data.trace_val[data.number_to_do++]=answer;
            answer=complex<double>(0.,0.);
          }
        }
      }
    }
  }
  parallel_cout ≪ "found "≪ data.number_to_do ≪ "/ 4^2 5^2 = 400"≪ endl;
}
```

Figure B.1: The spinor trace for the example Feynman Diagram. This subroutine is called by a function that calculates the spinor trace once and optionally writes it out to disk. The non-zero entries in the trace table are hashed for memory reasons because third order diagrams with Clover fermions can have 4 vertices and 4 propagators with more than half a million entries in the table. Several parameters are easily tuneable so that quarks with different types of spinors can be easily accomodated with the *same* code.

```
//1111111111111111111111111111111111111111111111111111111111111111111111111111111111
//1111111111111111111111111111111111111111111111111111111111111111111111111111111111
double diagram_1(double *k_in, const double *colour_1)
{
  static const Tr_data_cache cached_trace = cache(diagram_1_gamma);
  long sum_over = cached_trace.number_to_do;

      Qfourvector k_3 = QTransform(k_in);
      Qfourvector k_2 = QTransform(k_in+4);
  Gluonfourvector k_1 = Transform(k_in+8);
  if(QTransform_Check(k_3) || QTransform_Check(k_2)) {return 0.;}
  if(Transform_Check(k_1)) {return 0.;}

  Complex answer=Complex(0.,0.);
  // Twisted colour factor and colour checking code omitted here.
  double colour_fac[1]={colour_1[0]};
    VertexTable E2(2); Expec_2pt(k_1,-k_1,E2);
    VertexTable A3(3); Action_3pt(-k_1,k_1-k_2+k_3,k_2-k_3,A3);
    VertexTable A3_2(3); Action_3pt(k_1,-k_1+k_2-k_3,-k_2+k_3,A3_2);
    VertexTable GP_E2_to_A3(2); Gluon_Propagator(k_1,GP_E2_to_A3);
    VertexTable GP_E2_to_A3_2(2); Gluon_Propagator(-k_1,GP_E2_to_A3_2);
    VertexTable GP_A3_to_G1Q2(2); Gluon_Propagator(k_2-k_3,GP_A3_to_G1Q2);
    VertexTable GP_A3_to_A3_2(2); Gluon_Propagator(k_1-k_2+k_3,GP_A3_to_A3_2);
    VertexTable GP_A3_2_to_G1Q2_2(2);
                                  Gluon_Propagator(-k_2+k_3,GP_A3_2_to_G1Q2_2);
  CVertexTable G1Q2(2); Gluon_1_Quark_2(-k_2+k_3,-k_3,k_2,G1Q2);
  CVertexTable G1Q2_2(2); Gluon_1_Quark_2(k_2-k_3,-k_2,k_3,G1Q2_2);
  CVertexTable QP_G1Q2_to_G1Q2_2(1);
                                  Quark_Propagator(k_3,QP_G1Q2_to_G1Q2_2);
  CVertexTable QP_G1Q2_2_to_G1Q2(1);
                                  Quark_Propagator(k_2,QP_G1Q2_2_to_G1Q2);
   //  VertexTable Name(N) is a N-tensor in Lorentz indices of real doubles.
   // CVertexTable is complex, needed for quark-vertices.
```

Figure B.2: First part of the implementation of the example Feynman diagram. This fragment initialises and transforms the momenta, and evaluates the Feynman rules for those specific momenta. A linear transform should be applied by hand because of the poor routing.

```
36  long index_hash; int Z, Y, X, W;
37  for(long index=0;index<sum_over;index++) {
38    index_hash=cached_trace.indices[index];
39    Z=cached_trace.unhash(0,index_hash);
40    Y=cached_trace.unhash(1,index_hash);
41    X=cached_trace.unhash(2,index_hash);
42    W=cached_trace.unhash(3,index_hash);
43    Extern_sum(μ) {    // These macros are used to optimise for diagonal
44      Extern_sum(ν) { // propagators, or if the expectation E2(μ,ν) is not dense.
45        Sum_or_equ(σ,μ) {
46          Intern_sum(ρ) {          // In practice the sum should be rearranged
47            Intern_sum(ω) {        // to do the quark loop first (separately) and
48              Sum_or_equ(α,ν) { // then combine with the gluon loop.
49                Sum_or_equ(β,ρ) {
50                  Intern_sum(δ) {
51                    Sum_or_equ(ϵ,ω) {
52                      Sum_or_equ(ζ,δ) {
53                        answer+=-½×cached_trace.trace_val[index]×
54                                 E2(μ,ν)×A3(σ,ρ,ω)×A3_2(α,β,δ)×
55                                 G1Q2(ϵ,Z)×G1Q2_2(ζ,Y)×
56                                 GP_E2_to_A3(μ,σ)×GP_E2_to_A3_2(ν,α)×
57                                 GP_A3_to_A3_2(ρ,β)×GP_A3_to_G1Q2(ω,ϵ)×
58                                 GP_A3_2_to_G1Q2_2(δ,ζ)×
59                                 QP_G1Q2_to_G1Q2_2(X)×QP_G1Q2_2_to_G1Q2(W)×
60                                 colour_fac [0];
61                      }
62                    }
63                  }
64                }
65              }
66            }
67          }
68        } // Several macros are used to quickly change to differentiating the
69      }   // result with respect to parameters or momenta, twisted boundary
70    }     // conditions ( different volume factor) and to multiply the integrand by
71  }       // some common factor to change normalisation.
72  answer×=QJacobian(k_in)×QJacobian(k_in+4)×Jacobian(k_in+8);
73  return RE_IM_PART(RESULTS(answer)×factor(1))/
74         (VOL(k_1)×VOL(k_2)×VOL(k_3));
75}
```

Figure B.3: Second part of the implementation of the example Feynman diagram. This fragment does the sum over lorentz indices and multiplies by the colour, normalisation, Jacobian and volume factors.

```
int main(int argc,char **argv)
{
  PARALLEL_START;
  complex<double> colour_sum_1[1]={complex<double>(0.,0.)};

  for(int A=1;A<9;A++) {
    for(int B=1;B<9;B++) {
      for(int C=1;C<9;C++) {
        for(int E=1;E<9;E++) {
          for(int F=1;F<9;F++) {
            for(int a_5=1;a_5<4;a_5++) {
              for(int b_5=1;b_5<4;b_5++) {
                // Compute the usual colour factor
                colour_sum_1[0]+=colour_2pt(A,B)×
                  colour_3pt(A,C,E)×colour_3pt(B,C,F)×
                  Gluon_1_Quark_2_colour(E,b_5,a_5)×
                  Gluon_1_Quark_2_colour(F,a_5,b_5);
              }
            }
          }
        }
      }
    }
  }

  double colour_divisor=3.; // Colour normalisation.
  const double colour_1[1]={real(colour_sum_1[0]/colour_divisor)};

  parallel_cout ≪ "diagram 1 colour = "≪ colour_sum_1[0]/colour_divisor ≪ endl;
  parallel_cout ≪ " Doing "≪ first_iter() ≪ "@"≪ first_pts();
  parallel_cout ≪ " and "≪ second_iter() ≪ "@"≪ second_pts() ≪ endl;
  double total=0.,sd=0.;
  integrate(diagram_1,colour_1,1,3,&total,&sd,"0001");
  // subroutine, colour, number, #−momenta, total, error, logfile

  parallel_cout ≪ "total = "≪ total ≪ ", error = " ≪ sd ≪ endl;
  PARALLEL_CLOSE;
}
```

Figure B.4: Parallel main program to calculate colour factor and integrate the diagram.

APPENDIX C

STAGGERED CURRENTS

A detailed implementation of the currents is required for scenario 1: to explicitly remove the one-loop taste-changing effects. There are two pieces needed for the currents: the signs and factors for the point splitting, and the way that they are coupled to the scalars. The following implementation will remove the larger vector coefficients and assumes that the axial-vector ones are small enough that they can be neglected.

C.1 Projection Operator

The taste-changing interactions are calculated for specific momentum changes, $\zeta\pi/a$, so the counter-terms must make sure that only this momentum is being transfered along the non-propagating scalar line ϕ—ϕ. On the lattice using local operators this can only be approximated. A reasonably local projection operator which does a good job of selecting the correct transfer momentum around $\zeta\pi/a$ is therefore needed. Ideally the projection $\mathcal{P}(\zeta)$ would select only the momentum $\zeta\pi/a$: $\mathcal{P}(\zeta)f(k) = f(k)\delta_{k=\zeta'}$. On the lattice the following operator is a suitable replacement for the Dirac Delta function:

$$\mathcal{P}(\zeta) = (-1)^{4-\zeta^2} \prod_{\mu} \left((\zeta_\mu - 1) - \frac{\Delta_\mu^{(2)}}{4} \right) \Bigg|_{\text{sym}} . \tag{C.1}$$

This is $-\Delta_\mu^{(2)}/4$ in each direction $\zeta_\mu = 1$, with suppression $\sin^2(k_\mu/2)$, and $1+\Delta_\mu^{(2)}/4$ in directions $\zeta_\mu = 0$, with suppression $\cos^2(k_\mu/2)$. This property along with the approximate relation valid at this order: $\mathcal{P}(\zeta)\mathcal{P}(\zeta') \sim 1$ can be used to reduce the number of scalar fields.

The action of the projection operator depends on whether it is operating on a "colourful" 3×3 complex matrix link-scalar or a complex singlet scalar. In the case of the colorful scalar-matrix fields φ which live on links and transform like link fields under changes in gauge the derivatives in $\mathcal{P}(\zeta)$ act according to

$$\begin{aligned}\Delta^{(2)}_\nu \varphi_\mu(x) = \frac{1}{a^2 u_0^2}\Big[& U_\nu(x)\varphi_\mu(x+\hat{\nu})U^\dagger_\nu(x+\hat{\mu}+\hat{\nu}) \\ & - 2u_0^2\varphi_\mu(x) \\ & + U^\dagger_\nu(x-\hat{\nu})\varphi_\mu(x-\hat{\nu})U_\nu(x+\hat{\mu}-\hat{\nu})\Big],\end{aligned} \tag{C.2}$$

just as for the usual link-field. The tadpole improvement u_0 should be the same as for the rest of the action. Note that $\mathcal{P}\phi^\dagger = (\mathcal{P}\phi)^\dagger$. In the case of the singlet currents with $\phi_\mu(x)$ living on sites the operator $\Delta^{(2)}_\mu$ acts like an ordinary second derivative, without insertion of link variables:

$$\Delta^{(2)}_\nu \phi_\mu(x) = \frac{1}{a^2}\Big[\phi_\mu(x+a\hat{\nu}) - 2\phi_\mu(x) + \phi_\mu(x-a\hat{\nu})\Big], \tag{C.3}$$

C.2 Currents

Singlet currents with anti-hermitian matrices between the spinors:

$$J^{(1,C)}_\mu[\phi](x) = \begin{cases} \dfrac{1}{2}\left[\overline{\psi}(x)\gamma_\mu U_\mu(x)\phi_\mu(x)\psi(x+\hat{\mu}) - \overline{\psi}(x+\hat{\mu})\gamma_\mu\phi^\dagger_\mu(x)U^\dagger_\mu(x)\psi(x)\right] \\ \dfrac{i}{2}\left[\overline{\psi}(x)\gamma_\mu(U\phi)_\mu(x)\psi(x+\hat{\mu}) + \overline{\psi}(x+\hat{\mu})\gamma_\mu(U\phi)^\dagger_\mu(x)\psi(x)\right], \end{cases} \tag{C.4}$$

The upper current is used for $C = 1$ which is equivalent to $\zeta_\mu = 1$, and the lower for $C = -1, (\zeta_\mu = 0)$. Note that $\tilde{c}_V = c^{(1)}_V(\zeta^2, 1)$, and $c^{(1)}_V = c^{(1)}_V(\zeta^2, -1)$. The factors of $(-1)^{\zeta\cdot x}$, $(\overline{s} = \zeta)$ in (3.9) are not needed: here that factor is in the projection operator getting the right momentum. The singlet counter-term will be made up

from $\sum_{15\times\zeta,\mu} c_V^{(1)}(\zeta^2,C)J_\mu^C[\mathcal{P}(\zeta)\phi_\mu](x)$. C=1 when $\zeta_\mu = 1$.

The octet 4-quark operator has the structure $\sum_c \overline{\psi}T^c\psi\,\overline{\psi}T^c\psi$, which would require explicit insertion of a representation of the T-matrices. To avoid this an SU(3)-colour Fierz: $(T^a)_{ij}(T^a)_{kl} = \frac{1}{2}(\delta_{ik}\delta_{jl} - \frac{1}{3}\delta_{ij}\delta_{kl})$ can be applied. The second term is now a colour singlet, and can be treated in the same way as the rest of the colour singlet currents, whilst the first term is crossed in colour. If those identifications are cut new Hermitian 3x3 matrix "link"-fields $\varphi_\mu(x)_{ik}$ and $\varphi_\mu(x)_{jl}$ can be inserted in such a manner that when integrated out will have the same effect. The crossing happens in considering the leading terms in the perturbative expansion of $e^{-cJ[\varphi]+\mathrm{Tr}\,|\varphi|^2}$, using $\int \mathcal{D}\varphi e^{-\mathrm{Tr}\,\varphi\varphi^\dagger}\varphi_{ij}\varphi^\dagger_{kl}$=$\delta_{ik}\delta_{jl}$.

Crossed currents:

$$J_\mu^{(8,C)}[\varphi](x) = \begin{cases} \frac{1}{2}\left[\overline{\psi}(x)\gamma_\mu\varphi_\mu(x)\psi(x+\hat{\mu}) - \overline{\psi}(x+\hat{\mu})\gamma_\mu\varphi^\dagger_\mu(x)\psi(x)\right], & \zeta_\mu = 1, C = 1 \\ \frac{i}{2}\left[\overline{\psi}(x)\gamma_\mu\varphi_\mu(x)\psi(x+\hat{\mu}) + \overline{\psi}(x+\hat{\mu})\gamma_\mu\varphi^\dagger_\mu(x)\psi(x)\right], & \zeta_\mu = 0, C = \text{-}1 \end{cases} \tag{C.5}$$

The upper current is used for $C = 1$ ($\zeta_\mu = 1$), and the lower for $C = -1$, ($\zeta_\mu = 0$). Note that $\tilde{c}_V = c_V^{(1)}(\zeta^2, 1)$, and $c_V^{(1)} = c_V^{(1)}(\zeta^2, -1)$. The complete crossed counterterm will be made from a sum over ζ which involves all the different coefficients given in the tables: $\sum_{15\times\zeta,\mu} c_V^{(8)}(\zeta^2,C)\frac{1}{2}\left(J_\mu^{(8,C)}[\mathcal{P}(\zeta)\varphi](x) - \frac{1}{3}J_\mu^{(1,C)}[\mathcal{P}(\zeta)\phi_\mu](x)\right)$. The equivalence with four-quark currents is through the following trick:

$$\Delta\mathcal{L} = X\varphi - X'\varphi^\dagger + \mathrm{Tr}\,\varphi\varphi^\dagger \qquad \equiv \qquad \Delta\mathcal{L} = \frac{1}{2}XX' \tag{C.6}$$

with the assignment $J[\phi] = X\phi - X'\phi^\dagger$, ie $X \sim \overline{\psi}(x)\gamma_\mu\psi(x+\mu)$, the first piece of each current. This is the most local connection possible: $\overline{\psi}(x)\gamma_\mu\psi(x+\mu)\overline{\psi}(x+\mu)\gamma_\mu\psi(x)$, rather than shifting the second current by one lattice spacing, and having

the currents offset, as would happen with real scalars ϕ with

$$\Delta\mathcal{L} = \phi(x)\,[\overline{\psi}(x)\gamma_\mu\psi(x+\hat{\mu}) - \overline{\psi}(x+\hat{\mu})\gamma_\mu\psi(x)].$$

The final expression to be added to the Lagrangian $e^{-\mathcal{L}}$ is

$$\begin{aligned}\Delta\mathcal{L} = {} & \phi_\mu(x)\phi_\mu(x) + \mathrm{Tr}\left[\varphi_\mu(x)\varphi_\mu^\dagger(x)\right] \\ & + \sum_{\substack{15\times\zeta\neq 0 \\ 4\times\mu}} \alpha_s(\pi/a) \left\{ \begin{array}{c} \left(c_V^{(1)}(\zeta) - \frac{1}{6}c_V^{(8)}(\zeta)\right) J_\mu^{(1),C}[\mathcal{P}(\zeta)\phi_\mu](x) \\ +c_V^{(8)}(\zeta)\,\frac{1}{2}J_\mu^{(8),C}[\mathcal{P}(\zeta)\varphi](x) \end{array} \right\}\end{aligned} \tag{C.7}$$

which has a field $\phi_\mu(x)$ in each of the four directions, at every lattice site. There is one 3×3-complex matrix field $\varphi_\mu(x)$ on each link. The same "scalar" is used for each real light quark flavour.

For a generic smeared quark action of the form

$$\frac{1}{2}\sum_\mu \left[\overline{\psi}(x)\gamma_\mu V'_\mu(x)\psi(x+\mu) - \overline{\psi}(x)\gamma_\mu V'^\dagger_\mu(x-\mu)\psi(x-\mu)\right] + m\overline{\psi}\psi \tag{C.8}$$

the addition can be accumulated into new link-fields between the quarks:

$$\begin{aligned} V'_\mu(x) \to {} & V'_\mu(x) \\ & + \sum_{15\times\zeta\neq 0} i^{1-\zeta_\mu}\alpha_s(\pi/a)\left\{c'_V(\zeta)U_\mu(x)\mathcal{P}\phi_\mu(x) + c_V^{(8)}(\zeta)\frac{1}{2}\mathcal{P}\varphi_\mu(x)\right\} \end{aligned} \tag{C.9}$$

$$\begin{aligned} V'^\dagger_\mu(x-\mu) \to {} & V'^\dagger_\mu(x-\mu) \\ & + \sum_{15\times\zeta\neq 0} (-i)^{1-\zeta_\mu}\alpha_s\left\{c'_V(\zeta)\mathcal{P}\phi^\dagger_\mu(x-\mu)U^\dagger_\mu(x-\mu) + c_V^{(8)}(\zeta)\frac{1}{2}\mathcal{P}\varphi^\dagger_\mu(x-\mu)\right\} \end{aligned}$$

where the coefficient $c'_V(\zeta) = \left(c^{(1)}(\zeta) - \frac{1}{6}c^{(8)}(\zeta)\right)$. Finally the scalar "propagators" should be added:

$$\Delta\mathcal{L} = \sum_{4\times\mu}\left\{\phi_\mu(x)\phi^\dagger_\mu(x) + \mathrm{Tr}\left[\varphi_\mu(x)\varphi^\dagger_\mu(x)\right]\right\}, \tag{C.10}$$

for a complex scalar ϕ, and a 3×3 (colour) matrix φ. Accumulation of the change into V provides immense benefit as it means that no changes to the

inverter are required. Note, however that $V^\dagger \equiv (V)^\dagger$ and hence the quark determinant is anti-Hermitian (plus m) with no exceptional configurations *only* if the coefficients $c_V^{(1,8)}$ are *real*. α_s should be the same as that used in the 1-loop Symanzik gluon action.

REFERENCES

[1] K. G. Wilson, *Confinement of quarks*, *Phys. Rev.* **D10** (1974) 2445–2459.

[2] **HPQCD** Collaboration, C. T. H. Davies *et. al.*, *High-precision lattice QCD confronts experiment*, `hep-lat/0304004`.

[3] R. A. Briere *et. al.*, *CLEO–c and CESR–c: a new frontier of weak and strong*, . CLNS-01-1742.

[4] K. Hagiwara *et. al.*, *Review of Particle Physics*, *Physical Review D* **66** (2002) 010001+.

[5] G. P. Lepage and P. B. Mackenzie, *On the viability of lattice perturbation theory*, *Phys. Rev.* **D48** (1993) 2250–2264 [`hep-lat/9209022`].

[6] S. J. Brodsky, G. P. Lepage and P. B. Mackenzie, *On the elimination of scale ambiguities in perturbative quantum chromodynamics*, *Phys. Rev.* **D28** (1983) 228.

[7] G. P. Lepage, *Flavor-symmetry restoration and Symanzik improvement for staggered quarks*, *Phys. Rev.* **D59** (1999) 074502 [`hep-lat/9809157`].

[8] K. Gottfried and Y. Tung-Mow, *Quantum Mechanics: Fundamentals*. Springer-Verlag, New York, 2003.

[9] M. Luscher and P. Weisz, *Computation of the action for on-shell improved lattice gauge theories at weak coupling*, *Phys. Lett.* **B158** (1985) 250.

[10] M. G. Alford, W. Dimm, G. P. Lepage, G. Hockney and P. B. Mackenzie, *Lattice QCD on small computers*, *Phys. Lett.* **B361** (1995) 87–94 [`hep-lat/9507010`].

[11] S. Capitani, *Lattice perturbation theory*, *Phys. Rept.* **382** (2003) 113–302 [`hep-lat/0211036`].

[12] S. Gottlieb, *Dynamical Kogut-Susskind fermion results*, . Plenary presentation at Lattice 2003 in Tsukuba.

[13] M. Luscher and P. Weisz, *Efficient numerical techniques for perturbative lattice gauge theory computations*, *Nucl. Phys.* **B266** (1986) 309.

[14] H. J. Rothe, *Lattice gauge theories: An introduction*, *World Sci. Lect. Notes Phys.* **59** (1997) 1–512.

[15] J. Snippe, *Computation of the one-loop Symanzik coefficients for the square action*, *Nucl. Phys.* **B498** (1997) 347–396 [`hep-lat/9701002`].

[16] B. Sheikholeslami and R. Wohlert, *Improved continuum limit lattice action for QCD with wilson fermions*, *Nucl. Phys.* **B259** (1985) 572.

[17] S. Naik, *On-shell improved lattice action for QCD with Susskind fermions and asymptotic freedom scale*, *Nucl. Phys.* **B316** (1989) 238.

[18] K. Jansen, *Dynamical fermion simulations*, . Plenary presentation at Lattice 2003 in Tsukuba.

[19] M. Luscher and P. Weisz, *Background field technique and renormalization in lattice gauge theory*, *Nucl. Phys.* **B452** (1995) 213–233 [hep-lat/9504006].

[20] M. Luscher and P. Weisz, *Computation of the relation between the bare lattice coupling and the MS coupling in SU(N) gauge theories to two loops*, *Nucl. Phys.* **B452** (1995) 234–260 [hep-lat/9505011].

[21] L. F. Abbott, *The background field method beyond one loop*, *Nucl. Phys.* **B185** (1981) 189.

[22] G. P. Lepage, *A new algorithm for adaptive multidimensional integration*, *J. Comput. Phys.* **27** (1978) 192. Vegas.

[23] G. P. Lepage, VEGAS*: An adaptive multidimensional integration program*, . CLNS-80/447.

[24] M. Tentyukov and J. Fleischer, *A feynman diagram analyser DIANA*, *Comput. Phys. Commun.* **132** (2000) 124–141 [hep-ph/9904258].

[25] T. Hahn, *Generating feynman diagrams and amplitudes with feynarts 3*, *Comput. Phys. Commun.* **140** (2001) 418–431 [hep-ph/0012260].

[26] J. A. M. Vermaseren, *New features of FORM*, math-ph/0010025.

[27] R. Harlander and M. Steinhauser, *Automatic computation of feynman diagrams*, *Prog. Part. Nucl. Phys.* **43** (1999) 167–228 [hep-ph/9812357]. Introduces the COMPhep program.

[28] G. P. Lepage, P. B. Mackenzie, N. H. Shakespeare and H. D. Trottier, *Perturbative two- and three-loop coefficients from large beta Monte Carlo*, *Nucl. Phys. Proc. Suppl.* **83** (2000) 866–871 [hep-lat/9910018].

[29] H. D. Trottier, N. H. Shakespeare, G. P. Lepage and P. B. Mackenzie, *Perturbative expansions from Monte Carlo simulations at weak coupling: Wilson loops and the static-quark self- energy*, *Phys. Rev.* **D65** (2002) 094502 [hep-lat/0111028].

[30] T. Becher and K. Melnikov, *The asymptotic expansion of lattice loop integrals around the continuum limit*, *Phys. Rev.* **D66** (2002) 074508 [hep-ph/0207201].

[31] T. Becher and K. Melnikov, *Continuum methods in lattice perturbation theory*, *Nucl. Phys. Proc. Suppl.* **116** (2003) 407–411 [hep-ph/0211215].

[32] T. Becher and K. Melnikov, *The self-energy of improved staggered quarks*, *Phys. Rev.* **D68** (2003) 014506 [hep-lat/0302014].

[33] M. Luscher, *Some analytic results concerning the mass spectrum of Yang-Mils gauge theories on a torus*, *Nucl. Phys.* **B219** (1983) 233–261.

[34] E. G. Floratos and D. Petcher, *A two loop calculation of the mass gap for the 0(n) model in finite volume*, *Nucl. Phys.* **B252** (1985) 689.

[35] K. Hornbostel, G. P. Lepage and C. Morningstar, *Scale setting for alpha(s) beyond leading order*, *Nucl. Phys. Proc. Suppl.* **94** (2001) 579–583 [hep-lat/0011049].

[36] K. Hornbostel, G. P. Lepage and C. Morningstar, *Scale setting for alpha(s) beyond leading order*, *Phys. Rev.* **D67** (2003) 034023 [hep-ph/0208224].

[37] T. Blum *et. al.*, *Improving flavor symmetry in the Kogut-Susskind hadron spectrum*, *Phys. Rev.* **D55** (1997) 1133–1137 [hep-lat/9609036].

[38] D. Toussaint, *Spectrum results with Kogut-Susskind quarks*, *Nucl. Phys. Proc. Suppl.* **106** (2002) 111–116 [hep-lat/0110010].

[39] J. Hein, Q. Mason, G. P. Lepage and H. Trottier, *Mass renormalisation for improved staggered quarks*, *Nucl. Phys. Proc. Suppl.* **106** (2002) 236–238 [hep-lat/0110045].

[40] W.-j. Lee and S. R. Sharpe, *One-loop matching coefficients for improved staggered bilinears*, *Phys. Rev.* **D66** (2002) 114501 [hep-lat/0208018].

[41] W.-J. Lee and S. R. Sharpe, *Partial flavor symmetry restoration for chiral staggered fermions*, *Phys. Rev.* **D60** (1999) 114503 [hep-lat/9905023].

[42] **MILC** Collaboration, C. Bernard, *Chiral logs in the presence of staggered flavor symmetry breaking*, *Phys. Rev.* **D65** (2002) 054031 [hep-lat/0111051].

[43] C. Aubin *et. al.*, *Chiral logs with staggered fermions*, hep-lat/0209066.

[44] F. Knechtli and A. Hasenfratz, *Dynamical fermions with fat links*, *Phys. Rev.* **D63** (2001) 114502 [hep-lat/0012022].

[45] **HPQCD** Collaboration, Q. Mason *et. al.*, *Taste-changing in staggered quarks*, hep-lat/0209152.

[46] A. J. Buras, M. Jamin and M. E. Lautenbacher, *A 1996 analysis of the CP violating ratio epsilon'/epsilon*, *Phys. Lett.* **B389** (1996) 749–756 [hep-ph/9608365].

[47] M. Beneke and M. Neubert, *Flavor-singlet B decay amplitudes in QCD factorization*, *Nucl. Phys.* **B651** (2003) 225–248 [hep-ph/0210085].

[48] M. Beneke and M. Neubert, *QCD factorization for $B \to PP$ and $B \to PV$ decays*, hep-ph/0308039.

[49] S. R. Sharpe and N. Shoresh, *Physical results from unphysical simulations*, *Phys. Rev.* **D62** (2000) 094503 [hep-lat/0006017].

[50] G. P. Lepage *et. al.*, *Constrained curve fitting*, *Nucl. Phys. Proc. Suppl.* **106** (2002) 12–20 [hep-lat/0110175]. Bayesian Fitting.

[51] R. Sommer, *A new way to set the energy scale in lattice gauge theories and its applications to the static force and alpha-s in SU(2) Yang-Mills theory*, *Nucl. Phys.* **B411** (1994) 839–854 [hep-lat/9310022].

[52] C. W. Bernard *et. al.*, *The static quark potential in three flavor QCD*, *Phys. Rev.* **D62** (2000) 034503 [hep-lat/0002028].

[53] C. Bernard, *Pion and Kaon physics with improved staggered quarks*, . Poster presentation at Lattice 2003 in Tsukuba.

[54] K. Melnikov and T. v. Ritbergen, *The three-loop relation between the $\overline{\rm MS}$ and the pole quark masses*, *Phys. Lett.* **B482** (2000) 99–108 [hep-ph/9912391].

[55] G. Rodrigo, *Low-energy Yukawa input parameters for Yukawa coupling unification*, hep-ph/9507236.

[56] E. Gamiz, M. Jamin, A. Pich, J. Prades and F. Schwab, *Determination of m_s and $|V_{us}|$ from hadronic tau decays*, *JHEP* **01** (2003) 060 [hep-ph/0212230].

[57] R. Gupta and K. Maltman, *Light quark masses: A status report at DPF 2000*, *Int. J. Mod. Phys.* **A16S1B** (2001) 591–600 [hep-ph/0101132].

[58] H. Wittig, *Chiral effective lagrangian and quark masses*, hep-lat/0210025.

[59] Q. Mason and H. Trottier, *Two-loop quark mass renormalisation on the lattice*, . to appear.

[60] C. T. H. Davies *et. al.*, *A precise determination of alpha(s) from lattice QCD*, *Phys. Lett.* **B345** (1995) 42–48 [hep-ph/9408328].

[61] C. Davies *et. al.*, *The determination of alpha(s) from lattice QCD with 2+1 flavors of dynamical quarks*, hep-lat/0209122.

[62] M. Creutz, *Monte Carlo study of quantized SU(2) gauge theory*, *Phys. Rev.* **D21** (1980) 2308–2315.

[63] M. Peter, *The static potential in QCD: A full two-loop calculation*, *Nucl. Phys.* **B501** (1997) 471–494 [hep-ph/9702245]. mistake corrected by [64].

[64] Y. Schroder, *The static potential in QCD to two loops*, *Phys. Lett.* **B447** (1999) 321–326 [hep-ph/9812205].

[65] S. Weinberg, *The quantum theory of fields. Vol. 2: Modern applications.* Cambridge University Press, 1996.

[66] R. K. Ellis, *Perturbative corrections to universality and renormalization group behavior*, . Presented at ANL Workshop on Gauge Theory on a Lattice, Argonne, IL, Apr 5-7, 1984.

[67] C. Christou, H. Panagopoulos, A. Feo and E. Vicari, *The two loop relation between the bare lattice coupling and the* $\overline{\rm MS}$ *coupling in QCD with Wilson fermions*, *Phys. Lett.* **B426** (1998) 121–124.

[68] O. V. Tarasov, A. A. Vladimirov and A. Y. Zharkov, *The Gell-Mann-Low function of QCD in the three loop approximation*, *Phys. Lett.* **B93** (1980) 429–432.

[69] B. Alles, A. Feo and H. Panagopoulos, *Asymptotic scaling corrections in QCD with Wilson fermions from the 3-loop average plaquette*, *Phys. Lett.* **B426** (1998) 361–366 [hep-lat/9801003].

[70] A. Bode, H. Panagopoulos and Y. Proestos, *O(a) improved QCD: The 3-loop beta-function, and the critical hopping parameter*, *Nucl. Phys. Proc. Suppl.* **106** (2002) 832–834 [hep-lat/0110225].

[71] A. Bode and H. Panagopoulos, *The three-loop beta-fuction of QCD with the Clover action*, *Nucl. Phys.* **B625** (2002) 198–210 [hep-lat/0110211].

[72] B. Alles, M. Campostrini, A. Feo and H. Panagopoulos, *The three loop lattice free energy*, *Phys. Lett.* **B324** (1994) 433–436 [hep-lat/9306001].

[73] C. J. Morningstar and J. Shigemitsu, *One-loop matching of lattice and continuum heavy-light axial vector currents using NRQCD*, *Phys. Rev.* **D57** (1998) 6741–6751 [hep-lat/9712016].

[74] G. 't Hooft, *Some twisted selfdual solutions for the Yang-Mills equations on a hypertorus*, *Commun. Math. Phys.* **81** (1981) 267–275.

[75] I. Montvay and G. Munster, *Quantum fields on a lattice.* Cambridge monographs on mathematical physics. Cambridge University Press, 1994.

[76] G. Parisi, *Prolegomena to any future computer evaluation of the QCD mass spectrum*, . Invited talk given at Summer Inst. Progress in Gauge Field Theory, Cargese, France, Sep 1-15.

[77] P. Pascual and R. Tarrach, *QCD: Renormalization for the practitioner*, *Lect. Notes Phys.* **194** (1984) 1–277.

[78] R. Horgan, *Private communication*, .